TECHNICAL UNIVERSITY OF CRETE

DEPARTMENT OF ELECTRONIC & COMPUTER ENGINEERING

Control Optimization of Active-NPC Power Electronic Converters

Diploma Thesis

Achilladelis Nikolaos

Chania 2013

Acknowledgements

This thesis would not have been possible without the guidance and the help of several individuals, who in one way or another contributed and offered their valuable assistance in the preparation and completion of this study.

First and foremost, my gratitude to my advisor, Assistant Professor Eftychios Koutroulis, who gave me the possibility to complete this thesis with his super-vision, advice and guidance from the early stage of this research.

I am grateful for his encouragement and precious contribution throughout the elaboration of this study. I would also like to thank him for giving me the opportunity to work on his very interesting field of research.

Abstract

The grid-connected photovoltaic (PV) systems are an important part of renewable energy sources. In order to improve the efficiency, the reliability and the low prices of the PV systems many inverter topologies and respectively many SPWM strategies have been proposed to overcome problems and to find more effective approaches.

In this thesis, a new method is proposed to drive Active-NPC topology in order to derive the angles and the strategies that distribute better the power losses through semiconductors and consume less power. Genetic algorithms of the Matlab global optimization toolbox are used to optimize the power losses distribution and the total losses of the Active-NPC inverter topology. They are used to create an array of firing angles of the inverter output voltage waveform and a possible strategy. Then, Simulink simulates the circuit, exports the power losses of every power semiconductor and Matlab computes the minimum sum of the square differences of power losses between all devices and the total sum of them, which are the objective functions of the algorithm. Through this iterative model, genetic algorithm decides which set of angles and strategy should be extracted, in order to have more balanced and less power losses in the Active-NPC inverter semiconductors.

The results of this method indicate that the combination of angles detection and strategy selection give less and more balanced power losses. Having as objective function the total power, losses resulted in less power losses from 5.18% up to 20.51%. For the power losses distribution, the corresponding objective function value was reduced by 1.43% up to 176% with respect to the past-proposed SPWM strategies.

Table of Contents

1. Introduction

1. Power Electronic Technology and DC/AC Inverters

The growing needs in market for renewable energy technologies required a rapid growth in power electronics technology. [2] In most of the renewable energy technologies it is needed to convert the DC power, which is produced, into AC power and hence the development of power electronics and control equipment is a key factor. There are two types of DC/AC inverters: a) stand-alone and b) grid-connected. A stand-alone inverter differs from grid-connected in terms of control function and is used in off-grid applications e.g. with battery storage. [2] Grid-interactive inverters must follow the voltage and frequency characteristics of the utility generated power presented on the distribution line. They are suitable for grid-connected photovoltaic (PV) systems in rooftops and other large-scale applications.

The utility interactive inverters must not only condition the power output of the PV arrays, but also ensure that the PV system output is fully synchronized with the utility power, being the key link between them. It can be said that a grid connected inverter acts as an interface that converts DC current, produced by the solar cells, into utility grade AC current and consequently must produce good quality sine-wave following the frequency and voltage of the grid. A typical grid-connected inverter uses Pulse Width Modulation (PWM) schemes and operates in the range of 2-20 kHz.

The grid-connected photovoltaic (PV) systems integration is getting more and more widespread as being an important part of renewable energy sources. Multilevel inverter technology has gained much attention in the scientific research and power industrial area. These inverters involve less complexity, need less filtering and use no transformer. Multilevel converters can be beneficial for large systems in terms of cost and efficiency. In order to improve the efficiency, the reliability and the low prices of the PV systems, many kinds of new inverter topologies have been proposed to avoid using grid-isolation transformer, such as HERIC topology [1], Full-bridge with DC Bypass topology [1], H5 topology [1], conventional Neutral Point Clamped (NPC) [5], Conergy-NPC topology [1] and Active-NPC topology [4].

NPC is one of these topologies, connected to the grid, without using any transformer and compared with the traditional 2-level full bridge PWM inverters, can produce lower switch losses, less harmonic distortion and common-mode current, which significantly improve the efficiency of the inverters and make it appealing for photovoltaic application. Meanwhile, NPC inverter's main disadvantage is the unequal distribution of the losses in the power semiconductor devices (IGBTs, Diodes), which leads to an unequal distribution of temperature and limits the output power of the inverter. The conventional NPC topology was extended to a derivative topology with more zero-state paths reducing the above drawback, the Active-NPC structure.

The Active-NPC topology has more degrees of freedom and can be controlled by different PWM strategies. In contrast to the conventional NPC topology, Active-NPC has more than one ways to clamp the midpoint, which means that the current can be conducted through more clamping ways in both directions. The total losses in Active-NPC converter are not smaller, but the power losses are more balanced through the power semiconductor devices.

As already said, the main problem of these topologies is the unequal distribution of losses in circuit's semiconductors. In every inverter, the reduction of power losses is an essential aspect to increase efficiency and reduce costs and failures. When the energy losses are not well distributed, as in the NPC inverter, the junction temperature can be very different among the semiconductors. The highly stressed devices are prone to failures reducing also the overall performance of the cooling system. The difference of energy losses increases with the switching frequency, making the problem even worse.

There are many different strategies for Active-NPC inverter control, that use different zero states and conduction paths in order to solve the above problem. These strategies usually compare a reference voltage with one or more carrier waves, in different frequencies, same as in the traditional 2-level full-bridge PWM inverters. Strategies such as PWM1 [6], PWM2 [6], Natural Double-Frequency PWM strategy [6] and the Adjustable Losses Distribution (ALD) [1] strategy have been proposed to have better losses distribution performance.

In this thesis, Genetic Algorithms (GAs) are used to optimize the power losses distribution and the total losses of the Active-NPC topology. In particular, genetic algorithm creates a set of angles of the output voltage waveform and a strategy. Simulink simulates the circuit (Active-NPC topology), exports the power losses of every semiconductor to Matlab and then Matlab computes the minimum sum of the square differences of the power losses between all devices and the total sum of power losses. These are the objective functions of the algorithm. Through this iterative model, Genetic Algorithm decides which set of angles and strategy should be extracted, in order to have more balanced and less power losses through Active-NPC semiconductors. It has to be said that all possible switches transitions have been taken into consideration, in order to create all possible strategies, simulate them and decide which strategy of the optimized set of angles gives the best result. This set of angles, except from output voltage waveform's symmetry constraints, obeys IEEE standards for interconnecting distributed resources with Electric Power Systems, by examining the total demand distortion (TDD).

Simulations using Simulink have been performed for evaluating the efficiency of different Active-NPC strategies and comparing the already presented strategies with the method created in this thesis. The Genetic Algorithm's parameters have been initialized after optimization experiments through Matlab.

In chapter 2, the NPC topology and its derivative the Active-NPC topology are presented. Moreover, the past-proposed strategies, their drawbacks and their advantages, for these topologies, are described and analyzed. In chapter 3, the model constructed in this thesis is analyzed thoroughly. In chapter 4, the optimization results from the simulated model are presented. Additionally, a comparison is presented of the results between the approaches already presented in bibliography and the model developed in this thesis.

2. Active-NPC Inverter

2. Introduction

In order to improve the efficiency, the reliability and the low prices of the PV systems, many types of new inverter topologies have been proposed to avoid using a grid-isolation transformer, such as the Conventional Neutral Point Clamped Inverter and its derivative, the Active Neutral Point Clamped Inverter. There are different strategies for the Active-NPC inverter control, that use different zero states and conduction paths in order to distribute better the power losses through the power semiconductors. Strategies such as PWM1, PWM2, Natural Double-Frequency PWM strategy and the Adjustable Losses Distribution (ALD) strategy are described and analyzed in this chapter.

2.1 The Conventional Neutral Point Clamped Inverter

The Conventional Neutral Point Clamped (NPC) topology was introduced by Nabae, Takahasi and Akagi in 1981[5] showing great improvements in terms of lower dv/dt in comparison with the 2-level full-bridge inverter, without using any transformer, producing lower switching losses and common-mode current, reducing the harmonic distortion and as a result improving the total efficiency of the inverter [14]. In the case of the inverter, inductive loads can cause problems because an inductor cannot instantly stop conducting current, which must be dampened or diverted, so that it does not try to flow through the open switch, else the surges may destroy the IGBTs used to produce the output sine-wave. The Neutral Point Clamped inverter topology is presented in Fig. 2-1.

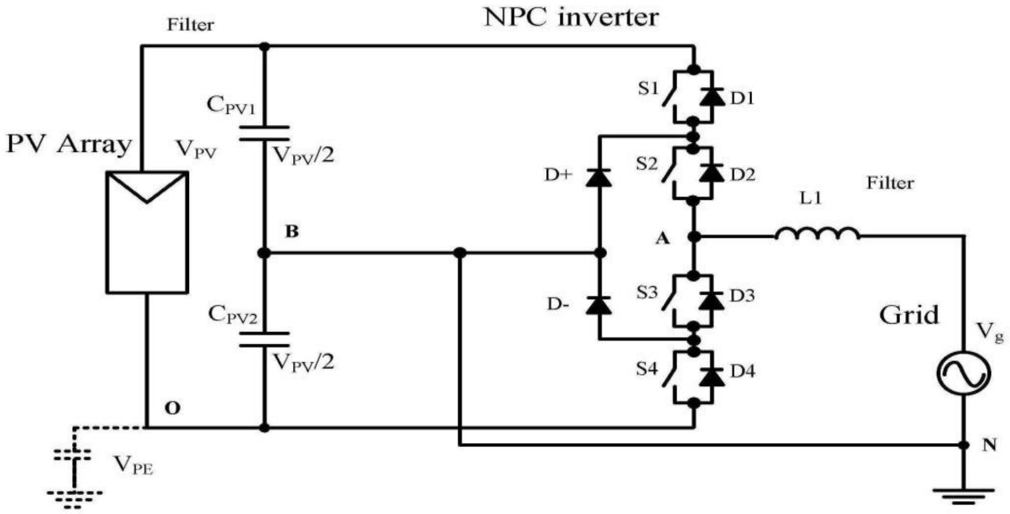

Figure 2-1 Conventional Neutral Point Clamped half-bridge inverter topology [1].

As presented in Fig. 2-1, the NPC half bridge is composed by four switches and two clamped diodes. The clamped diodes, D+ and D-, are used such that the zero voltage can be achieved by “clamping” the output to the grounded “middle point” of the DC bus, depending on the sign of the output current. However, the NPC topology has the disadvantage of an unequal distribution of losses among the power devices [4]. The maximum allowable power losses limit the switching frequency and output power. An unequal loss distribution- as in the case of the NPC inverter- yields an unequal junction temperature distribution among the semiconductors. Some devices become hot while others stay much cooler at the same time. The switching frequency and the maximum phase current of the entire inverter are limited because of the most stressed devices and as a result the overall switch utilization is low. At high-power inverters, separate heat sinks are installed per device to cause better thermal decoupling of the semiconductors. The maximum losses of a single device depend only by its own heat sink’s thermal characteristics. It has to be underlined that the losses of the respective devices depend on the operating points and the different modulation schemes being applied. The most critical operating points are located at the boundaries of the NPC inverter’s operating area, namely, being maximum and minimum modulation depth, at power factors of PF=1 and PF=-1. Here, the loss distribution is more unbalanced and all operating points in between are less critical. In order to overcome this drawback, the NPC topology was extended to the Active-NPC inverter which is examined in this thesis.

2.2 The Active-Neutral Point Clamped Inverter

The Active Neutral Point Clamped inverter (Active-NPC Fig.2-2) is a derivative of the conventional Neutral Point Clamped topology, having two more active switches, anti-parallel connected with the clamp diodes, which improve substantially the loss distribution. The Active-NPC voltage source inverter provides more degrees of freedom and it has more than one ways to clamp the midpoint. Compared to the NPC topology, the total losses are maintained but they are better balanced; hence a better thermal balance can be obtained.

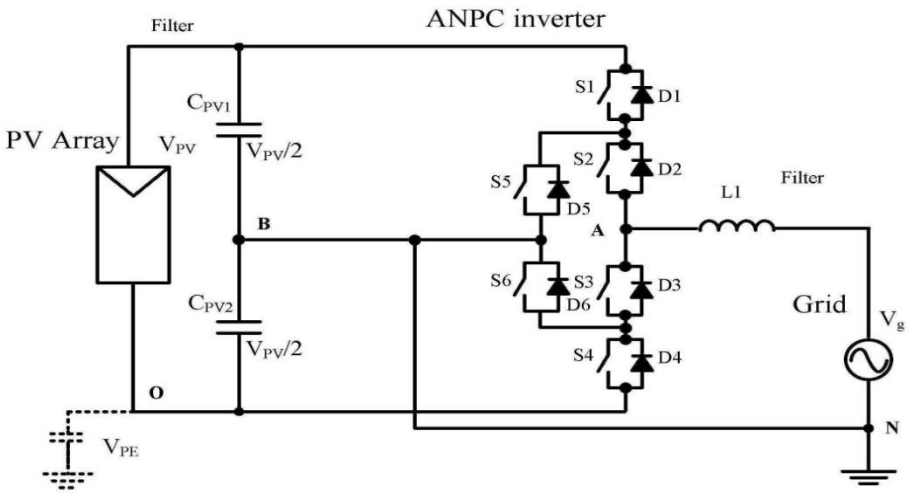

Figure 2-2 Active Neutral Point Clamped half-bridge inverter topology [1].

The Active-NPC structure is composed of six bidirectional switches capable to support a voltage equal to [$-V_{PV}/2$ $V_{PV}/2$]. Each switch is usually an Insulated-Gate Bipolar Transistor and it is connected with an anti-parallel diode. In the conventional NPC topology, the utilization of the upper or the lower NPC path is determined by the direction of the phase current, in difference with the Active-NPC topology, where by turning on S_5 and S_2, the phase current can be conducted through the upper path of the neutral tap in both directions (Fig. 2-3). In the same manner, by turning-on S_6 and S_3, the phase current can be conducted through the lower path of the neutral tap in both directions (Fig. 2-4). As a result, the Active-NPC inverter has more zero switching states. The different commutations and zero states in the Active-NPC inverter can be used to distribute the power losses more evenly among the semiconductors. The intention is not to save total inverter losses, but to distribute them equally. The total losses remain nearly unchanged. The commutations to or from the states determine the distribution of the switching losses. The distribution of conduction losses during the zero states can be controlled by the selection of the upper or lower current paths.

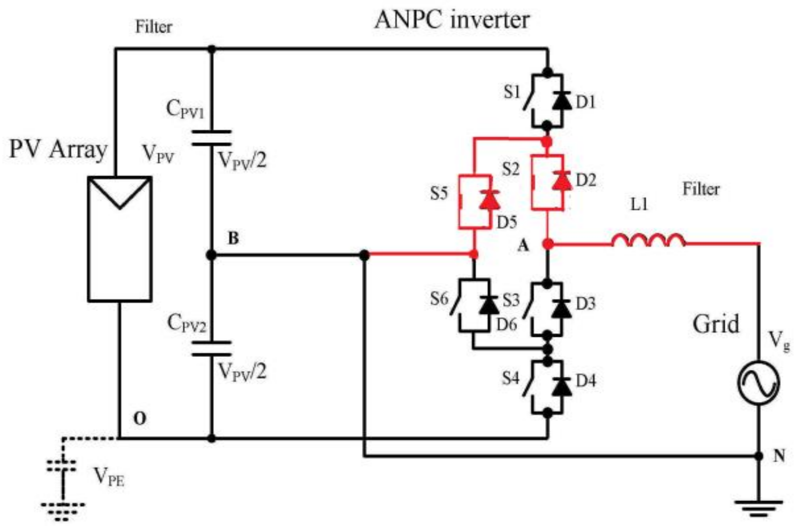

Figure 2-3 Upper current path.

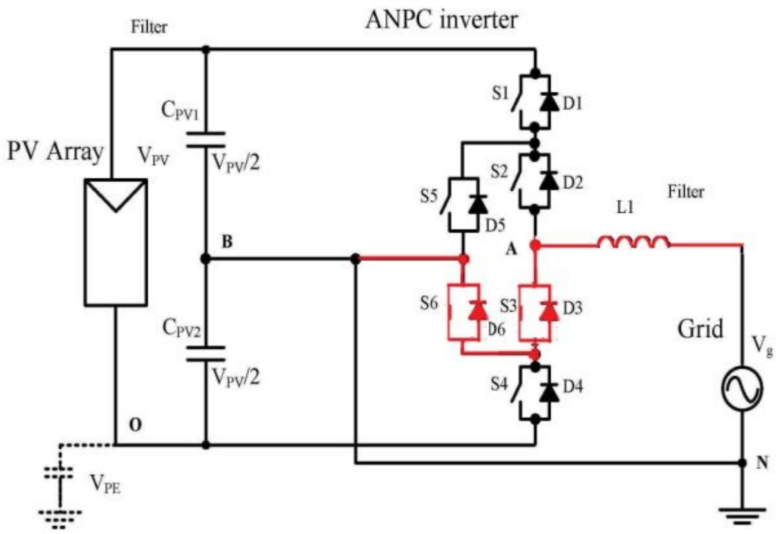

Figure 2-4 Lower current path.

There are many different PWM strategies for Active- NPC inverter control by using different zero states and conduction paths. [6] It has to be underlined that all commutation occurs between one active switch and one diode having essential switching losses, despite more than two devices are turned ON or OFF. The selection of the upper or the lower path during the zero states is a crucial choice referring to the distribution of conduction losses, in contrast to the influence of positive and negative states.

2.3 Past-Proposed PWM Strategies for the Active-NPC Inverter Topology

2.3.1 PWM-1 Strategy

In the case of strategy PWM-1 [6] the sets of switches S_1, S_5 and S_4, S_6 switch alternatively at different frequencies. The PWM-1 strategy uses two carrier signals, C_1 and C_2 (Fig. 2-5) with the same amplitude and switching frequency, but level-shifted on the vertical axis. In particular, the carrier associated to negative levels is in opposition phase with respect to the carrier associated to positive ones. The carrier signals are compared with the reference voltage which has the same frequency with the inverter output waveform. The control signals are obtained from the comparison of these waves and follow the strategy's characteristics. In PWM-1 strategy four states are obtained: P, N, O^+, O^- (Table 2-1). In the case of switching states P and N the paths of the load current through the switches are the same with the NPC structure (S_1, S_2 and S_3, S_4). During these states the conduction losses cannot be influenced. The zero voltage level is obtained with two switching states: O^+ and O^- . The state O^+ is obtained when the reference voltage is positive and the state O^- when it is negative. In particular, the state O^+ is obtained when the reference voltage is positive, S_2 and S_6 are turned on and S_1, S_3, S_4 and S_5 are turned off. The O^- is obtained when the reference voltage is negative, S_3, S_5 are turned on and S_1, S_2, S_4, S_6 are turned off (Table 2-1).

Table 2-1. Switching sequences of the Active-NPC PWM-1 strategy

Output Voltage	Switching State	S_1	S_2	S_3	S_4	S_5	S_6
$-V_{dc/2}$	N	0	0	1	1	0	0
0	O^-	0	0	1	0	0	1
0	O^+	0	1	0	0	1	0
$V_{dc/2}$	P	1	1	0	0	0	0

Fig. 2-5 shows the switches commutations during the positive and negative cycle depending on the comparison between the carrier and sinusoidal waveforms.

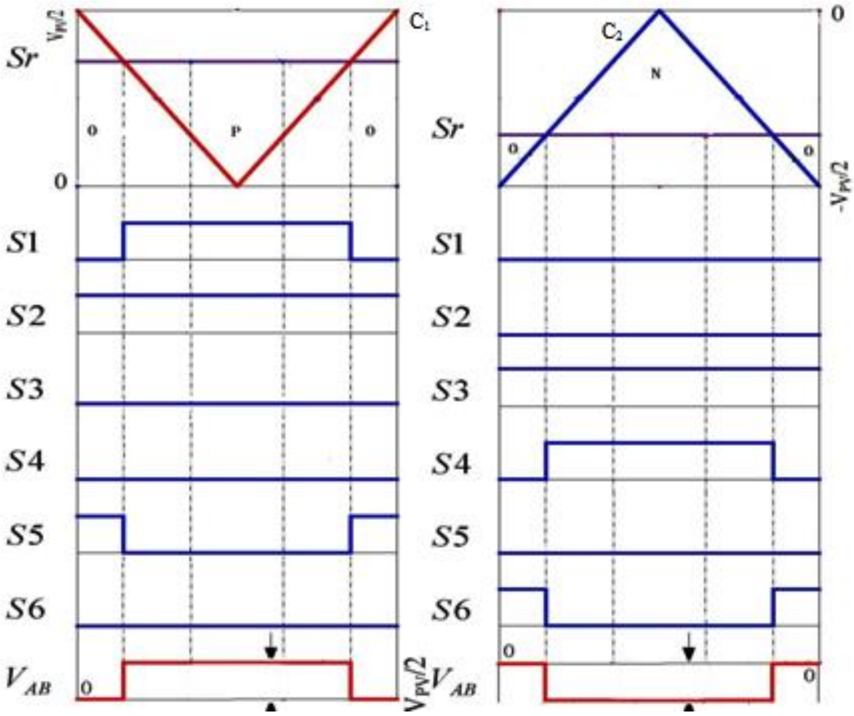

2-5 Sinusoidal PWM-1 strategy [6].

2.3.2 PWM-2 Strategy

In the case of PWM-2 [6], the set of S_2, S_3 switches alternatively at a high frequency (switching frequency), while the other switches at a low frequency, which is equal to the reference voltage frequency. The PWM-2 strategy uses two carrier signals, C_1 and C_2 (Fig. 2-6) with the same amplitude and frequency, but level-shifted on the vertical axis. In particular, the carrier associated to negative levels is in opposition phase with respect to the carrier associated to the positive ones. Following the comparison process, strategy PWM-2 has four switching states: P, N, O^+ and O^- . In the case of P and N commutation sequences, the paths of the load current through the switches are the same with the Active-NPC PWM-1 strategy and during these states the conduction losses cannot be influenced. The zero voltage level can be obtained with two switching states: O^+ and O^- . The state O^+ is obtained when the reference voltage is positive and S_1, S_3, S_6 are turned on, while S_5, S_2 and S_4 are turned off. The state O^- is obtained when the reference voltage is negative. In this case S_5, S_2 and S_4 must be turned on, while S_1, S_3, S_6 are turned off (Table 2-2). For O^+ and O^- states the load current can pass in both directions through S_5, S_2, or through S_6 and S_3.

Table 2-2. Switching sequences of the Active-NPC PWM-2 strategy							
Output Voltage	Switching State	S_1	S_2	S_3	S_4	S_5	S_6
$-V_{dc/2}$	N	0	0	1	1	1	0
0	O^-	0	1	0	1	1	0
0	O^+	1	0	1	0	0	1
$V_{dc/2}$	P	1	1	0	0	0	1

Fig. 2-6 shows the switches commutations during the positive and negative cycle depending on the comparison between the carrier waves and the sinusoidal waveform.

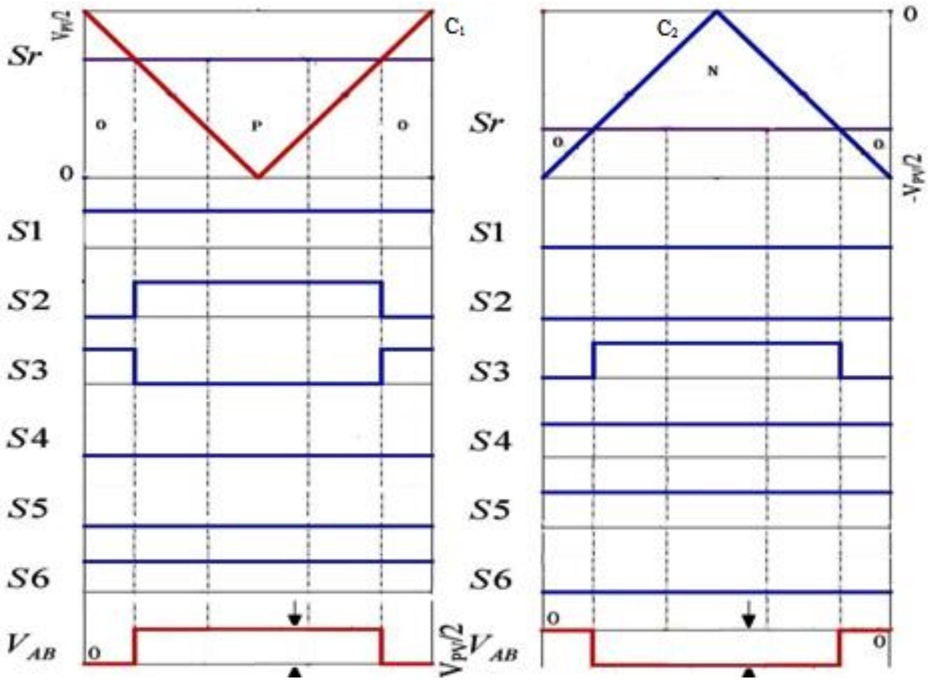

Figure 2-6 Sinusoidal PWM-2 strategy [6].

2.3.3 PWM-3 Strategy (Double Frequency Active-NPC strategy)

In the case of PWM-1, the set of switches S_2, S_3 switch “rarely” in comparison with the others, so they have mainly conduction losses. In the case of the PWM-2 strategy, the sets of switches S_1, S_5 and S_2, S_3 switch “rarely” (at low frequency) and have only conduction losses. PWM-3 [6] improves the static conversion efficiency, because at dead times (Sr≈0) two different sets of switches switch when $S_r < 0$ and $S_r > 0$. The switching states and sequences are analyzed in one switching period (T_s). In particular, the reference voltage (low frequency) is compared with two carrier waves C_1, C_2 (Fig. 2-7) that are phase-shifted on the horizontal axis by $T_s/2$. In difference with the other strategies, PWM-3 has six switching states, having two more states for zero voltage level: P, N, O_1^+, O_1^- , O_2^+ and O_2^- (Table 2-3).

Table 2-3. Switching sequences of the Active-NPC PWM-3 strategy

Output Voltage	Switching State	S_1	S_2	S_3	S_4	S_5	S_6
$-V_{dc/2}$	N	0	0	1	1	1	0
0	O_1^-	0	0	1	0	0	1
0	O_2^-	0	1	0	1	1	0
0	O_1^+	0	1	0	0	1	0
0	O_2^+	1	0	1	0	0	1
$V_{dc/2}$	P	1	1	0	0	0	1

The state P is obtained when the reference voltage is positive and S_1, S_2, S_6 are turned on, while S_3, S_4 and S_5 must be turned off. The state N is obtained by turning on the switches S_5, S_3 and S_4, while S_1, S_2, S_6 must be turned off. In these cases, the load current paths, through the switches, are the same with the other strategies, but during these active states two active switches and two diodes are conducting depending on the direction of the phase current.

The zero voltage level is obtained by four different control sequences: O_1^+, O_1^- , O_2^+ and O_2^-. The states O_1^- and O_2^- are obtained when the reference voltage is negative, while the states O_1^+ and O_2^+ are obtained when the reference voltage is positive.

In addition, the state O_1^- is obtained when the switches S_3 and S_6 are turned on and S_1, S_3, S_4, S_5 are turned off. The O_2^- is obtained when the switches S_5, S_2, S_4 are turned on and S_1, S_3, S_6 are turned off. The state O_1^+ is obtained when the switches S_5 and S_2 are turned on and S_1, S_3, S_4, S_6 are turned off. Finally, the state O_2^+ is obtained when S_1, S_3, S_6 are turned on and S_2, S_4, S_5 are turned off.

Fig.2-7 show the switches commutations during the positive and negative cycle depending on the comparison between the carrier waves and the sinusoidal waveform.

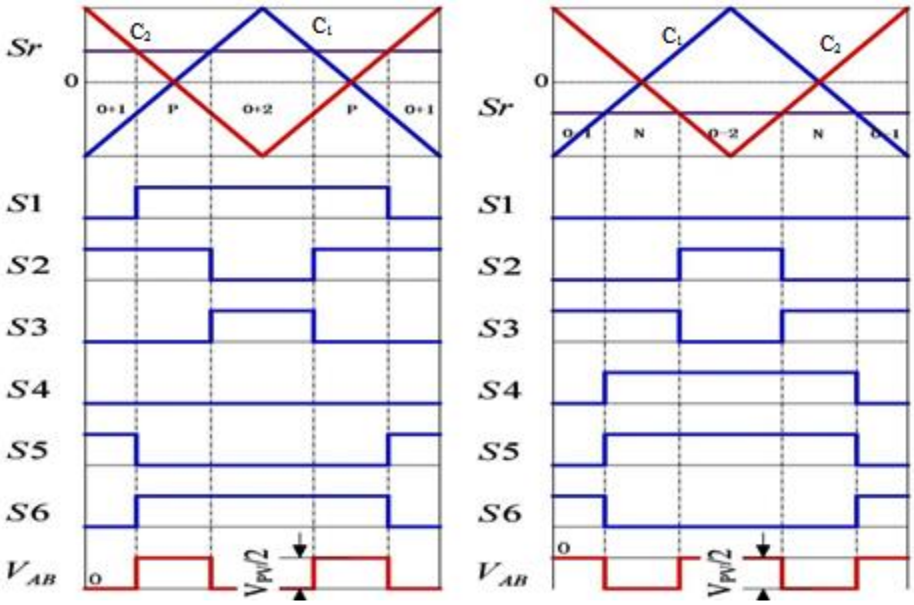

Figure 2-7 Sinusoidal PWM-3 strategy [6].

2.3.4 PWM-4 Strategy (Adjustable Losses Distribution Active-NPC strategy)

The Adjustable Losses Distribution (ALD) strategy [1] is a combination of the above classical PWM strategies, having two more zero states (six) and a total of 8 switches states: P, N, O_{in}^+, O_{in}^-, O_{out}^+ and O_{out}^-, O^+ and O^- (Table 2-4). In the case of classical strategies (PWM-1, PWM-2), the switching losses mainly stress the inner (PWM-1) and the outer (PWM-2) switches. In case of PWM-3, the switching losses are distributed by half between the inner and the outer switches (DF), improving the power losses distribution.

Table 2-4. Switching sequences of the Active-NPC PWM-4 strategy

Output Voltage	Switching State	S_1	S_2	S_3	S_4	S_5	S_6
$V_{dc/2}$	P	1	1	0	0	0	1
0	O_{in}^+	1	0	1	0	0	1
0	O_{out}^+	0	1	1	0	0	1
0	O^+	0	0	1	0	0	1
0	O^-	0	1	0	0	1	0
0	O_{out}^-	0	1	1	0	1	0
0	O_{in}^-	0	1	0	1	1	0
$V_{dc/2}$	N	0	0	1	1	1	0

ALD strategy is a combination of two similar sub-strategies and follows two sequences (Stress-In/Stress-Out mode) depending on the most stressed, inner or outer, devices. In particular, if the conduction power losses mainly stress the inner IGBTs (the conduction losses distribution depends on the modulation index, M and power factor, PF), then the ALD control strategy follows the Stress-Out mode (sequences:{ 0^+, 0_{out}^+, Positive, 0_{out}^+, 0^+} or {0^- , 0_{out}^-, Negative, 0_{out}^-, 0^- }), in order to increase the switching losses of the outer IGBTs. Respectively, if the conduction losses mainly stress the outer IGBTs, the ALD control strategy follows the Stress-In mode (sequences :{ 0^+, 0_{in}^+, Positive, 0_{in}^+, 0^+} or {0^- , 0_{in}^-, Negative, 0_{in}^-, 0^- }), increasing the switching power losses of the inner IGBTs. This mechanism balances better the total (conduction and switching) losses. Figs. 2-8 and 2-9 show the switches commutations during the positive and negative cycle for Stress-In and Stress-Out modes.

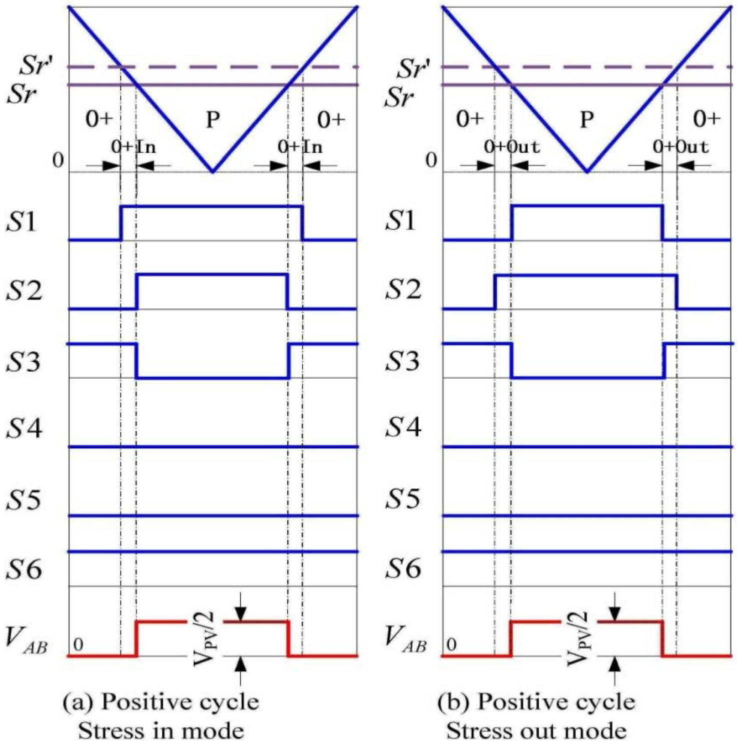

Figure 2-8 The switches states and the output voltage of ALD strategy for a positive cycle [1].

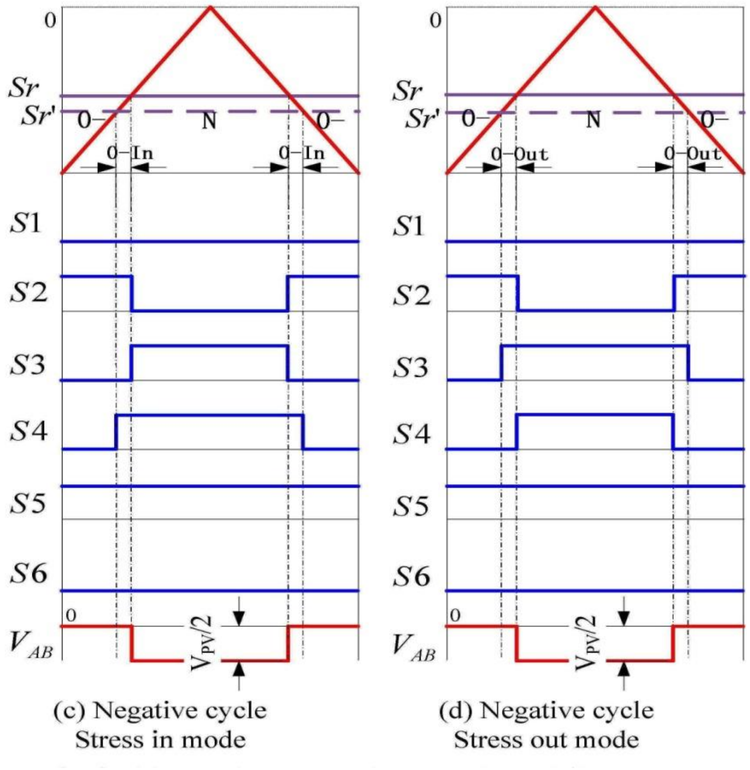

Figure 2-9 The switches states and the output voltage of ALD strategy for a negative cycle [1].

Referring to the mode rate, the ALD strategy takes as an input the percent of Stress-In/Stress-out mode in one output voltage cycle. Additionally, a new modulation signal Sr’ is composed by a synchronized sinusoidal wave added to the modulation wave Sr. In this thesis, the amplitude of Sr’ is 10% of the modulation wave Sr. Moreover, depending on the percentage of Stress-In mode at the positive half-cycle, S_1 uses as modulation signal the Sr’ signal instead of Sr, whereas during the negative half-cycle, S_4 uses the Sr’ signal instead of the Sr modulation signal. Respectively, during the percentage of Stress-Out mode at the positive half-cycle, S_2 uses the new modulation signal (Sr’), whereas during the negative half-cycle, S3 uses the Sr’ instead of the Sr modulation signal. If the amplitude of Sr’ exceeds carrier’s amplitude, the states of the inner (Stress-In) or the outer (Stress-Out) switches will not be changed during this period and the output current will not be influenced. For example at the positive state, in Stress-In mode during the positive half-cycle, S_1 and S_2 must be ON. If Sr’ amplitude exceeds the amplitude of the carrier , then S_1 keeps ON. However, since S_1 does not influence the active positive state, it is validated that the over-range of Sr’ does not influence the output current.

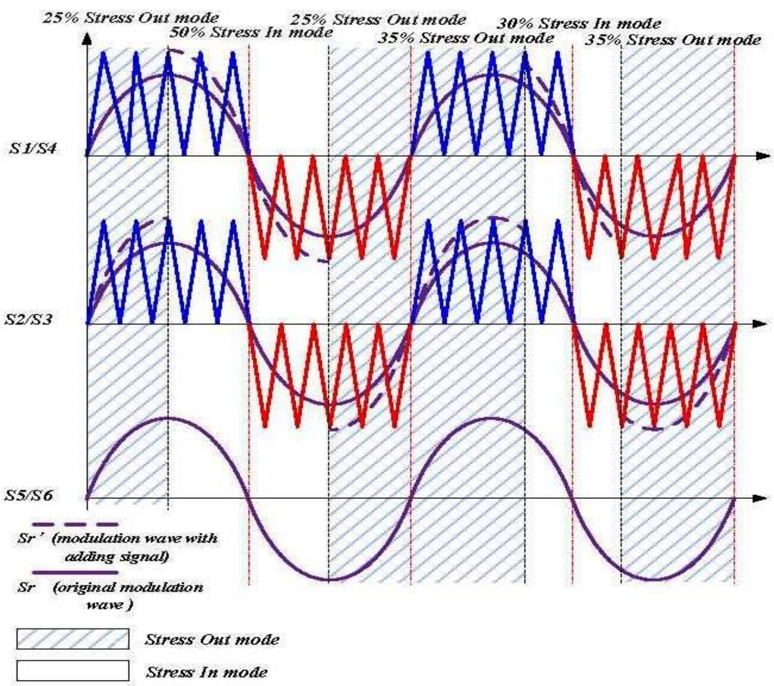

Figure 2-10 PWM generation for one cycle of 50%-50% Stress-In/Stress-Out mode and one cycle of 30%-70% Stress-In /Stress-Out mode[1].

Fig. 2-10 shows a combination of different rate modes in an output voltage cycle, in order to explain the ALD strategy flow. In case of 50%-50% Stress-In/Stress-Out mode, the switching losses are distributed between S_1 and S_4 equally during the first grid cycle. S_1, during the first quarter of a period, takes from positive Stress-Out mode switching losses and respectively S_4, at the fourth quarter of the period, suffers switching losses from negative Stress-Out mode. The Stress-In mode is also shared by the positive and negative cycle equally so as S_2 and S_3 take the same switching losses. Similarly, in case of 30%-70% Stress-In/Stress-Out mode during the second grid cycle, S_1, during the 35% of period, suffers switching losses from positive Stress-Out mode and S_4 suffers switching losses from 75% till the end of the period from the negative Stress-Out mode. S_2 takes 15% positive Stress-In mode and S_3 takes another 15% negative Stress-In mode. As a result the inner switches have less switching losses, in contrast to the outer switches.

Generally ALD's main features are [1]:

a) the switching losses distribution can be controlled by adjusting the adding sine wave Sr'.

b) there are two more zero states (six in total) in relation to other PWM strategies.

c) the new modulation wave (Sr’) and the classic modulation wave (Sr) have the same phase angle and frequency, but different amplitudes.

d) by adjusting Sr’ amplitude it is easy to control the switching distribution.

e) it is able to balance the conduction and the switching power losses between the outer and the inner switches, depending on Stress-In and Stress-Out percentages, by distributing the switching losses.

f) the efficiency of different Stress-In/Stress-Out rate ALD strategy is the same, because the total power losses are the same.

g) the total conduction and switching losses of the inner switches, S_2 and S_3, may be different, which is caused by the 0_{out}^{-} and 0_{out}^{+} zero states and they are dependent on the duration of the Stress-Out mode. The longer is the clamped period of Stress-Out mode, the more unbalanced the total power losses will be.

All PWM strategies for the Active-NPC topology described above produce the sinusoidal output voltage at the desired frequency by comparing a sinusoidal control signal at the desired frequency, with a triangular waveform having frequency equal to the switching frequency. In this thesis, a new approach is presented using a combination of the sinusoidal PWM output voltage characteristics, the possible commutations of switches at the Active-NPC topology and Genetic Algorithms.

3. The Proposed Optimization Method

3. Introduction

In this thesis, Genetic Algorithms (GAs) are used to optimize the total power losses and the loss distribution of the Active-NPC topology. In particular, genetic algorithm produces a set of angles that compose the output voltage waveform and a possible strategy. Simulink simulates the circuit, exports the power losses of every semiconductor to Matlab and Matlab and computes the minimum sum of the squared difference of power losses between all devices, which is the objective function of the algorithm referring to the distribution of losses. The same functionality is followed for the total losses and in this case the objective function of the genetic algorithm is the sum of every semiconductor power losses. Through this iterative model, the genetic algorithm decides which set of angles and strategy should be extracted, in order to have less and more balanced power losses through Active-NPC semiconductors. It has to be underlined that all possible switches transitions have been taken into consideration, in order to create all possible strategies, simulate them and decide which strategy of the optimized set of angles gives us the best result. This array of angles, except from the output voltage waveform symmetry constraints, obeys IEEE standards for interconnecting distributed power sources with Electric Power Systems, by examining the total demand distortion (TDD).

3.1 Optimization Model Structure

The model consists of two connected parts constructing an iterative model (Fig. 3-1). The first part uses Matlab software and contains genetic algorithms (Matlab gaoptimset global optimization toolbox), 3L-PWM waveforms construction, all possible strategies, according to the possible commutations between [$+V_{dc}$ 0 $-V_{dc}$] states, the objective function computations and the connection with the second part of the optimization model.

The second part uses Simulink toolbox and simulates the operation of the Active-Neutral Pointed Clamped (Active-NPC) inverter. It is controlled from the previous part that defines all possible commutations and switches transitions. After simulating the Active-NPC inverter, Simulink extracts the power losses of every semiconductor to the first part. These simulation results are used to compute the objective function of genetic algorithm, which is optimized.

The following schema shows the full model structure, every part of which will be described and analyzed in the following paragraphs.

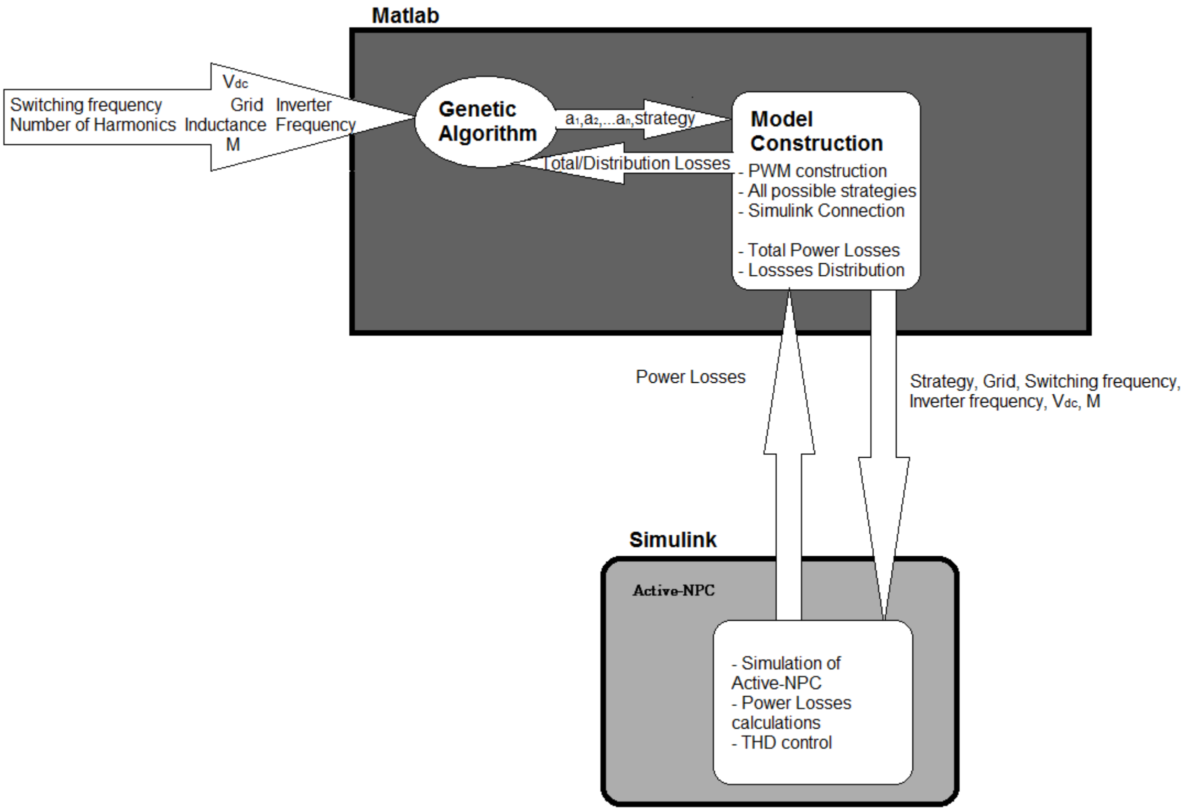

Figure 3-1 The iterative optimization model developed in this thesis.

3.1.1 The Matlab optimization model

This part of the optimization algorithm receives the angles from the genetic algorithm and drives them to Simulink, having constructed the PWM waveform, the switches transitions and setting up the characteristics of the power semiconductors and other electronic parts of the circuit.

For every such setup, the total demand distortion and modulation index constraints are examined in order to verify that it satisfies the optimization problem constraints.

Starting from the Modulation index constraints, the fundamental output's amplitude is computed from the given function for a 3-level PWM waveform [8]. In general, a non-sinusoidal waveform $\mathrm{f}(\mathrm{t})$ repeating with an angular frequency ω can be expressed as:

$$f(t) = F_0 + \sum_{h=1}^{\infty} f_h(t) = \frac{1}{2} a_0 + \sum_{h=1}^{\infty} \{a_h \cos(h\omega t) + b_h \sin(h\omega t)\} \qquad (3.1)$$

where $F_0 = \frac{1}{2} a_0$ is the average value of the waveform and a_h and b_h are given from the following equations:

$$\mathrm{a_h} = \frac{1}{\pi} \int_0^{2\pi} f(t) \cos(h\omega t) d(\omega t) \ , \ \mathrm{h} = 0, \ldots .\ \infty \qquad (3.2)$$

and

$$\mathrm{b_h} = \frac{1}{\pi} \int_0^{2\pi} f(t) \sin(h\omega t) d(\omega t) \ , \ \mathrm{h} = 1, \ldots ... \infty \qquad (3.3)$$

From (3.1) and (3.2), the average value is given by:

$$F_0 = \frac{1}{2} a_0 = \frac{1}{2\pi} \int_0^{2\pi} f(t) d(\omega t) = \frac{1}{T} \int_0^{T} f(t) d(t) \qquad (3.4)$$

where, $\omega = \frac{2\pi}{\mathrm{T}}$.

In (3-1), each frequency component $\{f_h = a_h \cos(h\omega t) + b_h \sin(h\omega t)\}$ can be represented as a phasor in terms of its rms value:

$$\boldsymbol{F_h} = F_h e^{j\varphi_h} \tag{3.5}$$

where, the rms magnitude and phase φ_h are given by:

$$\mathrm{F_h} = \frac{\sqrt{a_h^2 + b_h^2}}{\sqrt{2}} \tag{3.6}$$

and

$$\tan(\varphi_h) = \frac{(-b_h)}{a_h} \tag{3.7}$$

The rms value of $f(t)$ can be expressed in terms of the rms values of its Fourier series components:

$$F = \left(F_0^2 + \sum_{h=1}^{\infty} F_h^2 \right)^{\frac{1}{2}} \tag{3.8}$$

It should be noted that many AC waveforms have a zero average value ($F_0 = 0$). Moreover, by using the waveform symmetry, it is often possible to simplify the calculations of a_h and b_h in (3.6) and (3.7). The table below (Fig.3-2) summarizes the types of symmetry, required conditions and the resulting expressions for a_h and b_h.

Symmetry	*Condition Required*	a_h and b_h
Even	$f(-t) = f(t)$	$b_h = 0 \qquad a_h = \frac{2}{\pi}\int_0^{\pi} f(t)\cos(h\omega t)\, d(\omega t)$
Odd	$f(-t) = -f(t)$	$a_h = 0 \qquad b_h = \frac{2}{\pi}\int_0^{\pi} f(t)\sin(h\omega t)\, d(\omega t)$
Half-wave	$f(t) = -f(t + \frac{1}{2}T)$	$a_h = b_h = 0$ for even h $a_h = \frac{2}{\pi}\int_0^{\pi} f(t)\cos(h\omega t)\, d(\omega t)$ for odd h $b_h = \frac{2}{\pi}\int_0^{\pi} f(t)\sin(h\omega t)\, d(\omega t)$ for odd h
Even quarter-wave	Even and half-wave	$b_h = 0$ for all h $a_h = \begin{cases} \frac{4}{\pi}\int_0^{\pi/2} f(t)\cos(h\omega t)\, d(\omega t) & \text{for odd } h \\ 0 & \text{for even } h \end{cases}$
Odd quarter-wave	Odd and half-wave	$a_h = 0$ for all h $b_h = \begin{cases} \frac{4}{\pi}\int_0^{\pi/2} f(t)\sin(h\omega t)\, d(\omega t) & \text{for odd } h \\ 0 & \text{for even } h \end{cases}$

Figure 3-2 Symmetries in Fourier analysis [8].

The waveform of the Active-NPC inverter power stage output is shown in Fig. 3-3. It has an odd and half-wave symmetry.

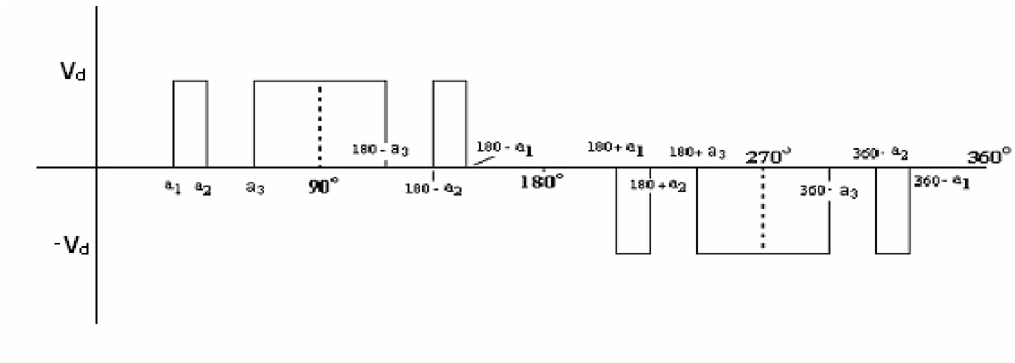

Figure 3-3 3-Level PWM waveform of the Active-NPC output voltage [9].

According to the above table and the symmetry of the waveform shown in Fig. 3-3 [9]:

$$\mathrm{V}_{\mathrm{a0,h}} = \frac{4}{\pi}\left[\int_{\alpha_1}^{\alpha_2} V_d \sin(h\omega t)dt + \int_{\alpha_3}^{90} V_d \sin(h\omega t)dt\right] \Rightarrow \tag{3.9}$$

$$\mathrm{V}_{\mathrm{a0,h}} = \frac{4}{\pi}V_d \frac{1}{h}\left[-\cos\left(ha_2\right) + \cos\left(ha_1\right) - \cos(90) + \cos\left(ha_3\right)\right] \Rightarrow$$

$$\mathrm{V}_{\mathrm{a0,h}} = \frac{4}{\pi}V_d \frac{1}{h}\left[\cos\left(ha_1\right) - \cos\left(ha_2\right) + \cos\left(ha_3\right)\right] \Rightarrow$$

So the general Fourier analysis of the 3-Level equation for m angles is:

$$V_{a0,h} = \frac{4\mathrm{V}_d}{h\pi}[\sum_{k=1}^{m}(-1)^{k+1}\cos(ha_k)] \tag{3.10}$$

Defining the fundamental amplitude as $\mathrm{b}_1 = \sqrt{2}\mathrm{V}_1$, where V_1 is the RMS fundamental amplitude, it results that for h=1:

$$\sqrt{2}V_1 = \frac{4\mathrm{V}_d}{\pi}[\sum_{k=1}^{m}(-1)^{k+1}\cos(a_k)] \Rightarrow$$

$$\frac{\sqrt{2}V_1\pi}{4V_d} = [\sum_{k=1}^{m}(-1)^{k+1}\cos(a_k)]$$

The first angle a_1 can be computed by solving the above equation. So:

$$\frac{\sqrt{2}V_1\pi}{4V_d} = \cos a_1 + [\sum_{k=2}^{m}(-1)^{k+1}\cos(a_k)] \Rightarrow$$

$$\mathrm{a}_1 = \cos^{-1}\left(\frac{\sqrt{2}V_1\pi}{4V_d} - \left[\sum_{k=2}^{m}\left(-1\right)^{k+1}\cos\left(a_k\right)\right]\right) \tag{3.11}$$

The Modulation Index, M, is an input parameter of the optimization algorithm and it is desired to be parameterized. Thus:

$$M = \frac{b_1}{V_d} \Rightarrow M = \frac{\sqrt{2}\mathrm{V}_1}{V_d} \tag{3.12}$$

Using (3.12), it results that (3.11) is modified as follows:

$$\mathrm{a}_1 = \cos^{-1}\left(\frac{M\pi}{4} - \left[\sum_{k=2}^{m}(-1)^{k+1}\cos(a_k)\right]\right) \tag{3.13}$$

Reconstructing and inserting the new computed angle to the set of angles that the genetic algorithm produced, we have to check if the resulting Total Demand Distortion is within the limit set by the IEEE standard for interconnecting distributed power sources with Electric Power Systems [10]. During inverting DC to AC the voltage waveform is not purely sinusoidal because in addition to a dominant component at the fundamental frequency, the waveform contains components at unwanted frequencies that are harmonics of the fundamental frequency. According to this standard, when the distributed power source is serving balanced linear loads, then the harmonic current injection at the Point of Common Coupling should not exceed the limit stated in Table (3-1).

Table 3-1. Maximum Harmonic Current Distortion In Percent Of Rated Voltage

Individual harmonic order h (odd harmonics)	h<11	11≤h<17	17≤h<23	23≤h<35	35≤h	**Total demand distortion (TDD)**
Percent (%)	4.0	2.0	1.5	0.6	0.3	5.0

It must be checked for every odd harmonic, if the angles produced by the genetic algorithm comply with each cell of the above table. Additionally, an L-type filter is inserted at the output of the Active-NPC inverter in order to comply with the above restrictions. This value of L is a parameter input by the user in the proposed algorithm. The current harmonics injected into the electric grid are given by:

$$\mathrm{I_h} = \frac{V_{a0,h}}{Lw_h} \tag{3.14}$$

where $\omega_h = 2\pi f_h$ and $V_{a0,h}$ is given by (3.10), thus:

$$\mathrm{I_h} = \frac{V_{a0,h}}{L2\pi f_h} \Rightarrow \mathrm{I_h} = \frac{V_{a0,h}}{L2\pi f_{inv} h} \tag{3.15}$$

where h is the harmonic number.

From (3.10) and (3.15), it results that the Root Mean Square value of the harmonic current inserted into the electric grid is given by:

$$I_{2<h<n}^{rms} = \sqrt{\sum_{h=2}^{n} I_h^2} \tag{3.16}$$

The total demand distortion is calculated as follows:

$$TDD = \frac{I_{h\neq 1}^{rms}}{I_0} \tag{3.17}$$

where:

$$I_{h\neq 1}^{rms} = \sqrt{I_{2<h<11}^{rms\ 2} + I_{11<h<17}^{rms\ 2} + I_{17<h<23}^{rms\ 2} + I_{23<h<35}^{rms\ 2} + I_{35<h}^{rms\ 2}} \tag{3.18}$$

and

$$\mathrm{I_o} = \frac{P_o}{V_o} \tag{3.19}$$

where V_0 is the fundamental amplitude of the voltage output waveform and P_0 is the power rate. It has to be noted that TDD is checked for every individual cell of Table (3-1).

After checking the Total Demand Distortion, the algorithm creates the 3-Level PWM waveform. The first step is to compute all possible switches combinations where the Active-NPC inverter output waveform gets the 3 states [P, 0, N].

It has been observed that the positive state can be obtained when S_1, S_2 and S_1, S_2, S_6 switches are ON, the negative state can be obtained when S_3, S_4 and S_3, S_4, S_5 switches are ON and the zero state has 6 possible combinations taken from the all past-proposed PWM strategies described in chapter 2. The following Table (3-2) shows all possible switch commutations.

Table 3-2. All possible switches commutations of the past-proposed PWM strategies

Strategy	**Switching State**	S_1	S_2	S_3	S_4	S_5	S_6
PWM1	P_1	ON	ON	OFF	OFF	OFF	OFF
PWM2/DF*/ALD*	P_2	ON	ON	OFF	OFF	OFF	ON
PWM2/ALD	0^-	OFF	ON	OFF	ON	ON	OFF
PWM2/DF/ALD	$0^+/0_2^+/0_{IN}^+$	ON	OFF	ON	OFF	OFF	ON
DF/ALD	$0_1^+/0^-$	OFF	ON	OFF	OFF	ON	OFF
PWM1/DF/ALD	$0^-/ 0_1^-/0^+$	OFF	OFF	ON	OFF	OFF	ON
ALD	0_{out}^+	OFF	ON	ON	OFF	OFF	ON
ALD	0_{out}^-	OFF	ON	ON	OFF	ON	OFF
PWM1	N_1	OFF	OFF	ON	ON	OFF	OFF
PWM2/DF/ALD	N_2	OFF	OFF	ON	ON	ON	OFF

By examining the above table, we can create all possible strategies using every state and combine them according to the PWM output. It has to be underlined that strategies do not have only one way to clamp the midpoint in every period. The past-proposed PWM strategies lead us to clamp the midpoint with up to six different zero states in a period. In this way, all possible commutations can be obtained.

Moreover, taking into account all possible commutations and transitions of the switches for each state and assigning ON as ‘1’ and OFF as ‘0’, we can create strategies at every combination of them. The total number of the resulting strategies is 6408 and they are stored as ones and zeros in cells of another matrix, every cell of which can be accessed. The cell index is the strategy that generated from the genetic algorithm. After selecting the appropriate strategy and configuring the selected cell, matrices of ones and zeros (from the ON, OFF assignments) are used to drive the gates of the IGBT semiconductors.

The next step is to construct the PWM output voltage of the Active-NPC inverter that has odd and half-wave symmetry. The Active-NPC inverter output voltage is assumed to have odd and quarter-wave symmetry with N switching angles per quarter-cycle. Because of this symmetry, the DC component and the even harmonics are equal to zero.

The symmetries allow us to construct a 3-Level PWM waveform, knowing the firing angles a_1, a_2…, a_n and the strategy of commutations. Assigning the angles to times and creating an array with zeros and ones (+,-) for the three possible levels of the output voltage, we can control the Active-NPC switches.

As an example, supposing that we choose to combine the first P state, the final N state and the first O state from the above table, we have the following vectors:

$P_1:[110000], N_2:[001110]$ and $O:[011000]$

As said before, genetic algorithm generates the set of angles in degrees (°), which can be transformed to time according to the following equation:

$$t_i = T_{inv} \frac{a_i}{360^0} \qquad (3.20)$$

where:

i is number of the angle and T_{inv} is the inverter output waveform Period.

The symmetry and structure of a PWM waveform give us the opportunity to model the possible amplitude-state of the constructed waveform. As a result, it is easy to assign every possible state to the above vectors in a period. For every positive output states the vector referring to P is stored in a matrix, for every zero output the vector is stored in the same matrix below the previous vector and for every negative output state the second vector is stored below the “zero” vector in the same matrix. When all states are stored, we have already created a strategy that can drive all semiconductors of the Active-NPC inverter.

Table 3-3. The example switches commutations

Switches	**S_1**	**S_2**	**S_3**	**S_4**	**S_5**	**S_6**
O	0	1	1	0	0	0
P	1	1	0	0	0	0
O	0	1	1	0	0	0
P	1	1	0	0	0	0
O	0	1	1	0	0	0
P	1	1	0	0	0	0
O	0	1	1	0	0	0
O	0	1	1	0	0	0
N	0	0	1	1	1	0
O	0	1	1	0	0	0
N	0	0	1	1	1	0
O	0	1	1	0	0	0
N	0	0	1	1	1	0
O	0	1	1	0	0	0

The matrix presented in Table (3-3) for the previous example drives all semiconductors because every column is an array of zeros and ones that drive each semiconductor. It represents the above 3-Level PWM waveform with three angles per quarter.

Thus:

$$S_1 = \left[\, 1\ 0\ 1\ 0\ 1\ 0\ 0\ 0\ 0\ 0\ 0\ 0\ 0\ 0 \,\right]$$

$$S_2 = \left[1\ 1\ 1\ 1\ 1\ 1\ 1\ 1\ 0\ 1\ 0\ 1\ 0\ 1\right]$$

$$S_3 = \left[1\ 0\ 1\ 0\ 1\ 0\ 1\ 1\ 1\ 1\ 1\ 1\ 1\ 1\right]$$

$$S_4 = \left[0\ 0\ 0\ 0\ 0\ 0\ 0\ 0\ 1\ 0\ 1\ 0\ 1\ 0\right]$$

$$S_5 = \left[0\ 0\ 0\ 0\ 0\ 0\ 0\ 0\ 1\ 0\ 1\ 0\ 1\ 0\right]$$

$$S_6 = \left[0\ 0\ 0\ 0\ 0\ 0\ 0\ 0\ 0\ 0\ 0\ 0\ 0\ 0\right]$$

These transition matrices are synchronized with the times that are computed and the model imports them to the Simulink part of the optimization algorithm. In particular, these matrices are imported to the Timer Simulink blocks, as analyzed next.

Finally, when Simulink returns the power losses of every semiconductor, the objective function is computed. For total losses, the sum of these losses is computed. The objective function for the optimal distribution of total losses is the minimum sum of the squared differences of power losses between all devices.

$$\min\{\sum_{i} p_i\} \text{, where } i = 1 \ldots 12 \qquad \textit{(3.21)}$$

$$\min\{\sum_{\forall i \neq k} (p_i - p_k)^2\} \text{ , where } i = 1 \ldots 12 \text{ and } k = 1 \ldots 12 \qquad \textit{(3.22)}$$

3.1.2 Genetic Algorithms Using Matlab

The genetic algorithm [11] is an adaptive heuristic search algorithm based on the ideas of natural selection and genetics. Actually, the genetic algorithm is a repetitive, iterative procedure in which a population of candidate solutions (called individuals) is evolved towards better solutions. The optimal solution is achieved through generated generations, in each of which, the fitness function of every individual in the population is evaluated. The more fit individuals are selected from the population and each individual's genome is modified to form a new generation. The algorithm uses the new generation in the next iteration and terminates when either the

number of generations is reached, or there is no improvement in the objective function. In this thesis genetic algorithms are applied because of their ability to solve a variety of optimization problems that are not well suited for standard optimization algorithms, including problems in which the objective function is discontinuous, non-differentiable, stochastic, or highly nonlinear [11]. Additionally, a large scale of solutions can be investigated thoroughly and quickly. Finally, it has to be noted that the optimal solutions are achieved through the best combination of the selection, the crossover and the mutation rules, which are key factors to avoid local minimum and making the algorithm more efficient for the proposed optimization problem.
The genetic algorithm uses three main types of rules at each step, as already said to create the next generation from the current population:

- **Selection rules** select according to the objective function's fitness, the best individuals, called parents, which contribute to the population at the next generation.
- **Crossover rules** combine two parents to form children for the next generation.
- **Mutation rules** randomly change the individual parents to form children. The mutation action is applied after crossover.

The genetic algorithm differs from a classical, derivative-based, optimization algorithm in two main ways. Firstly, Genetic Algorithm generates a population of solutions at each generation. The best solution in the population approaches an optimal solution in difference with a classical algorithm, that generates a single solution and the optimal solution is approached by a sequence of solutions. Secondly, Genetic Algorithm selects the next population by the action of computation, using random number generators, while a classical algorithm selects by a deterministic computation the next solution [11].

Genetic algorithm is a small but important part of this thesis. It is the algorithm that decides which set of angles and which strategy give the best result, given the input parameters, bounds and constraints of our problem.

Genetic Algorithm part gets as input the number of angles subject to the optimization process and has some constraints and bounds. The algorithm must produce angles that obey to:

- $0 < a_i < 90^0$

In order to have better results, algorithm produces numbers in between 0 and 1 that are then multiplied by 90°. The same method is followed in strategy extraction by multiplying with the number of possible strategies. Additionally, the bounds have been set as [0,1] for all genetic algorithm variables.

- $a_{i+1} > a_i$

In this constraint because the number of inputs is defined by the Active-NPC inverter designer, configurable matrices are constructed depending on the number of variables. In particular, following Matlab's documentation, the matrix for linear inequality constraints of the form $A\,x \leq b$ has the following characteristics: If the problem has m linear inequality constraints and n_{vars} variables, then:

- A is a matrix of size m-by-n_{vars}
- b is a vector of length m.

So in the problem studied in this thesis, A is a (n_{vars} x n_{vars+1}) matrix containing ones (1,-1) and zeros. In every line there is one "angle", which is compared with another "angle" in the next column. Also, B is a (n_{vars}-1 x 1) matrix containing zeros.

For example for number of angles=3 and number of algorithm's variables=4, then matrices A and B are given by:

$$A = \begin{bmatrix} 1 & -1 & 0 & 0 & 0 \\ 0 & 1 & -1 & 0 & 0 \\ 0 & 0 & 1 & -1 & 0 \\ 0 & 0 & 0 & 0 & 1 \end{bmatrix}$$

$$B = \begin{bmatrix} 0 \\ 0 \\ 0 \\ 1 \end{bmatrix}$$

And as a result of the above inequality:

$$\begin{bmatrix} 1 & -1 & 0 & 0 & 0 \\ 0 & 1 & -1 & 0 & 0 \\ 0 & 0 & 1 & -1 & 0 \\ 0 & 0 & 0 & 0 & 1 \end{bmatrix} \mathrm{x_i} \le \begin{bmatrix} 0 \\ 0 \\ 0 \\ 1 \end{bmatrix} \Rightarrow$$

$$x_1 \le x_2$$

$$x_2 \le x_3$$

$$x_3 \le x_4$$

In the above inequalities, every line corresponds to an inequality between variables and complies with our constraints between angles.

- Angles comply with IEEE standards for interconnecting distributed power sources with Electric Power Systems, by examining the total demand distortion (TDD).

  In order to add as constraint the above compliance, the genetic algorithm is forced to assign the “inf” value to the objective function of decision variables which do not comply with this constraint and as a result, these set of angles and strategy are rejected.

  .

- The fundamental voltage amplitude must be of the desirable value and it is checked by the model.

  The above method is also applied to check the amplitude of the fundamental voltage, by assigning the “inf” value to the objective function in case that the constraint is not satisfied.

Matlab’s global optimization toolbox [11] contains the ga() function to find the minimum of a given (objective) function using genetic algorithm. The syntax is:

[x ,fval, exitflag] = ga(fitnessfcn ,nvars, A,b,[],[],LB,UB,nonlcon,IntCon,options)

This function minimizes the objective function “fitnessfcn”, with the default optimization parameters replaced by values in the structure options, which can be created using the gaoptimset function [12] and returns f_{val}, the optimal value of the fitness function at the resulting optimal vector of decision variables, x, and exitflag, an integer identifying the reason the algorithm terminated.

Gaoptimset() creates genetic algorithm options structure and has the following syntax.

Syntax:
options=gaoptimset('PlotFcns',{@gaplotbestf},'Display','iter','PopulationSize',60,'EliteCount',5,'SelectionFcn',@selectionroulette,'CrossoverFraction',0.5,'CrossoverFcn',@crossovertwopoint,'MutationFcn',@mutationadaptfeasible,'Generations',1000);

Any unspecified parameters are set to their default values.

The **Population size** field, in **Population** options, determines the size of the population and specifies how many individuals exist in each generation. The larger the population size is selected, the more thoroughly the genetic algorithm searches the solution space by searching more points. As a result the possibility of returning a local minimum and not a global minimum is decreased. However, a large population size also causes the algorithm to run more slowly. In the problem studied in this thesis depending on the number of angles inserted as input, the population size is adjusted accordingly.

Elite count is the number of individuals with the best fitness values in the current generation that are guaranteed to survive to the next generation. These individuals are called “elite children”.

SelectionFcn option handles the function that selects the parents of crossover and mutation children. In this thesis, selection roulette is selected. In roulette selection option, the parents are chosen by simulating a roulette wheel, in which the area of the section of the wheel corresponding to an individual is proportional to the individual's expectation. The algorithm uses a random number to select one of the sections with a probability equal to its area.

The **Crossover fraction** is the fraction of the population at the next generation, not including elite children, that is created by the crossover function.

CrossoverFcn option handles the function that the algorithm uses to perform the crossover function. In general, by selecting a specific crossover option, it is specified how the genetic algorithm combines two individuals, or parents, to form a crossover child for the next generation.

In this thesis, two possible crossover functions, provided in Matlab, were chosen in order to test which option gives the best results. The first crossover option was the "crossoversinglepoint" and the second was "crossovertwopoint". Both of those options produced similar results. In **Single point** crossover (@crossoversinglepoint) genetic algorithm chooses a random integer, N, between 1 and "Number of variables" and then [12]:

- Selects vector entries numbered less than or equal to N from the first parent.
- Selects vector entries numbered greater than N from the second parent.
- Concatenates these entries to form a new child vector.

For example, if p_1 and p_2 are the parents, where:

$$p_1 = [a\ b\ c\ d\ e\ f\ g\ h]$$

$$p_2 = [1\ 2\ 3\ 4\ 5\ 6\ 7\ 8]$$

then if the crossover point is 2, the function returns the following child:

$$\text{child} = [a\ b\ 3\ 4\ 5\ 6\ 7\ 8]$$

In **Two point** crossover (@crossovertwopoint), the genetic algorithm selects two random integers M and N between 1 and "Number of variables". The function selects [12]:

- Vector entries numbered less than or equal to M from the first parent
- Vector entries numbered from M+1 to N from the second parent
- Vector entries numbered greater than N from the first parent.

The algorithm then concatenates these genes to form a new single gene. For example, if p_1 and p_2 are the parents,where:

$$p_1 = [a\ b\ c\ d\ e\ f\ g\ h]$$

$$p_2 = [1\ 2\ 3\ 4\ 5\ 6\ 7\ 8]$$

Then if the crossover points are M= 3 and N= 7, the function returns the following child:

$$\text{child} = [\text{a b c 4 5 6 7 h}]$$

MutationFcn is the option that handles the function that produces mutation children. Adaptive Feasible (@mutationadaptfeasible) is the default option and it is selected in this thesis. Adaptive Feasible randomly generates directions that are adaptive with respect to the last successful or unsuccessful generation. The feasible region is bounded by the constraints and inequality constraints. A step length is chosen along each direction so that linear constraints and bounds are satisfied.

Generations is a positive integer specifying the maximum number of iterations before the algorithm converges. By increasing the generations, the final result is often improved. The algorithm stops when the number of number of generations evolved reaches the maximum number of generations set, or when there is no improvement in the objective function for an interval of time.

As a general comment, because of the nature of genetic algorithm and its ability to search and solve a large variety of optimization problems, the above parameters are selected and initialized after tests

The genetic algorithm exports an array of angles and a strategy in the Active-NPC inverter model. The results of genetic algorithm are reconstructed in order to be inserted to the Simulink part of the optimization method and to start the simulation of the Active-NPC inverter operation, as described in the following.

3.2 Simulink Part of the optimization method

Simulink® is an environment for multidomain simulation that provides the opportunity to design, simulate, implement and test, with graphic user interfaces and customizable set of blocks, the Active-NPC inverter [11]. Its ability to interact with Matlab environment helps the realization of the proposed optimization method.

For our purpose, the Active-Neutral Point Clamped inverter is built using the electronic parts described next according to its structural elements. The parameters of the semiconductors were set according to the MITSUBISHI PM75DSA120 intelligent power module (IPM) datasheet and

Simulink model's characteristics. Also, ideal DC voltage sources are used, as well as ideal AC voltage sources (grid simulation), ground connections, bus selectors, integrators for continuous-time integrations, multipliers, gain blocks, voltmeters, ampere meters, an ideal RLC branch (filter), scopes, timers and "To Workspace" blocks that export results from Simulink to Matlab.

3.2.1 Diode Blocks

The diode is a semiconductor device that is controlled by its own voltage V_{ak} and current I_{ak}.

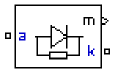

Figure 3-4 Diode block in Simulink.

The Diode block is simulated by a resistor, an inductor, and a DC voltage source connected in series with a switch. The switch operation is controlled by the voltage V_{ak} and the current I_{ak}. It also contains a series R_s-C_s snubber circuit that can be connected in parallel with the diode device (between nodes A and K). Finally, the diode block has an output ("m"), as shown in Fig.3-5, which is a vector output containing two signals, the diode measured current (A) and voltage (V).

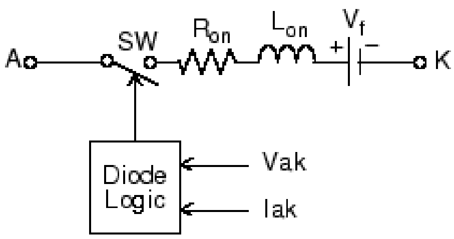

Figure 3-5 The model of diode block in Simulink.

When a diode is forward biased ($V_{ak} > 0$), it starts to conduct with a small forward voltage V_f across it. It turns off when the current flow into the device becomes 0. When the diode is reverse biased ($V_{ak} < 0$), it stays in the off state. Fig. 3-6 shows diode's functionality:

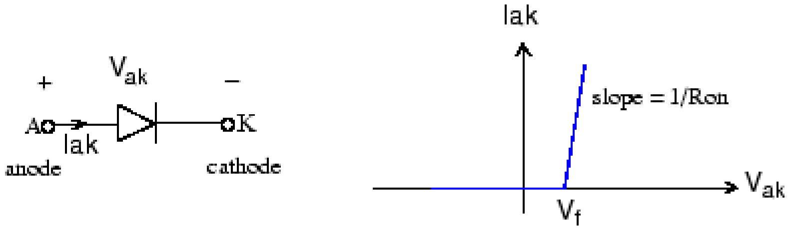

Figure 3-6 Diode block functionality.

The diode block parameters were set as follows:

- Resistance R_{on}: 0.044 Ohms
- Inductance L_{on}: 0 H
- Forward Voltage V_f: 0.5 V
- Initial Current I_c: 0 A
- Snubber Resistance R_s: inf
- Snubber Capacitance C_s: 0 F

3.2.2 Insulated Gate Bipolar Transistor (IGBT) Blocks

The IGBT block implements a semiconductor device controllable by the gate signal.

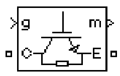

Figure 3-7 IGBT block in Simulink.

It is simulated as a series combination of a resistor R_{on}, inductor L_{on}, and a DC voltage source V_f in series with a switch controlled by a logical signal ($g > 0$ or $g = 0$).

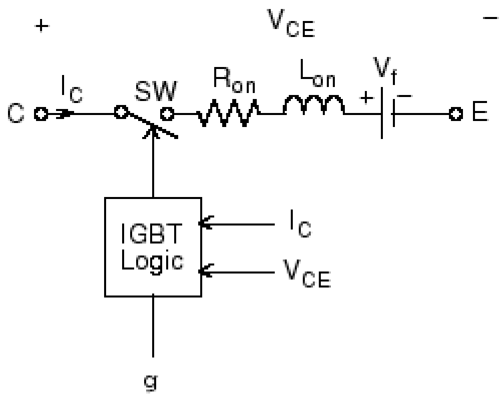

Figure 3-8 The model of IGBT in Simulink.

The IGBT turns on when the collector-emitter voltage is positive and greater than V_f and a positive signal is applied at the gate input (g > 0). It turns off when the collector-emitter voltage is positive and a zero signal is applied at the gate input (g = 0). The IGBT block contains a series R_s-C_s snubber circuit, which is connected in parallel with the IGBT device (between terminals C and E). The turn-off characteristic of the IGBT model is approximated by two segments. When the gate signal falls to 0, the collector current decreases from I_{max} to $0.1 \cdot I_{max}$ during the fall time (T_f), and then from 0.1·Imax to 0 during the tail time (T_t). Fig. 3-9 shows IGBT’s functionality:

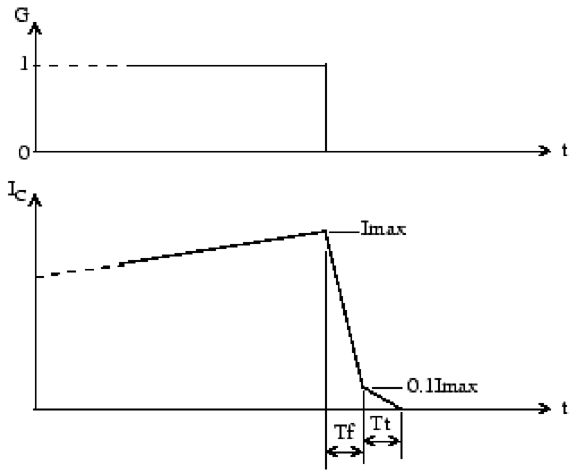

Figure 3-9 IGBT block functionality.

The IGBT parameters were set as follows:

- Resistance R_{on}: 0.076 Ohms
- Inductance L_{on}: 0 H
- Forward Voltage V_f: 0.75 V

- Current 10% fall time T_f : 0 s
- Current tail time T_t: 4.5e-6 s
- Initial Current I_c: 0 A
- Snubber Resistance R_s: inf
- Snubber Capacitance C_s: 0 F

The IGBT block has an “m” output, as shown in Fig.3-7, which is a vector containing two signals. This output is used to measure the IGBT current (A) and voltage (V).

3.2.3 DC Voltage Source Blocks

The DC Voltage Source block implements an ideal DC voltage source.

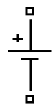

Figure 3-10 DC voltage source block in Simulink.

3.2.4 AC Voltage Source Block

The AC Voltage Source block implements an ideal AC voltage source.

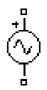

Figure 3-11 AC voltage source block in Simulink.

The generated voltage, *U*, is described by the following relationship:

$$U = A\sin(\omega t + \varphi)$$

where $\omega = 2\pi f$ and φ=phase in radians.

The following values were set to simulate the electric grid using the AC voltage source block in this thesis:

- Peak amplitude: $220\cdot\sqrt{2}$ V
- Phase: 0° and
- Frequency: 50 Hz.

3.2.5 RLC Branch Block (Filter)

The Parallel RLC Branch block implements a single resistor, inductor and capacitor or a parallel combination of them (Fig.3-12).

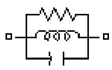

Figure 3-12 RLC branch block in Simulink.

Only existing elements are displayed in the block icon. In Active-NPC inverter model developed in this thesis, the parameters were used to simulate the output filter inductor using this block set as follows:

- Branch type: L
- Inductance: H

The value of filter inductance is an input parameter of the algorithm, provided by the designer.

3.2.6 Power Computation Subsystem

The Power Computation Subsystem has been created to compute the power losses for every semi-conductor of the Active-NPC inverter:

Figure 3-13 Power computation subsystem.

In order to compute the power losses for every semiconductor, this subsystem (Fig.3-15) takes as inputs the voltage and current measured. Then, the subsystem computes the average power losses of the i^{th} semiconductor according to the following operation:

$$P_{avg_i} = \frac{1}{T}\int_{t}^{t+T} I_i V_i dt \qquad (3.23)$$

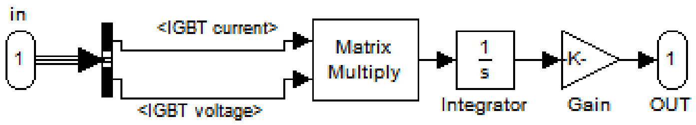

Figure 3-14 Power computation subsystem functionality.

The semiconductors currents and voltages have been measured from the "m" outputs of their Simulink blocks and are vectors, each of them containing two signals. These vectors are demultiplexed using Bus Selector blocks provided in the Simulink library. The Matrix multiply block multiplies $V_{semicon}$ and $I_{semicon}$, the Integrator block integrates the product over a period (T) and the Gain block multiplies the result with $\frac{1}{T}$. The result is imported to the "To Workspace" block that export results from Simulink to Matlab arrays.

3.2.7 Timer Blocks

The Timer block (Fig.3-15) is a very important block for this model, because it drives the IGBTs, according to the strategies that are loaded from the Matlab part of the optimization algorithm. In general, it generates a logical signal (0 or 1 logical levels) changing at times specified by the angles computed by the genetic algorithm.

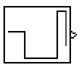

Figure 3-15 Timer block of Simulink.

The parameters of this block are the following:

- Times: the transition times, in seconds, where the output of the block changes its value as defined by the "Amplitude parameter". The Time parameter must be a vector of the same length as the vector defined in the "Amplitude" parameter.

- Amplitude: the vector of amplitudes of the signal to be generated by the Timer block. The amplitude is kept constant between the transition times defined in the Time vector.

It has to be noticed that all power electronic elements parameters have been configured through the Matlab part of the optimization algorithm and in every loop, for optimization reasons, only the Timers blocks are updated to drive the IGBTS.

3.2.8 Total Harmonic Distortion Subsystem

The Total Harmonic Distortion subsystem is used to check and ensure that Active-NPC inverter output current waveform obeys to the IEEE standard for interconnecting distributed power sources with Electric Power Systems. The subsystem presented in Fig.3-16 receives as input the inverter current and has a Boolean output, which is inserted to Matlab workspace, in order to check IEEE constraints. The subsystem contains Fourier blocks, math blocks, comparators and AND logical Operators. The inserted signal is analyzed, according to TDD equation (3.17) and checked with Fourier and math blocks according to IEEE rules (Table 3-1). The output is a logical result after checking every set of harmonics.

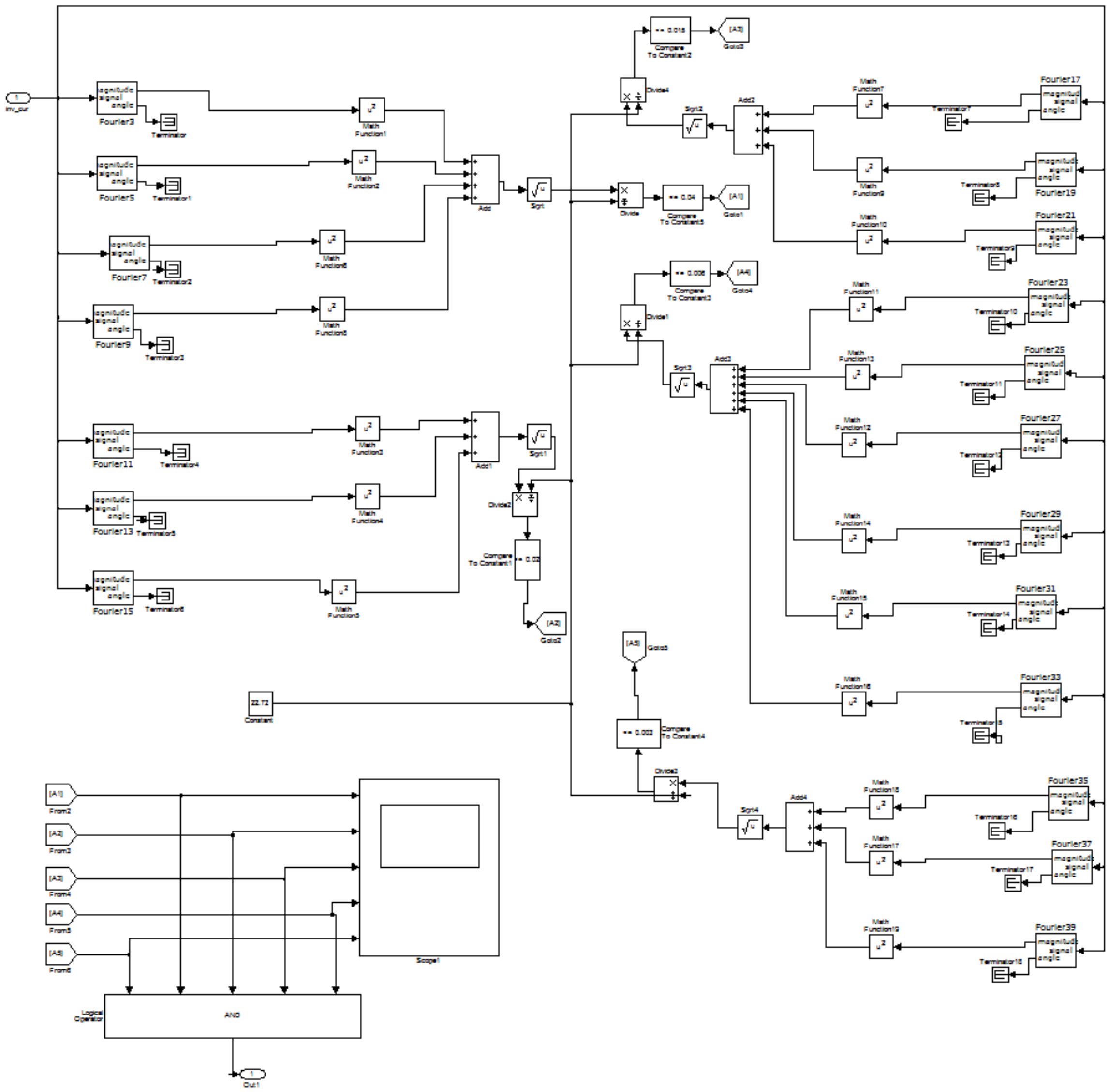

Figure 3-16 Subsystem for checking compliance with the IEEE standard for interconnecting distributed power sources with electric power systems.

3.3 Active Neutral- Point Clamped Inverter block

The Active-NPC topology has been modeled in Simulink in order to be simulated with the above power electronic elements. It has to be noticed that the simulation runs for a specific simulation time according to the period of the inverter output waveform. During simulations, it was observed that the semiconductor devices need some periods to operate in steady-state, thus more than one period needed to be examined. This attitude created some problems in our computations referring to overall time performance.

The Simulink model of the Active-NPC inverter is shown in Fig.3-17.

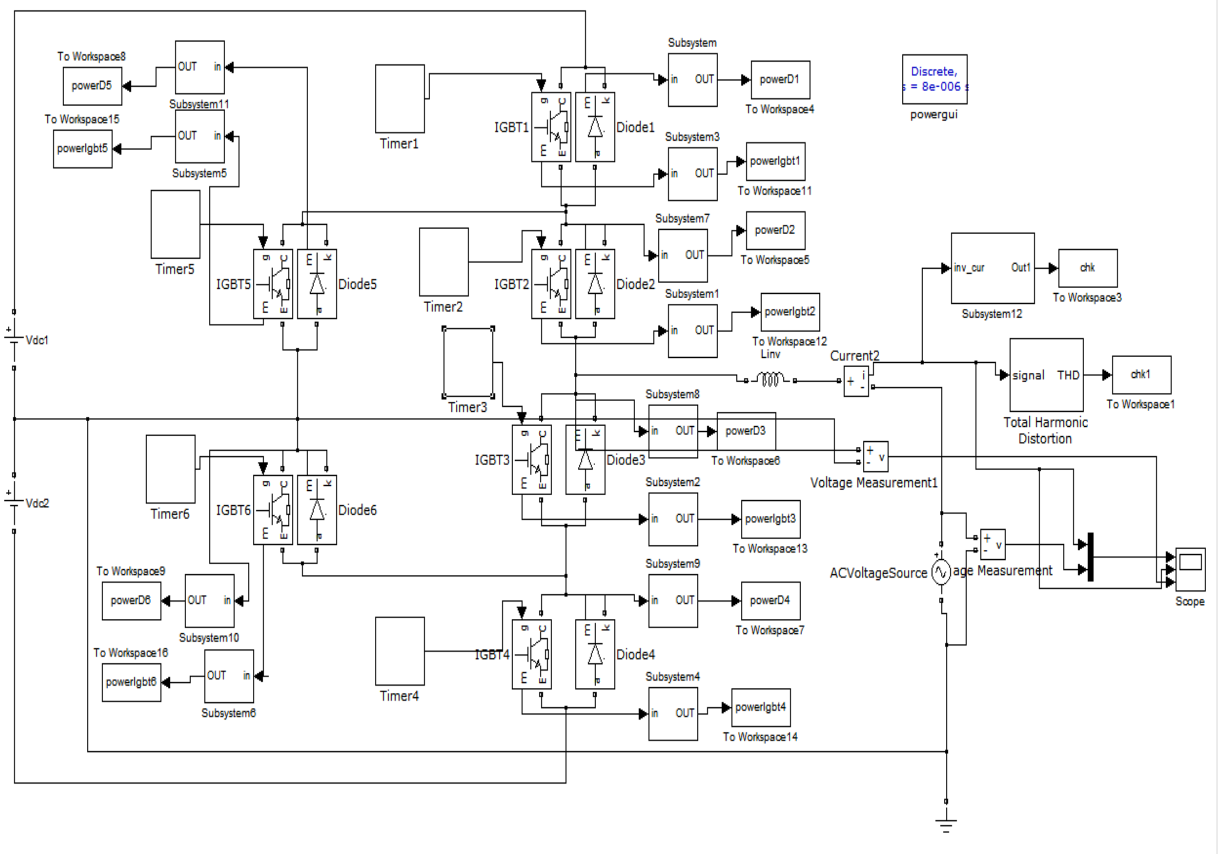

Figure 3-17 The Active-NPC inverter model in Simulink.

4. Optimization Results and Comparison with Past-Proposed Strategies for Active-NPC inverters

4. Introduction

In this chapter, the optimization results, after executing genetic algorithms, are presented. There are results depending on the switching frequency, referring to the number of firing angles per quarter period and the filter L. Additionally, the TDD factor is computed and checked, taking under consideration Simulink's FFT Analysis option of the power graphic user interface (powergui). The time that was required to compute the best solution for every case, is variable, depending on the switching frequency (number of optimized angles) and the filter inductance value. Moreover, using the grid computer of Technical University of Crete, parallel multi-processing has been achieved, which reduced the overall time of every experiment and gave the opportunity to run the genetic algorithm for more generations. For a switching frequency of 3000Hz and the grid computer using 50-60 workers, required 8 hours to perform the optimization process for 600 generations. For a switching frequency of 5000Hz, which is 50 firing angles per quarter period, the grid computer was running for 10 hours, for a filter of 8mH. For a switching frequency of 8000Hz and a filter of 8mH, the system needed at least 12 hours, using more than 50 workers, to compute the best result and at least 30 hours without parallel multi-processing. For a switching frequency of 10 kHz, the system needed at least 15 hours to terminate. Finally, for a 10 kHz switching frequency, about three days were needed to find the best result without parallel multi-processing. The number of generations in genetic algorithm is an important factor so as the filter, because the larger filter is used, the more periods are required by the simulation system to run, until the Active-NPC inverter circuit reaches steady-state. It has to be noted that exhaustive searches were developed and they demonstrated that the optimization method results of the genetic algorithms are optimal.

4.1 Past-proposed PWM strategies for the Active-NPC inverter

In the following paragraphs, the results of the past-proposed PWM strategies will be presented in order to demonstrate the Active-NPC behavior, using Matlab and Simulink environments, with these strategies with an inductance L=8 mH as output filter.

4.1.1 PWM 1

Figs. 4-1 to 4-3 present the power loss distribution for f_s=3000 Hz, M=0.8 and PF=1, the Active-NPC inverter current injected to the electric grid, the PWM output voltage and the spectrum of the Active-NPC inverter output current.

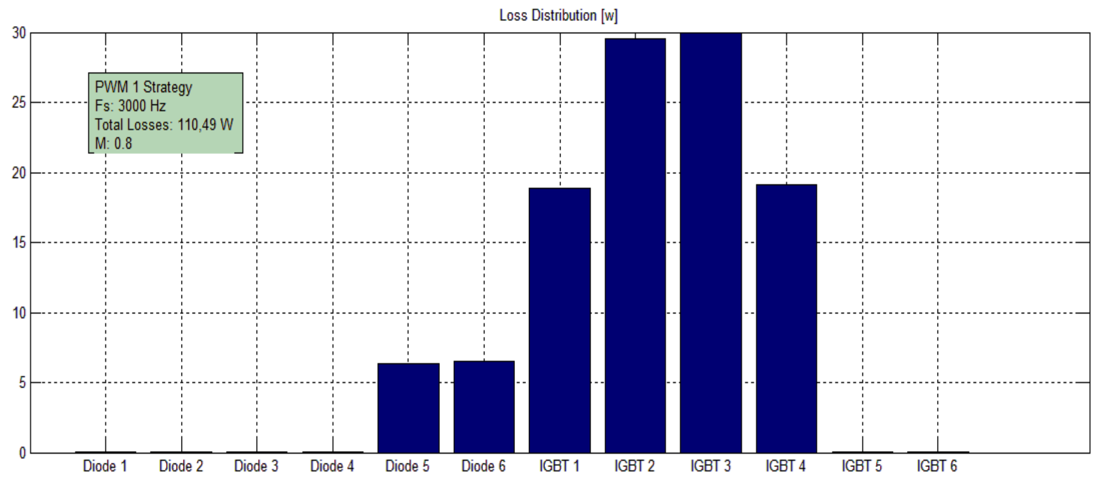

Figure 4-1 Power loss distribution for fs=3000 Hz, L=8mH, M=0.8, PF=1.

(a)

(b)

(c)

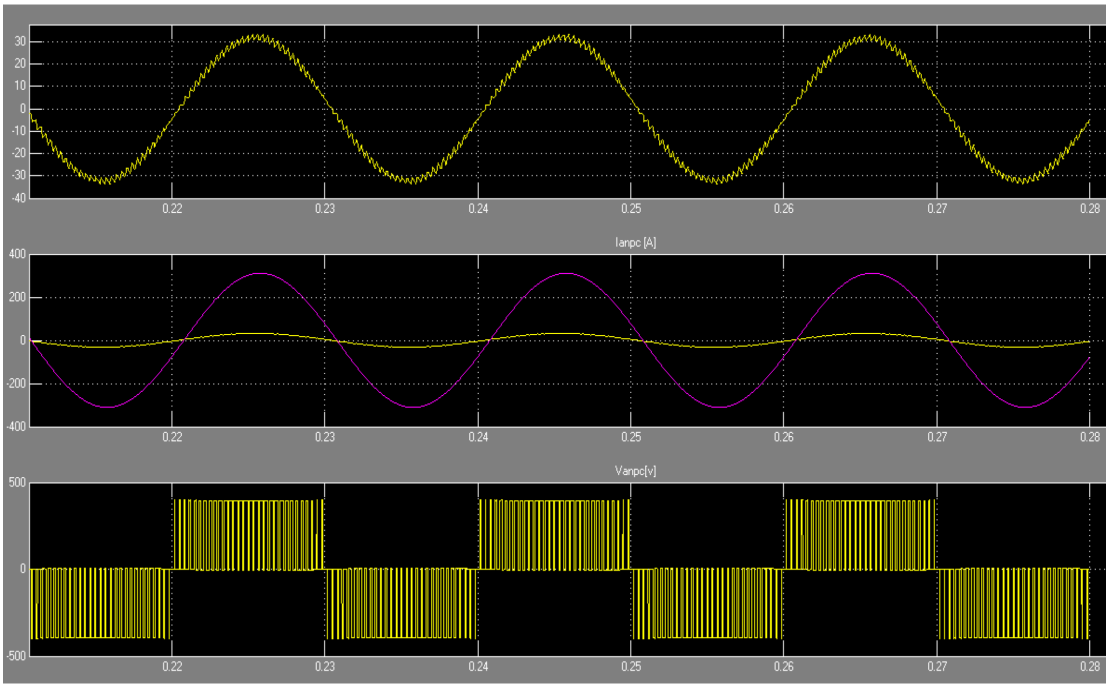

Figure 4-2(a) Inverter current injected into the electric grid (A), (b) Active-NPC inverter output current and grid voltage,(c) Active-NPC inverter PWM output voltage (V).

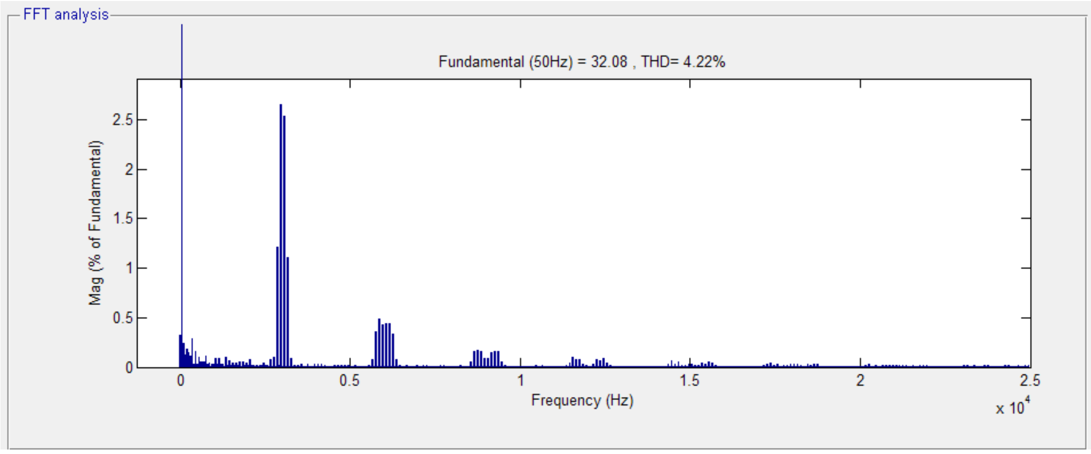

Figure 4-3 The spectrum of the Active-NPC inverter output current for fs=3000 Hz, L=8mH, M=0.8, PF=1.

Figs. 4-4 to 4-6 present the power loss distribution for f_s=5000 Hz, M=0.8 and PF=1, the Active-NPC inverter current injected to the electric grid, the PWM output voltage and the spectrum of the Active-NPC inverter output current.

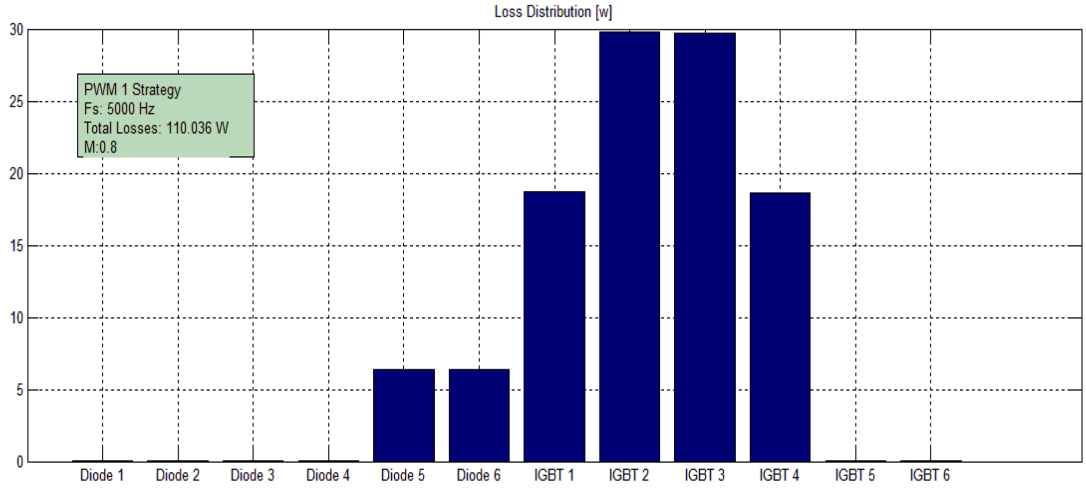

Figure 4-4 Power loss distribution for f_s=5000 Hz, L=8mH, M=0.8, PF=1.

(a)

(b)

(c)

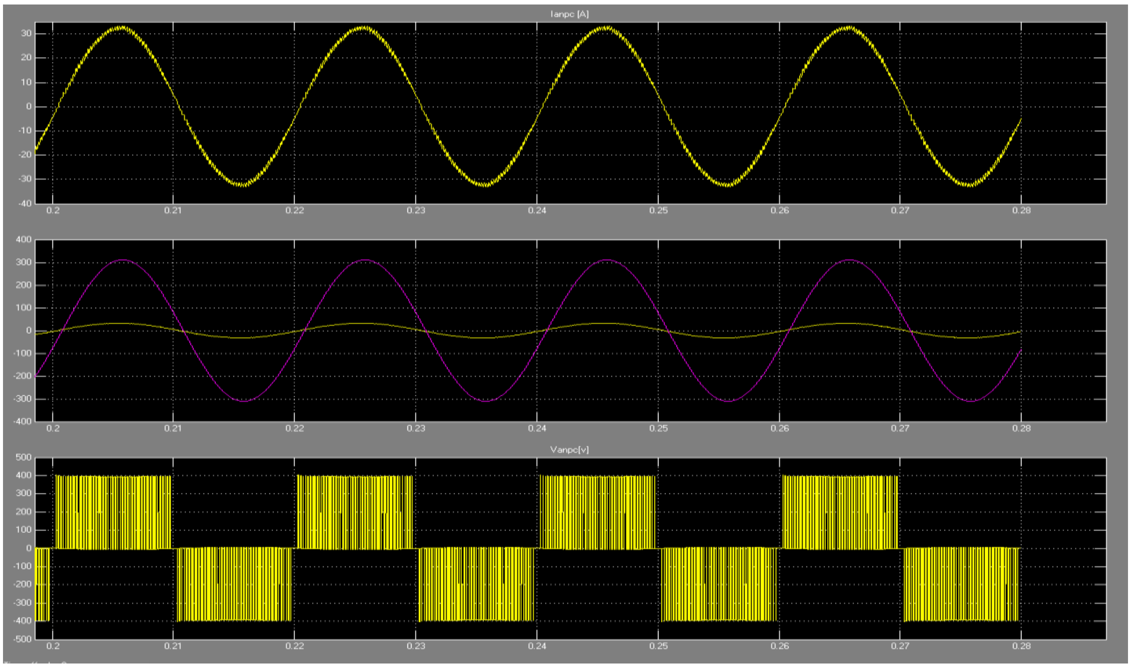

Figure 4-5(a) Inverter current injected into the electric grid (A), (b) Active-NPC inverter output current and grid voltage,(c) Active-NPC inverter PWM output voltage (V).

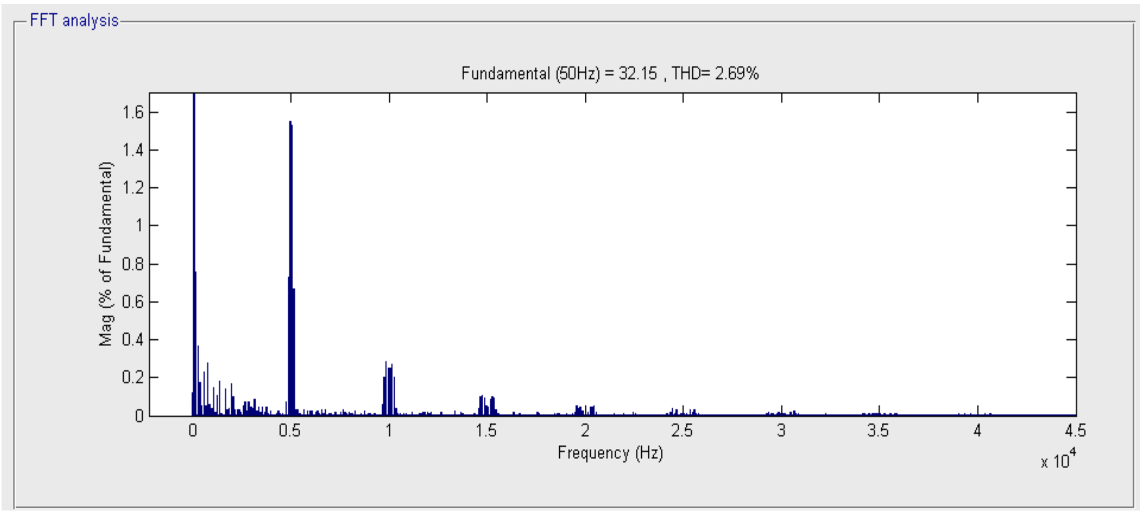

Figure 4-6 The spectrum of the Active-NPC inverter output current for f_s=5000 Hz, L=8mH, M=0.8, PF=1.

Figs. 4-7 to 4-9 present the power loss distribution for f_s=8000 Hz, M=0.8 and PF=1, the Active-NPC inverter current injected to the electric grid, the PWM output voltage and the spectrum of the Active-NPC inverter output current.

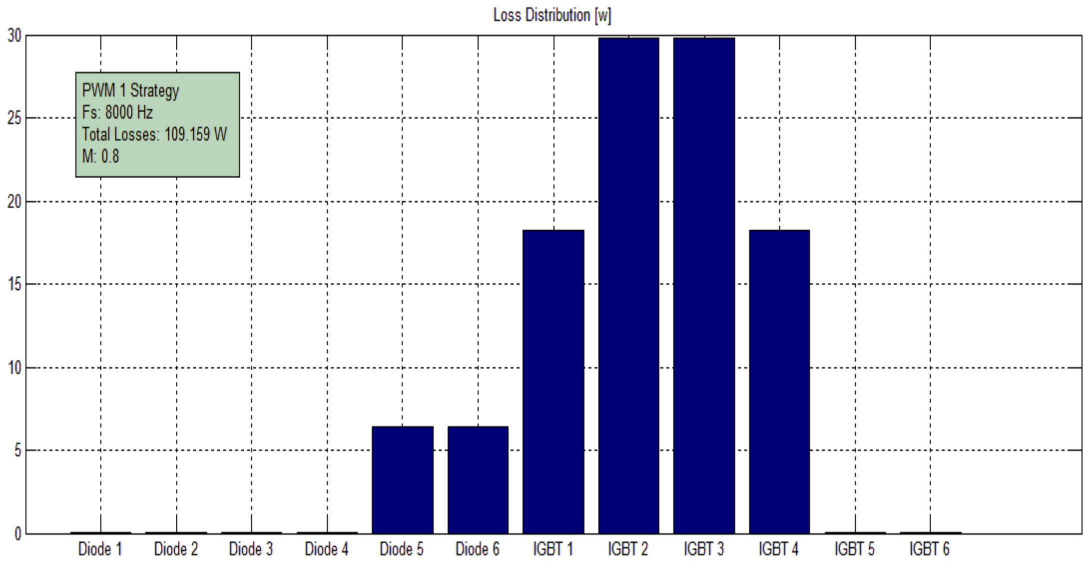

Figure 4-7 Power loss distribution for f_s=8000 Hz, L=8mH, M=0.8, PF=1.

(a)

(b)

(c)

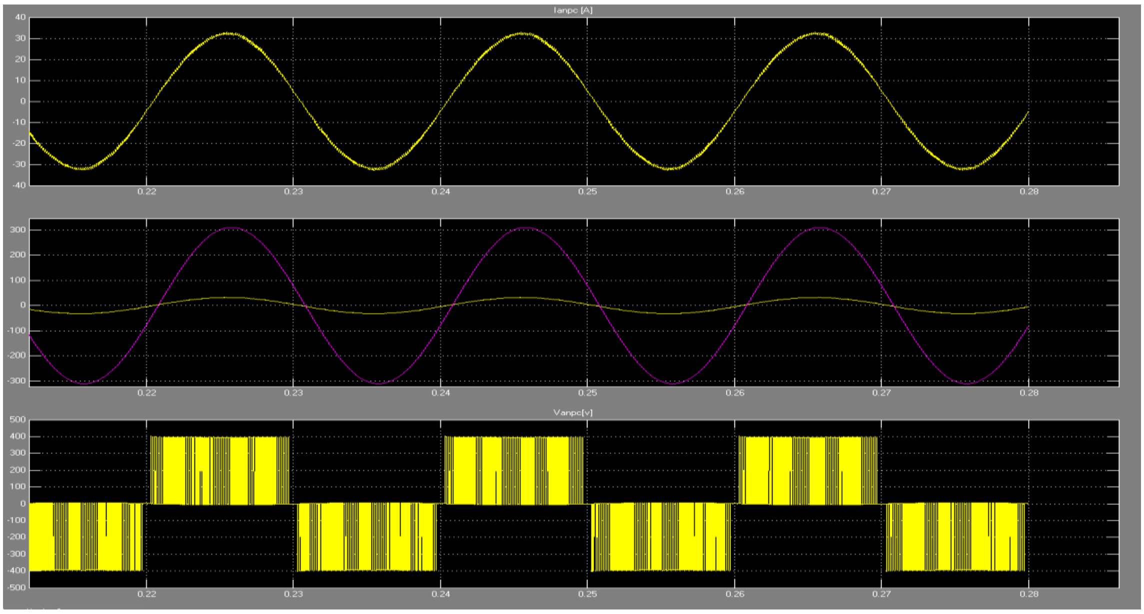

Figure 4-8(a) Inverter current injected into the electric grid (A), (b) Active-NPC inverter output current and grid voltage,(c) Active-NPC inverter PWM output voltage (V).

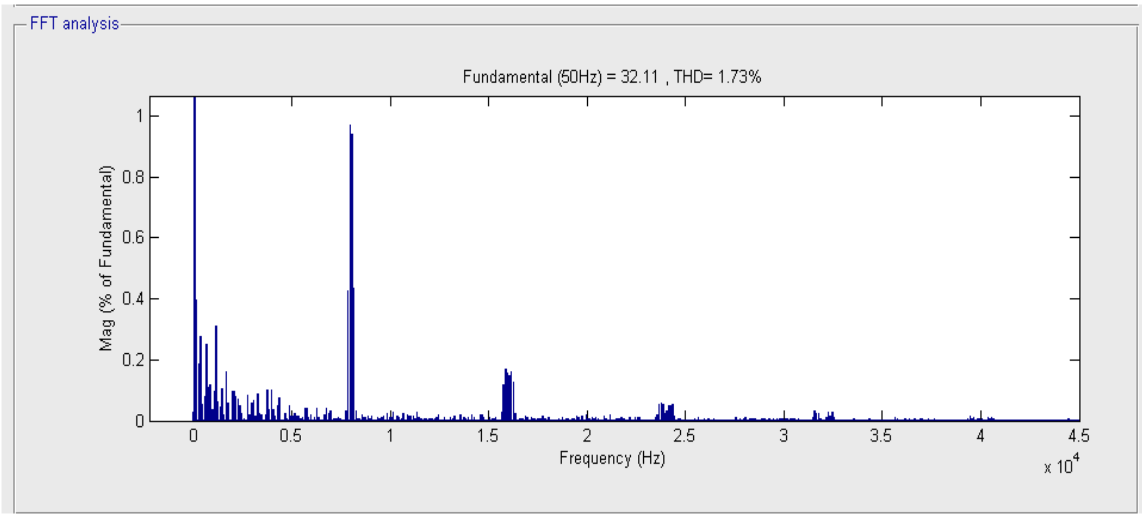

Figure 4-9 The spectrum of the Active-NPC inverter output current for f_s=8000 Hz, L=8mH, M=0.8, PF=1.

Figs. 4-10 to 4-12 present the power loss distribution for f_s=10000 Hz, M=0.8 and PF=1, the Active-NPC inverter current injected to the electric grid, the PWM output voltage and the spectrum of the Active-NPC inverter output current.

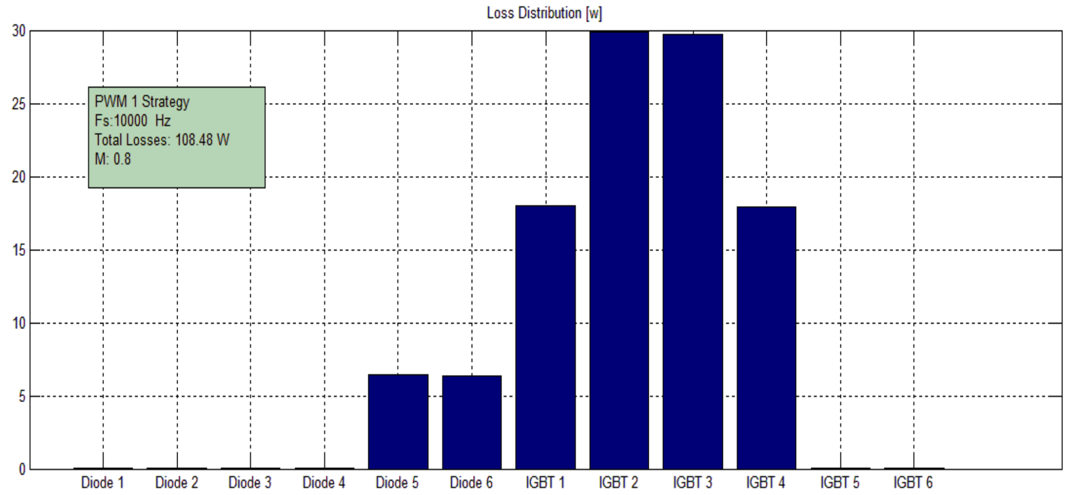

Figure 4-10 Power loss distribution for f_s=10000 Hz, L=8mH, M=0.8, PF=1.

(a)

(b)

(c)

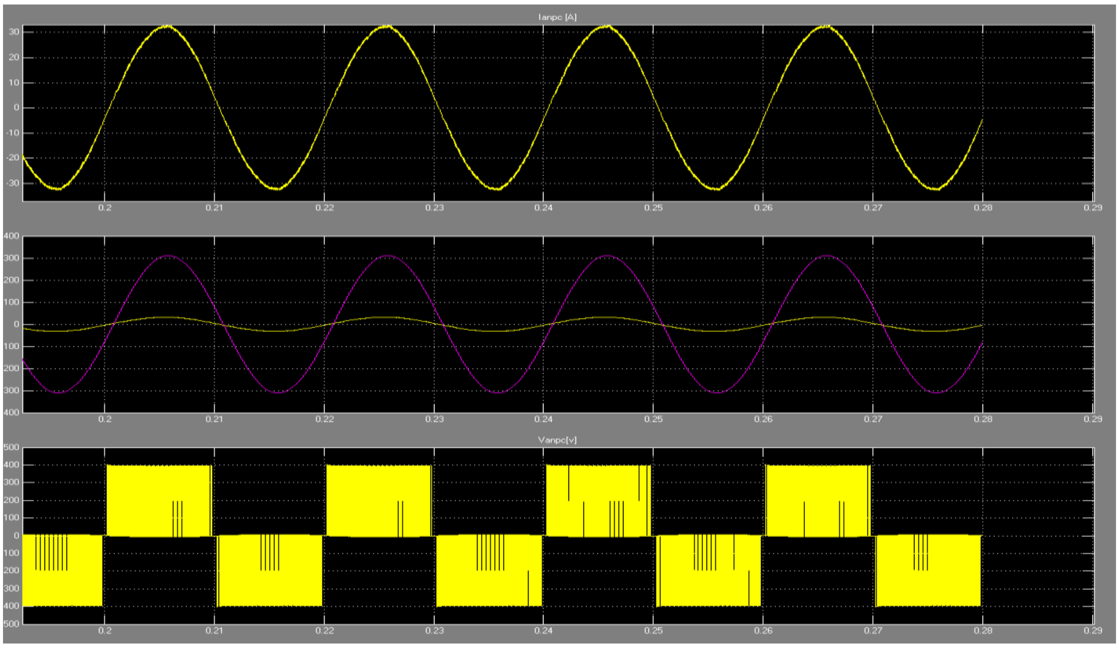

Figure 4-11(a) Inverter current injected into the electric grid (A), (b) Active-NPC inverter output current and grid voltage,(c) Active-NPC inverter PWM output voltage (V).

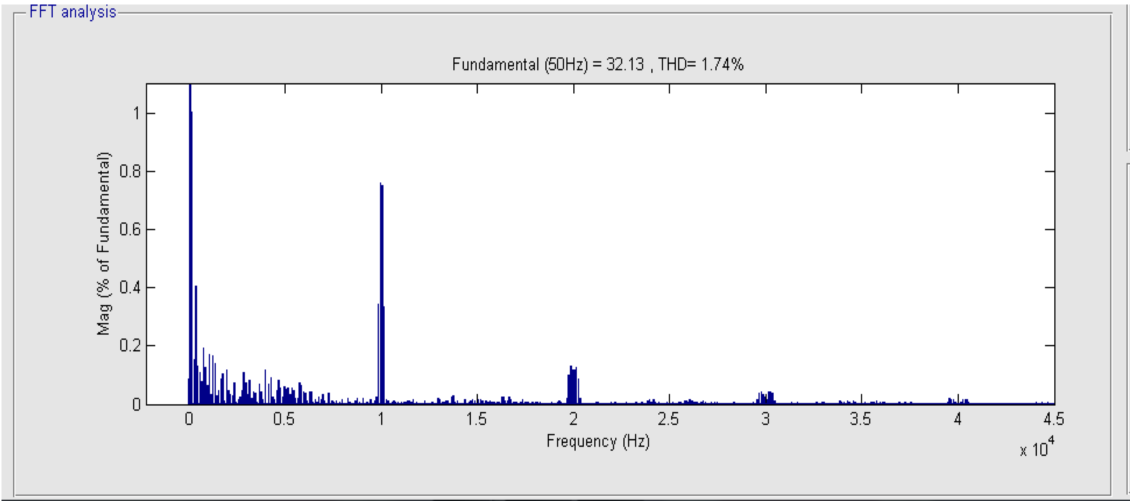

Figure 4-12 The spectrum of the Active-NPC inverter output current for f_s=10000 Hz, L=8mH, M=0.8, PF=1.

4.1.2 PWM 2

Figs. 4-13 to 4-15 present the power loss distribution for f_s=3000 Hz, M=0.8 and PF=1, the Active-NPC inverter current injected to the electric grid, the PWM output voltage and the spectrum of the Active-NPC inverter output current.

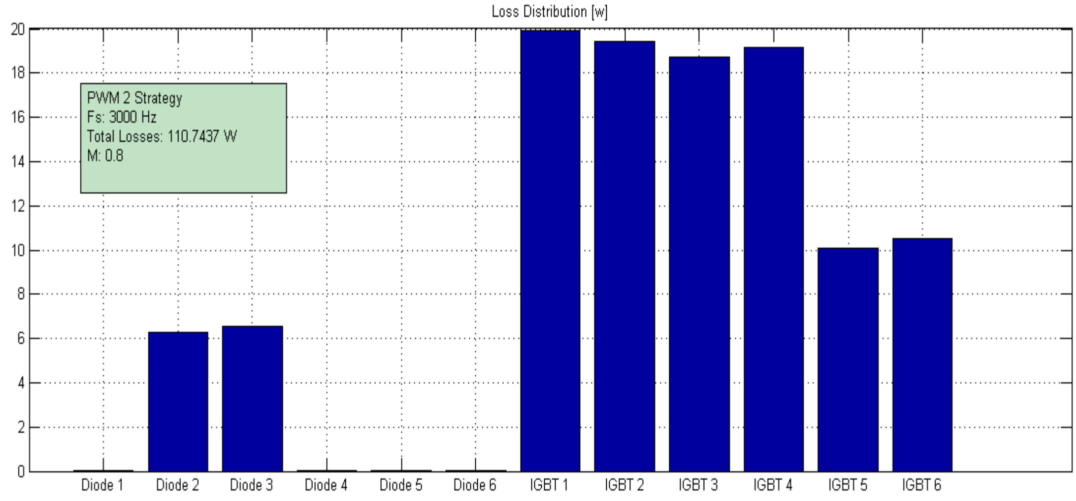

Figure 4-13 Power loss distribution for f_s=3000 Hz, L=8mH, M=0.8, PF=1.

(a)

(b)

(c)

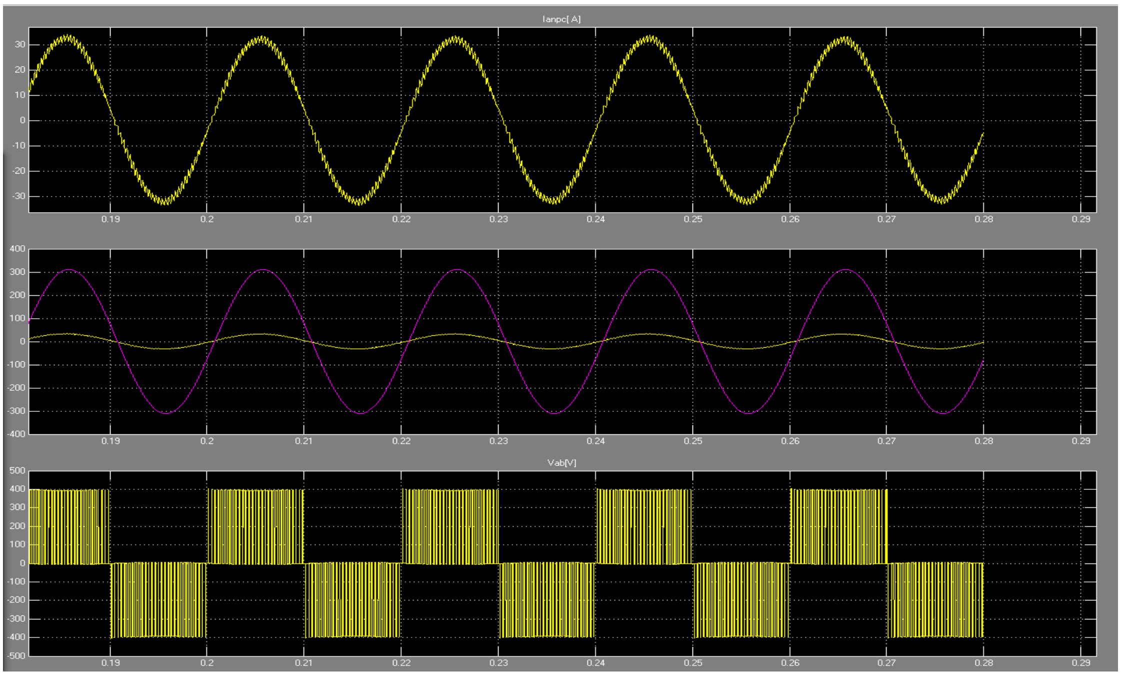

Figure 4-14(a) Inverter current injected into the electric grid (A), (b) Active-NPC inverter output current and grid voltage,(c) Active-NPC inverter PWM output voltage (V).

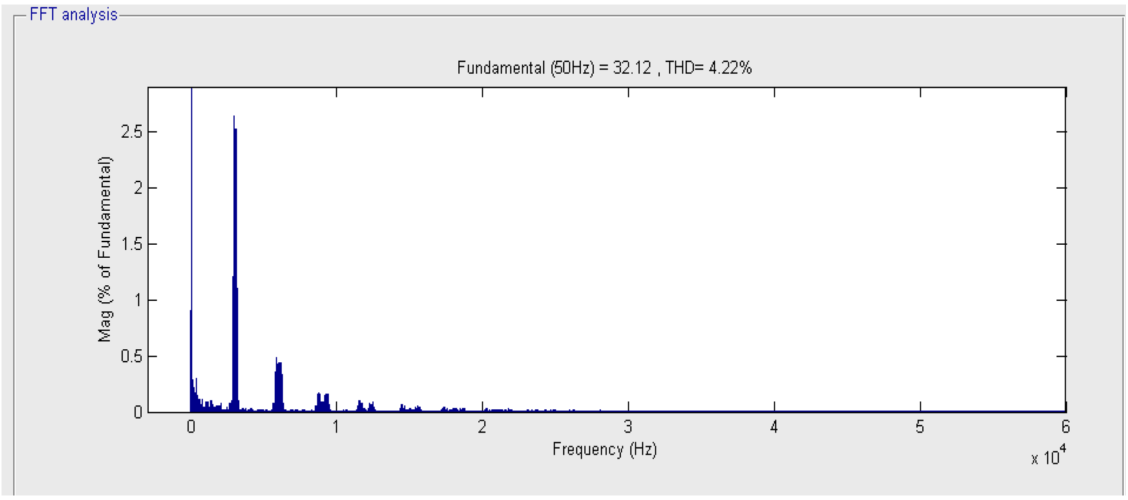

Figure 4-15 The spectrum of the Active-NPC inverter output current f_s=3000 Hz, L=8mH, M=0.8, PF=1.

Figs. 4-16 to 4-18 present the power loss distribution for f_s=5000 Hz, M=0.8 and PF=1, the Active-NPC inverter current injected to the electric grid, the PWM output voltage and the spectrum of the Active-NPC inverter output current.

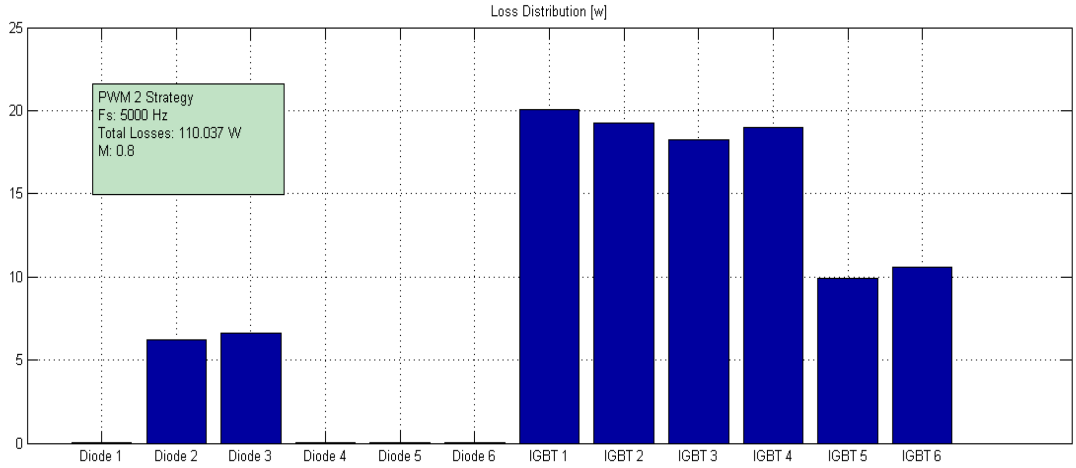

Figure 4-16 Power loss distribution for f_s=5000 Hz, L=8mH, M=0.8, PF=1.

(a)

(b)

(c)

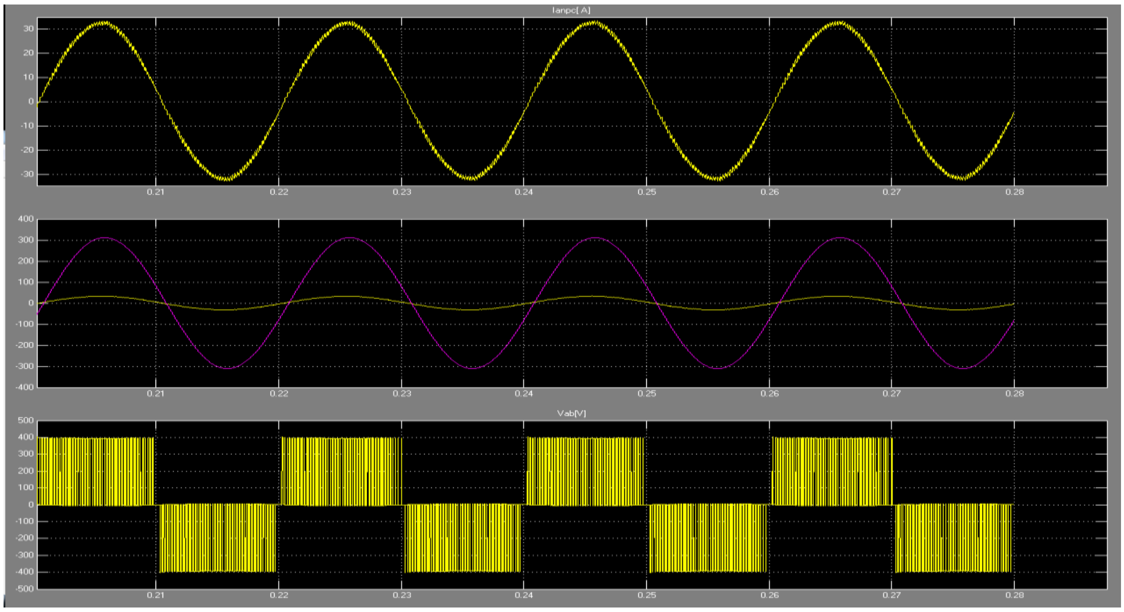

Figure 4-17(a) Inverter current injected into the electric grid (A), (b) Active-NPC inverter output current and grid voltage,(c) Active-NPC inverter PWM output voltage (V).

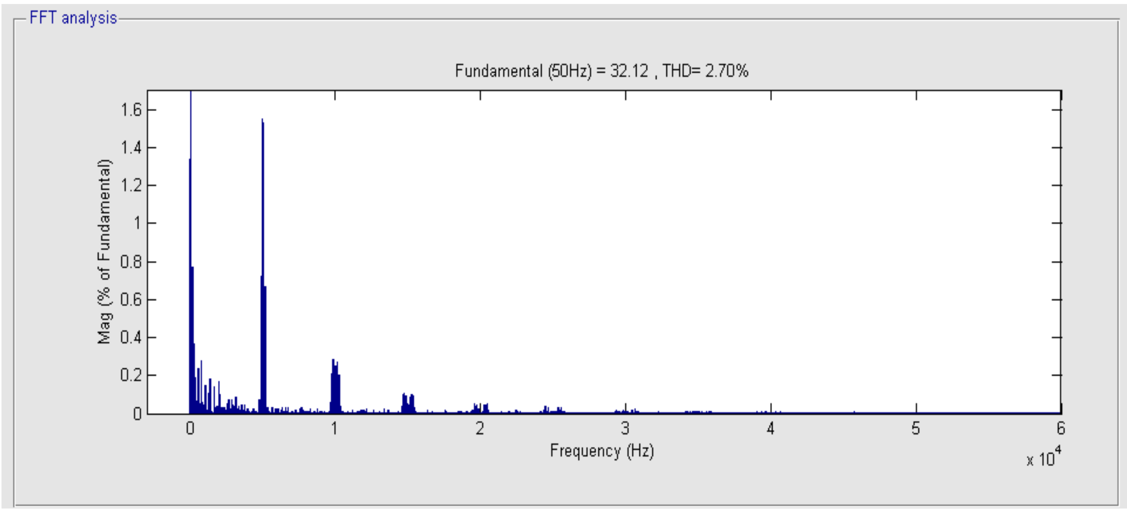

Figure 4-18 The spectrum of the Active-NPC inverter output current for f_s=5000 Hz, L=8mH, M=0.8, PF=1.

Figs. 4-19 to 4-21 present the power loss distribution for f_s=8000 Hz, M=0.8 and PF=1, the Active-NPC inverter current injected to the electric grid, the PWM output voltage and the spectrum of the Active-NPC inverter output current.

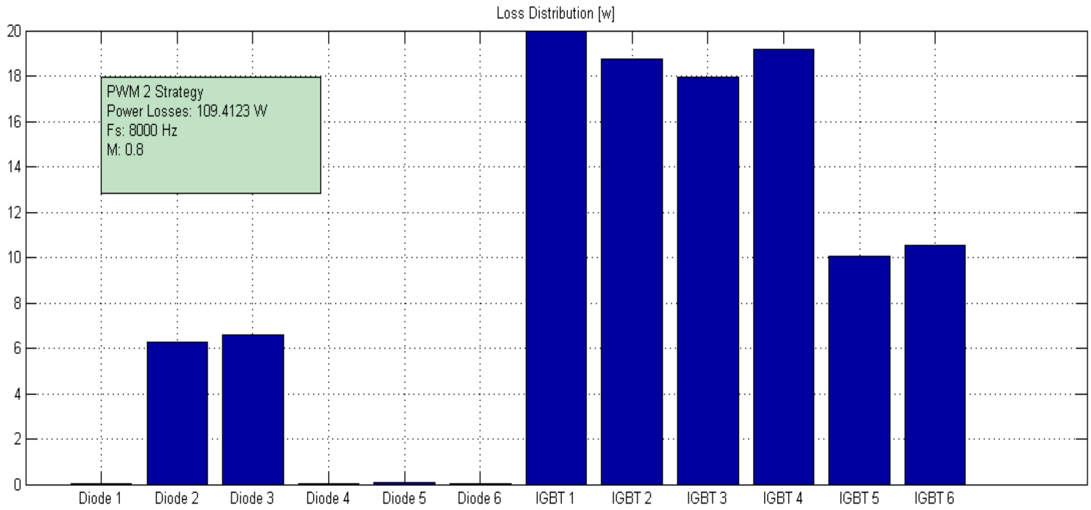

Figure 4-19 Power loss distribution for f_s=8000 Hz, L=8mH, M=0.8, PF=1.

(a)

(b)

(c)

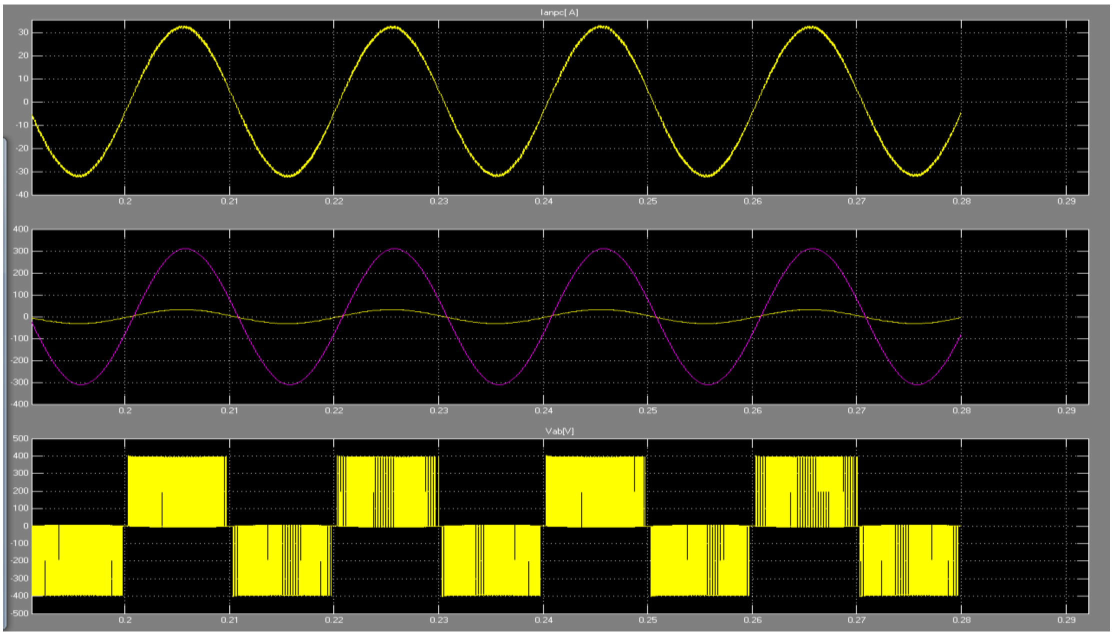

Figure 4-20(a) Inverter current injected into the electric grid (A), (b) Active-NPC inverter output current and grid voltage,(c) Active-NPC inverter PWM output voltage (V).

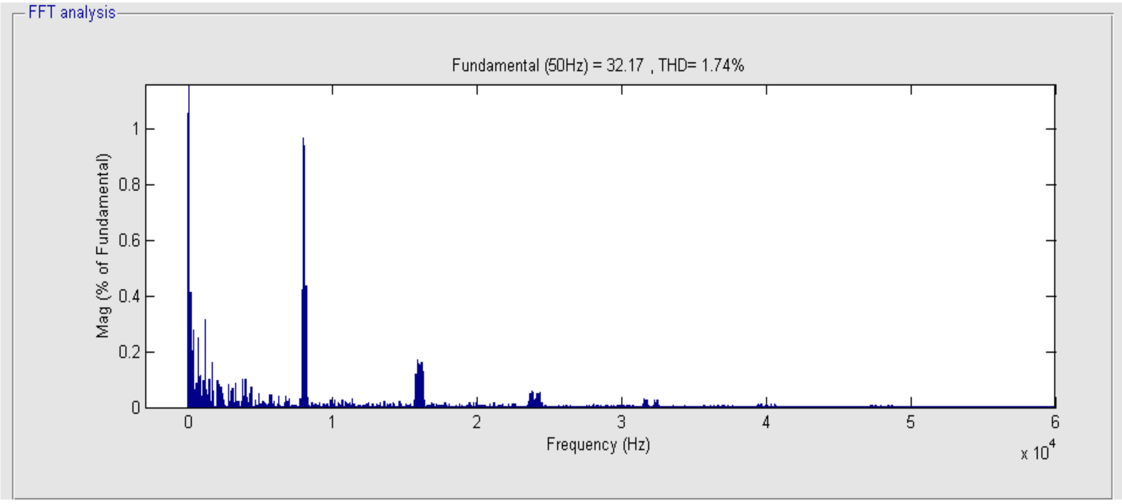

Figure 4-21 The spectrum of the Active-NPC inverter output current f_s=8000 Hz, L=8mH, M=0.8, PF=1.

Figs. 4-22 to 4-24 present the power loss distribution for f_s=10000 Hz, M=0.8 and PF=1, the Active-NPC inverter current injected to the electric grid, the PWM output voltage and the spectrum of the Active-NPC inverter output current.

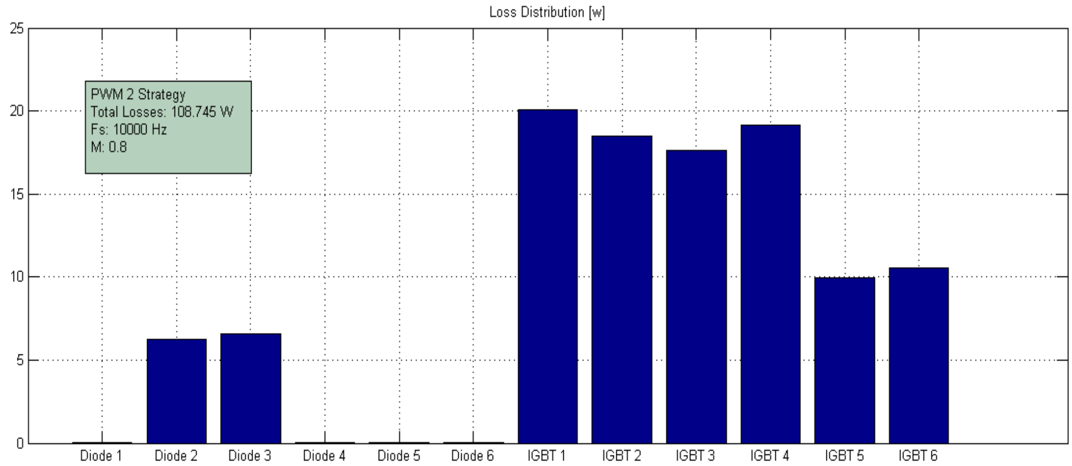

Figure 4-22 Power loss distribution for f_s=10000 Hz, L=8mH, M=0.8, PF=1.

(a)

(b)

(c)

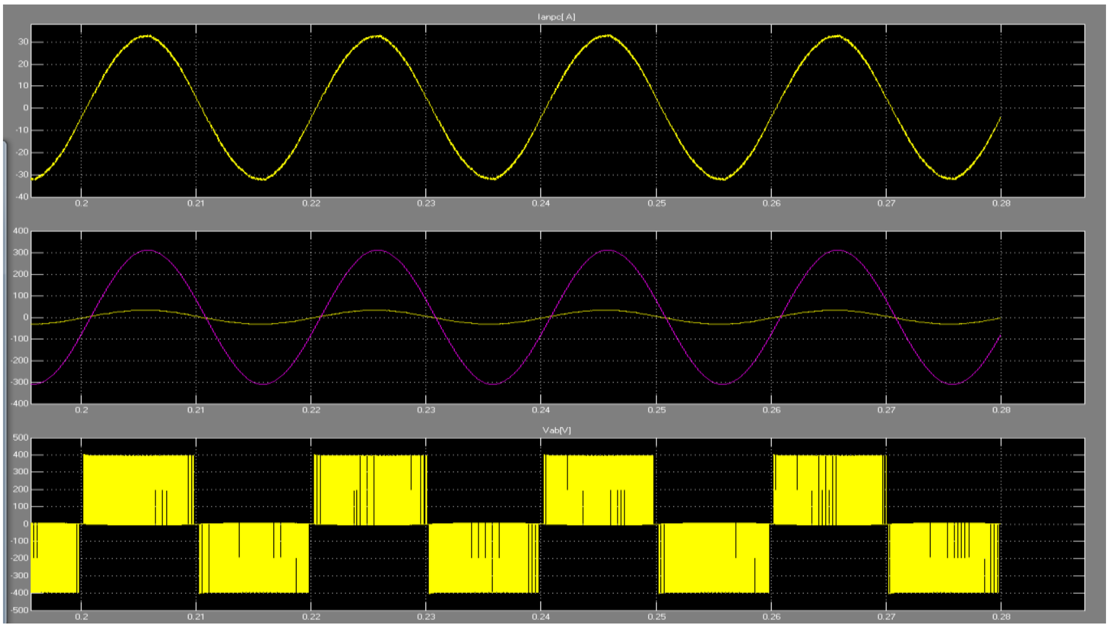

Figure 4-23(a) Inverter current injected into the electric grid (A), (b) Active-NPC inverter output current and grid voltage,(c) Active-NPC inverter PWM output voltage (V).

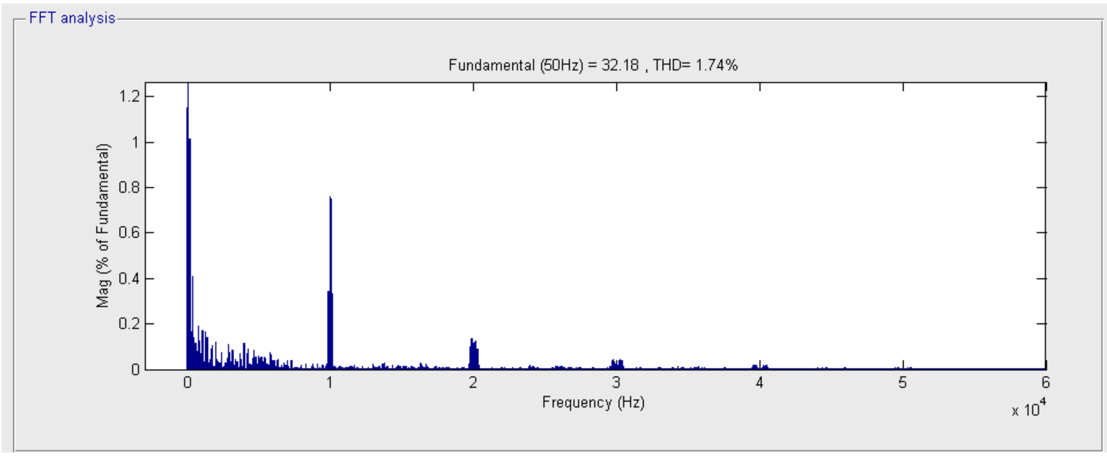

Figure 4-24 The spectrum of the Active-NPC inverter output current f_s=10000 Hz, L=8mH, M=0.8, PF=1.

4.1.3 PWM 3 (Double Frequency Active-NPC strategy)

Figs. 4-25 to 4-27 present the power loss distribution for f_s=3000 Hz, M=0.8 and PF=1, the Active-NPC inverter current injected to the electric grid, the PWM output voltage and the spectrum of the Active-NPC inverter output current.

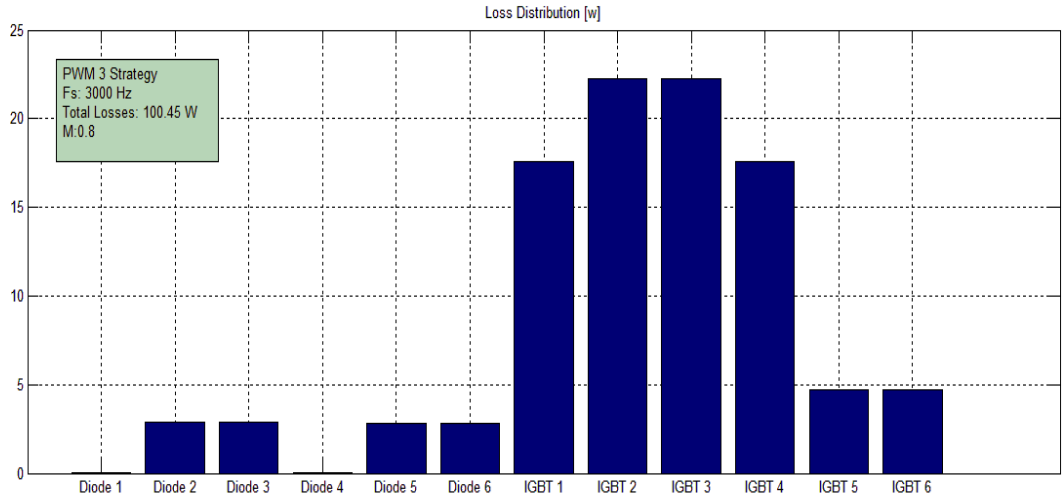

Figure 4-25 Power loss distribution for f_s=3000 Hz, L=8mH, M=0.8, PF=1.

(a)

(b)

(c)

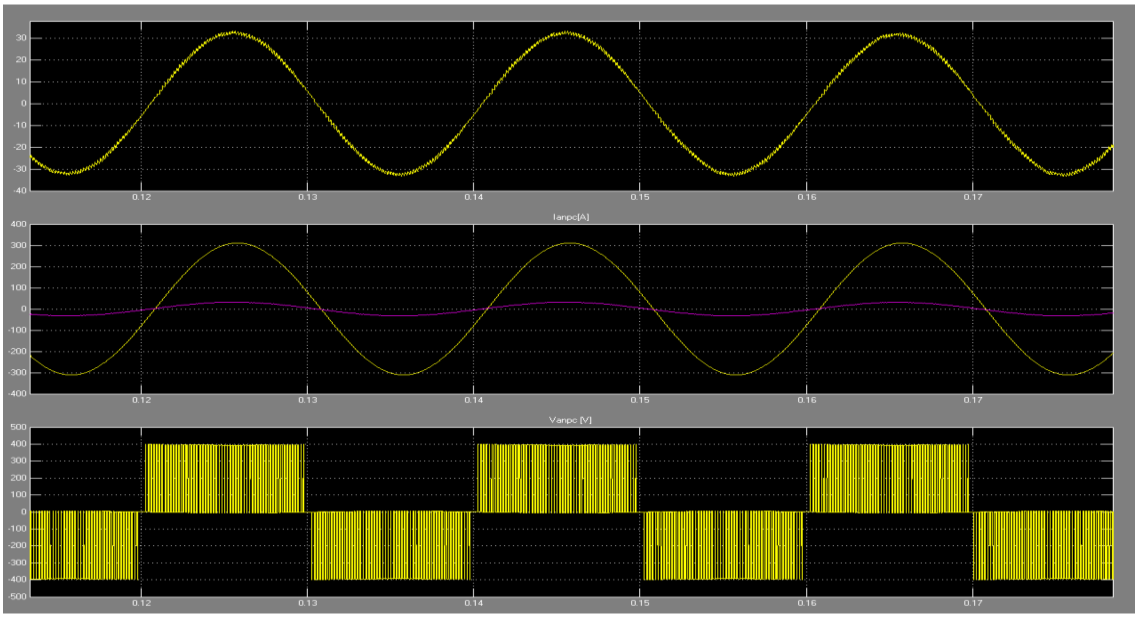

Figure 4-26(a) Inverter current injected into the electric grid (A), (b) Active-NPC inverter output current and grid voltage,(c) Active-NPC inverter PWM output voltage (V).

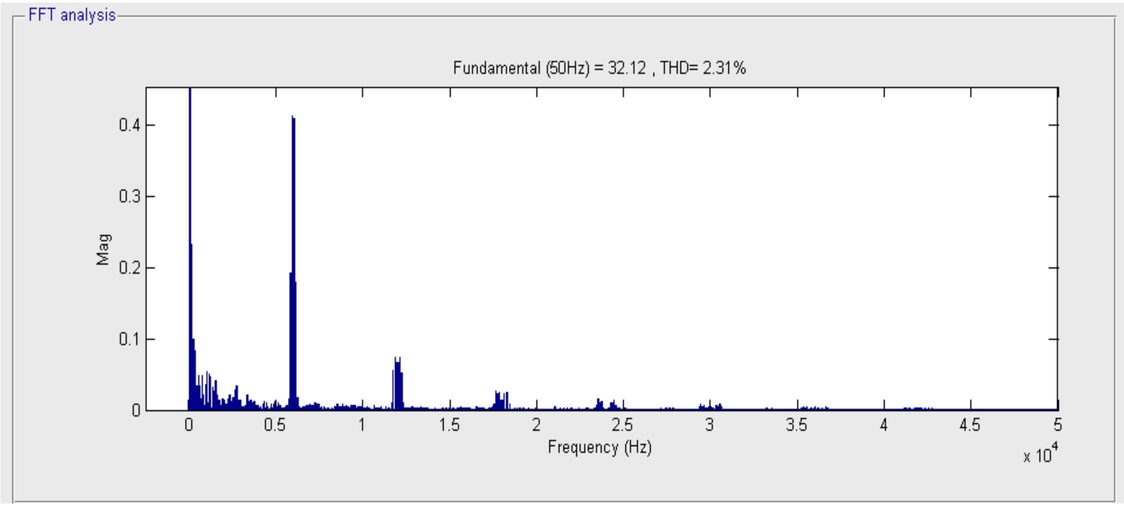

Figure 4-27 The spectrum of the Active-NPC inverter output current for f_s=3000 Hz, L=8mH, M=0.8, PF=1.

Figs. 4-28 to 4-30 present the power loss distribution for f_s=5000 Hz, M=0.8 and PF=1, the Active-NPC inverter current injected to the electric grid, the PWM output voltage and the spectrum of the Active-NPC inverter output current.

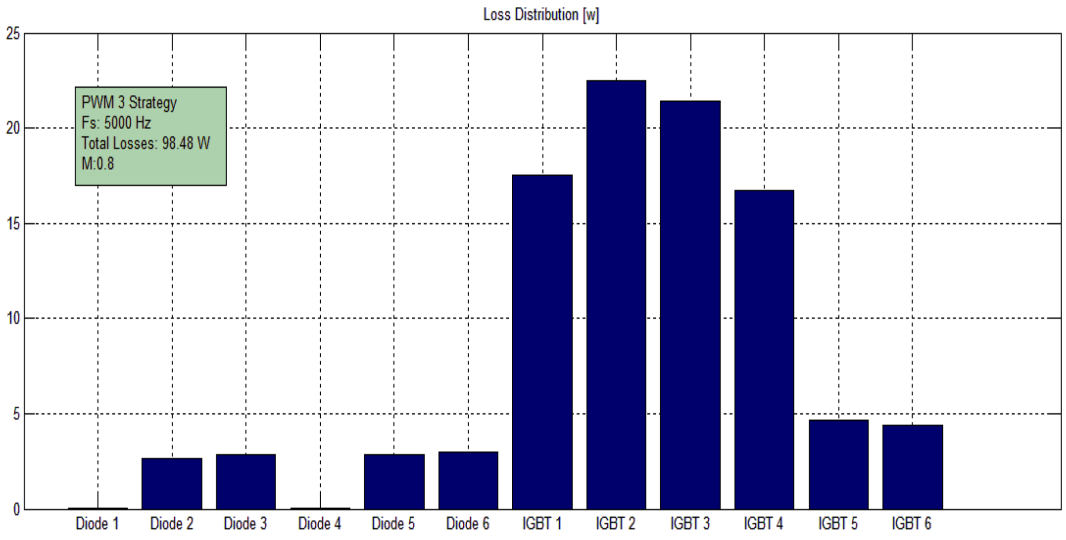

Figure 4-28 Power loss distribution for f_s=5000 Hz, L=8mH, M=0.8, PF=1.

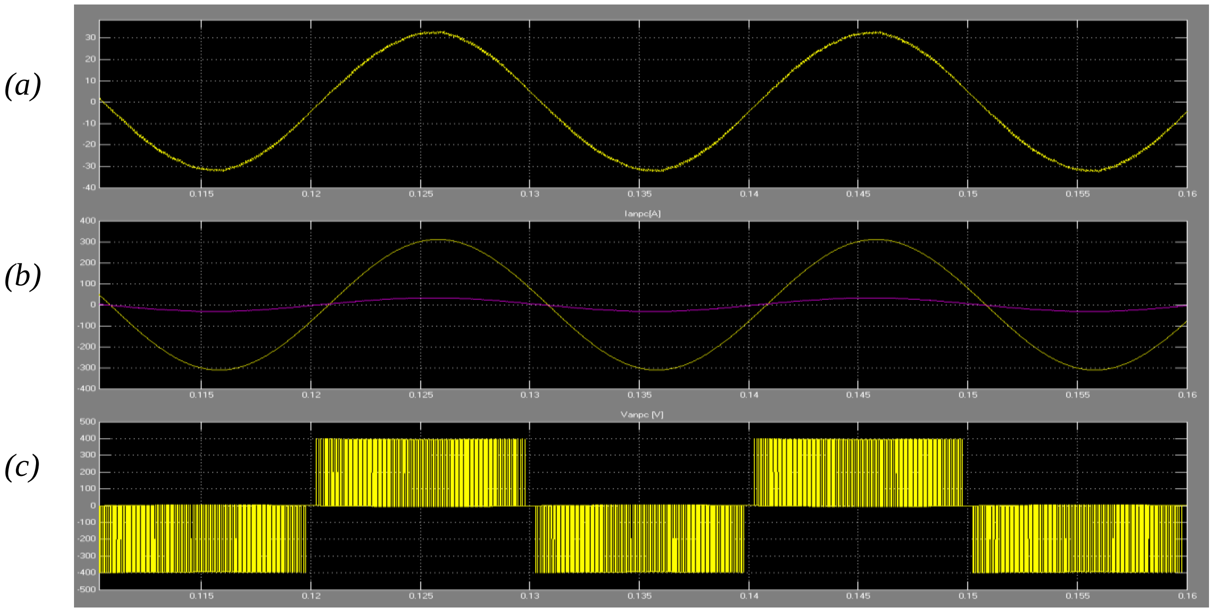

Figure 4-29(a) Inverter current injected into the electric grid (A), (b) Active-NPC inverter output current and grid voltage,(c) Active-NPC inverter PWM output voltage (V).

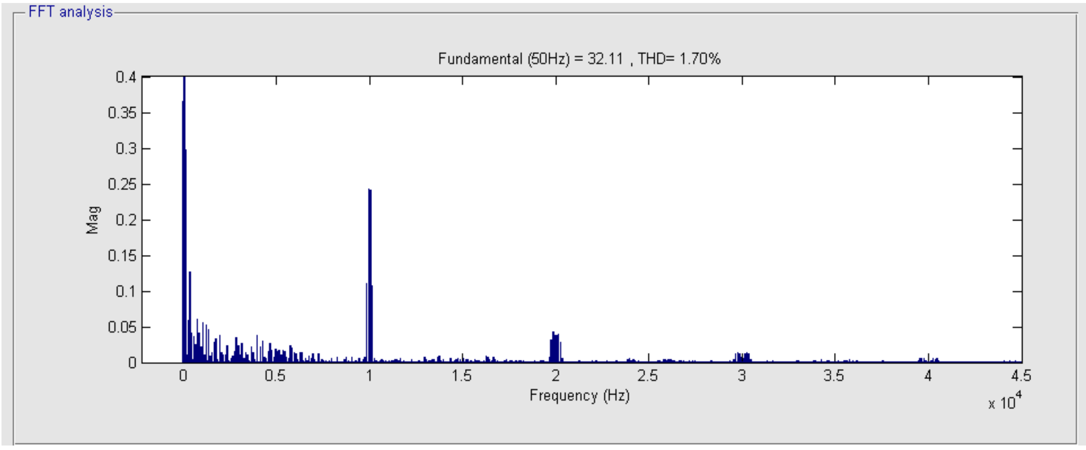

Figure 4-30 The spectrum of the Active-NPC inverter output current f_s=5000 Hz, L=8mH, M=0.8, PF=1.

Figs. 4-31 to 4-33 present the power loss distribution for f_s=8000 Hz, M=0.8 and PF=1, the Active-NPC inverter current injected to the electric grid, the PWM output voltage and the spectrum of the Active-NPC inverter output current.

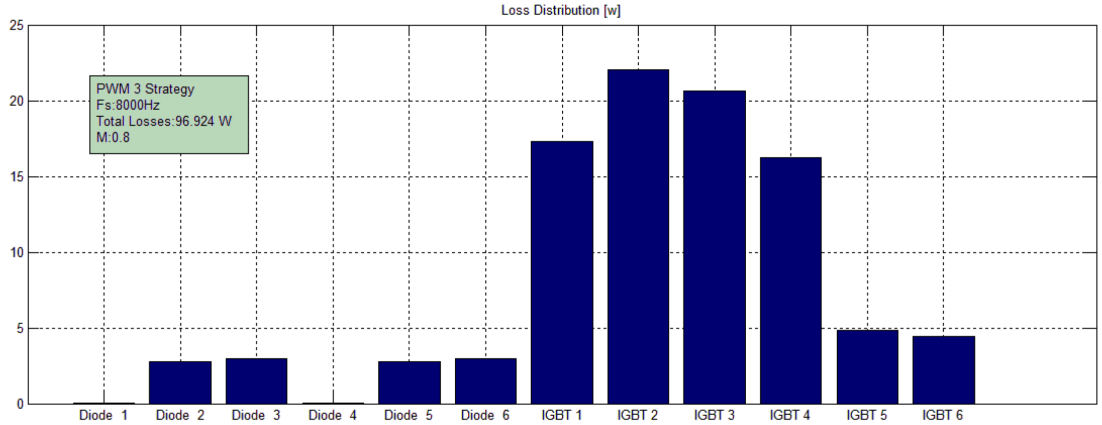

Figure 4-31 Power loss distribution for f_s=8000 Hz, L=8mH, M=0.8, PF=1.

(a)

(b)

(c)

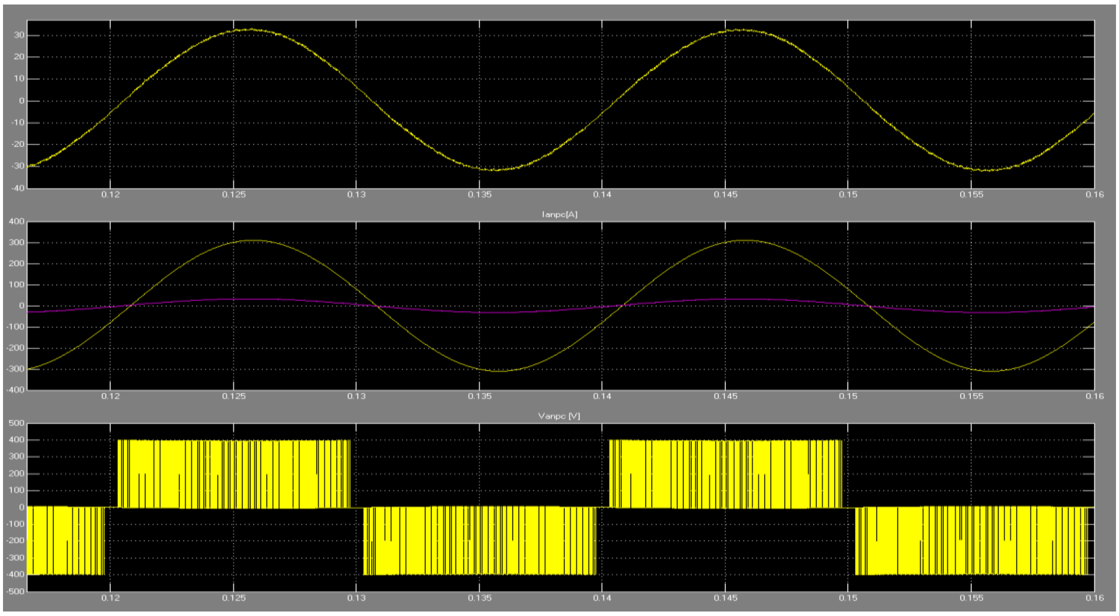

Figure 4-32(a) Inverter current injected into the electric grid (A), (b) Active-NPC inverter output current and grid voltage,(c) Active-NPC inverter PWM output voltage (V).

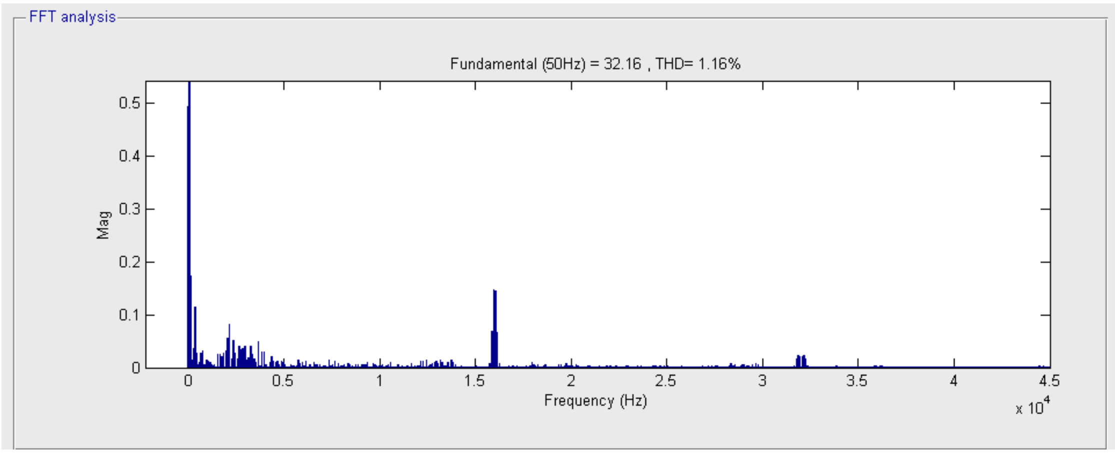

Figure 4-33 The spectrum of the Active-NPC inverter output current for f_s=8000 Hz, L=8mH, M=0.8, PF=1.

Figs. 4-34 to 4-36 present the power loss distribution for f_s=10000 Hz, M=0.8 and PF=1, the Active-NPC inverter current injected to the electric grid, the PWM output voltage and the spectrum of the Active-NPC inverter output current.

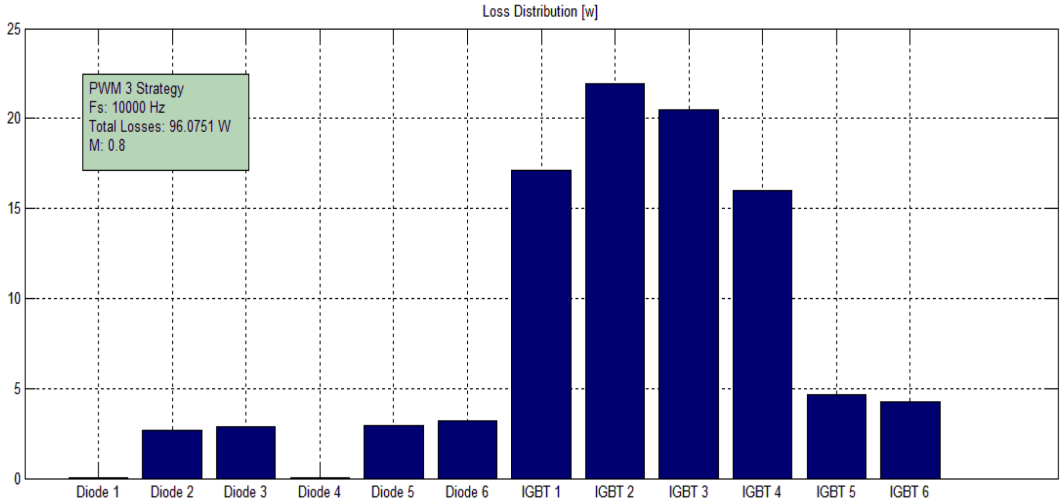

Figure 4-34 Power loss distribution for f_s=10000 Hz, L=8mH, M=0.8, PF=1.

(a)

(b)

(c)

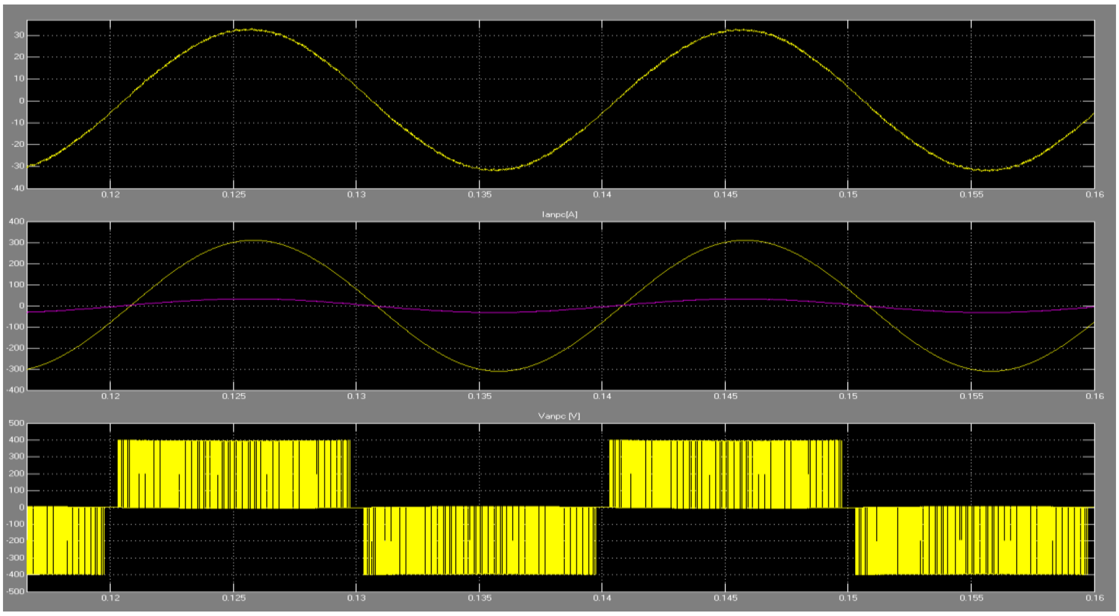

Figure 4-35(a) Inverter current injected into the electric grid (A), (b) Active-NPC inverter output current and grid voltage,(c) Active-NPC inverter PWM output voltage (V).

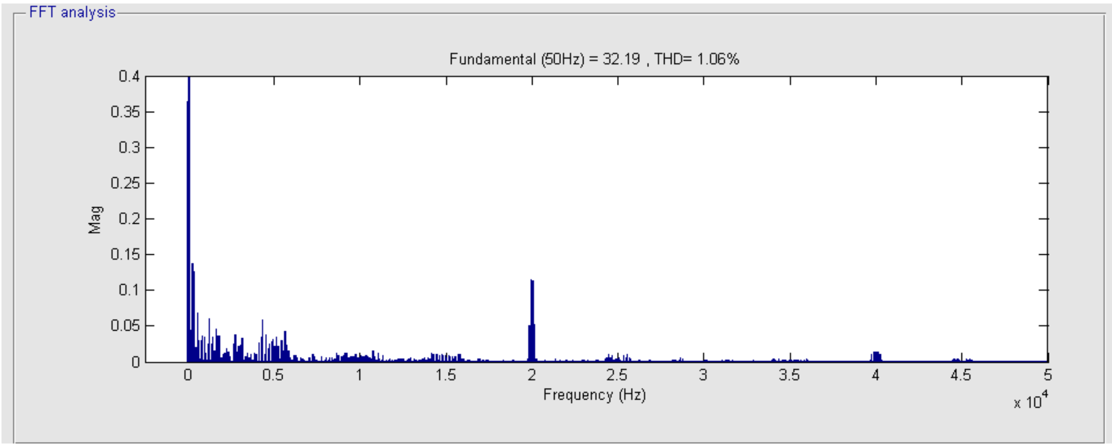

Figure 4-36 The spectrum of the Active-NPC inverter output current for f_s=10000 Hz, L=8mH, M=0.8, PF=1.

4.1.4 PWM-4 Strategy (Adjustable Losses Distribution Active-NPC) 50-50 Stress In-Stress Out

Figs. 4-37 to 4-39 present the power loss distribution for f_s=3000 Hz, M=0.8 and PF=1, the Active-NPC inverter current injected to the electric grid, the PWM output voltage and the spectrum of the Active-NPC inverter output current.

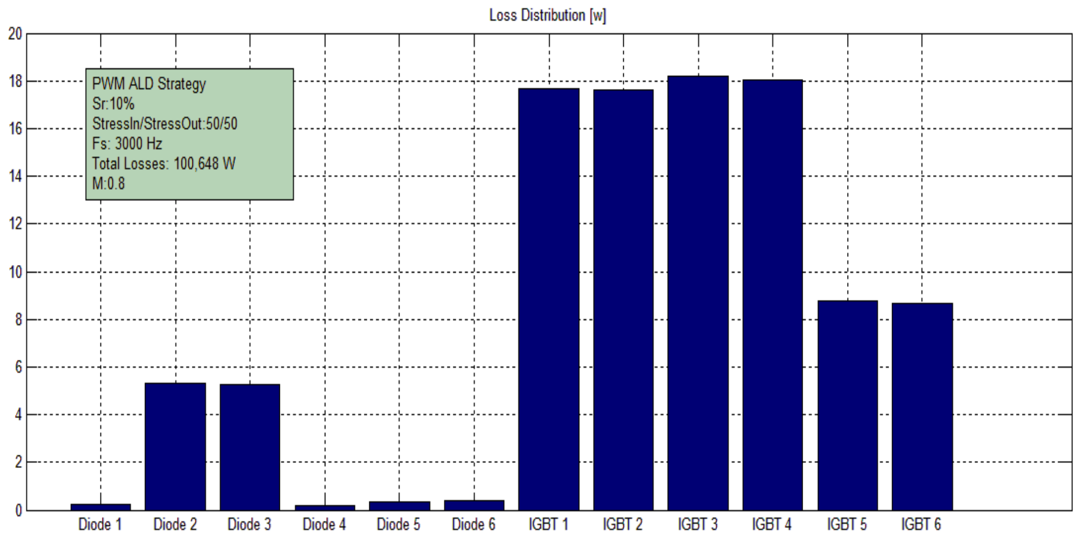

Figure 4-37 Power loss distribution for f_s=3000 Hz, L=8mH, M=0.8, PF=1.

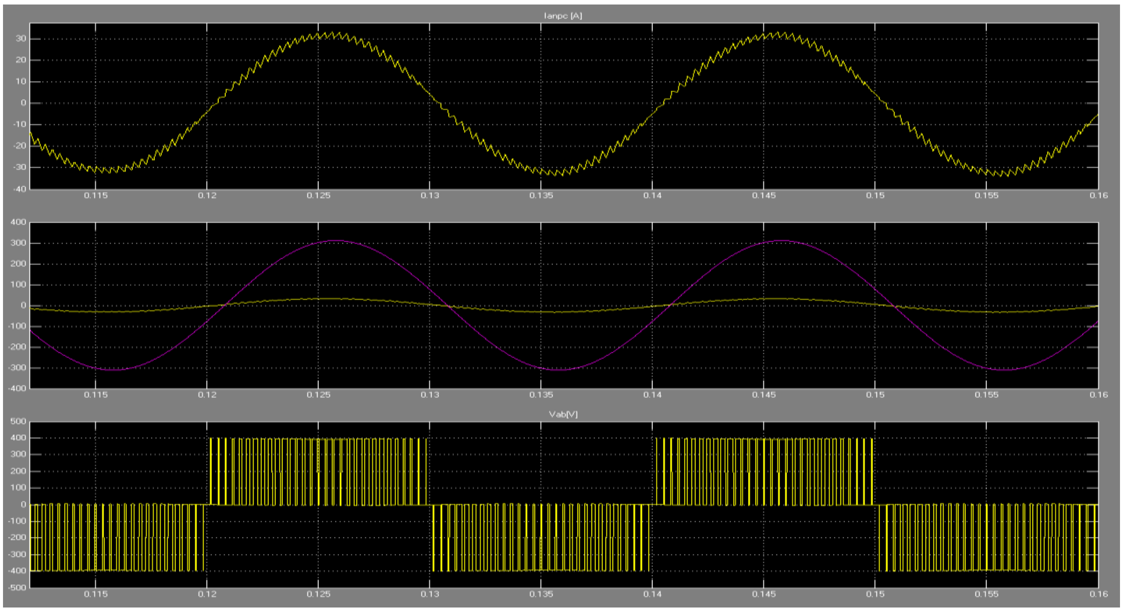
(a)
(b)
(c)

Figure 4-38(a) Inverter current injected into the electric grid (A), (b) Active-NPC inverter output current and grid voltage,(c) Active-NPC inverter PWM output voltage (V).

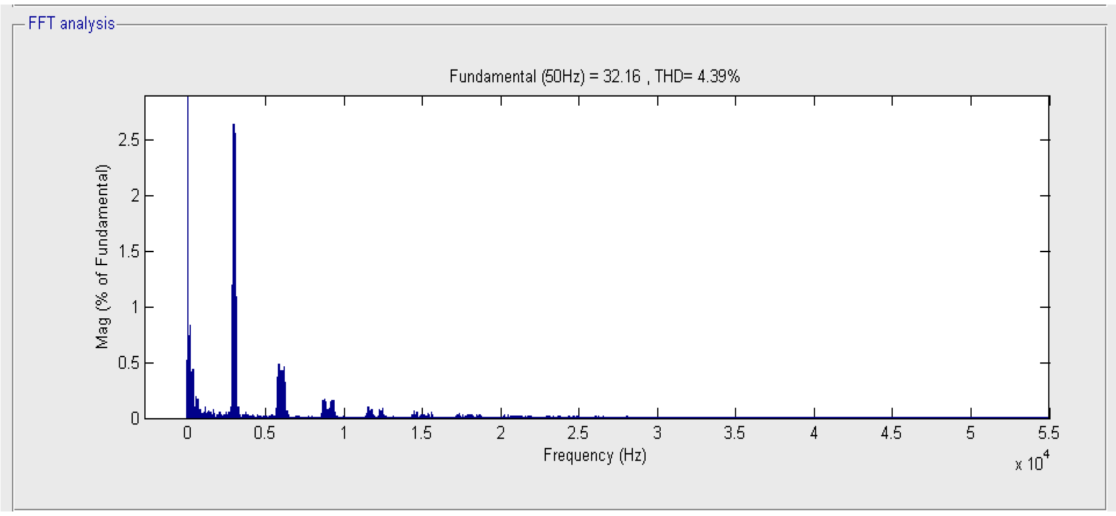

Figure 4-39 The spectrum of the Active-NPC inverter output current f_s=3000 Hz, L=8mH, M=0.8, PF=1.

Figs. 4-40 to 4-42 present the power loss distribution for f_s=5000 Hz, M=0.8 and PF=1, the Active-NPC inverter current injected to the electric grid, the PWM output voltage and the spectrum of the Active-NPC inverter output current.

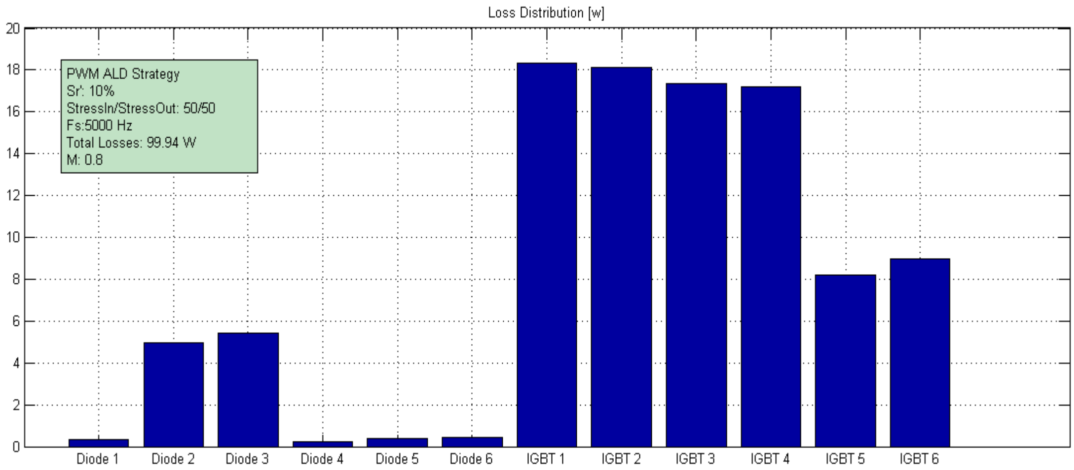

Figure 4-40 Power loss distribution for f_s=5000 Hz, L=8mH, M=0.8, PF=1.

(a)

(b)

(c)

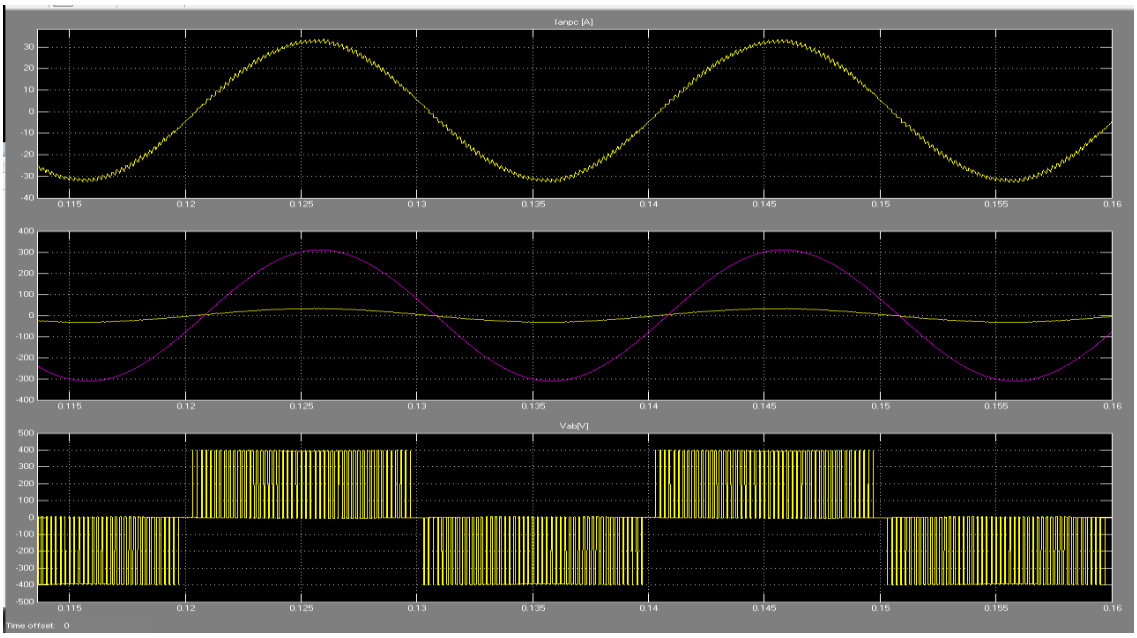

Figure 4-41(a) Inverter current injected into the electric grid (A), (b) Active-NPC inverter output current and grid voltage,(c) Active-NPC inverter PWM output voltage (V).

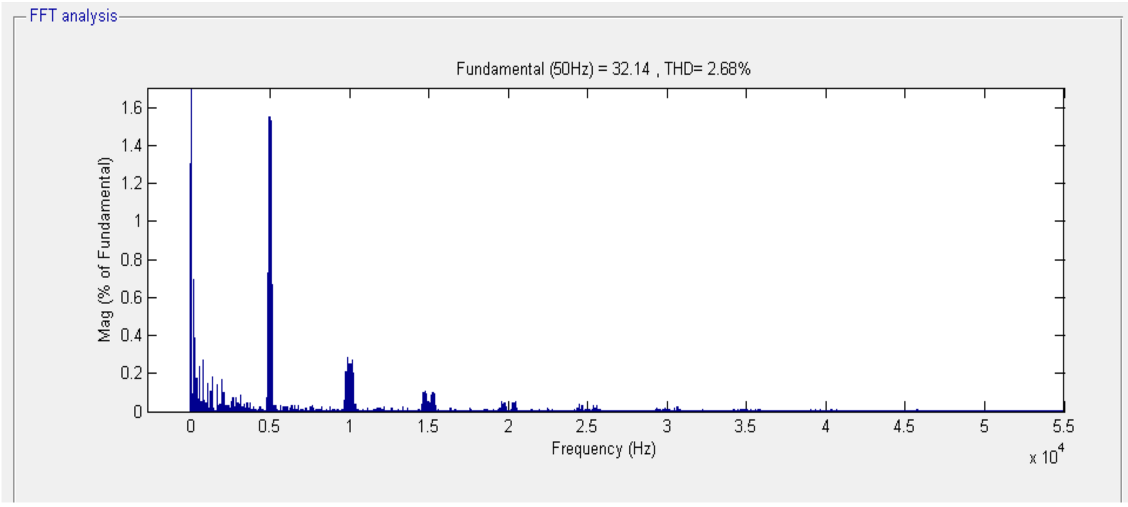

Figure 4-42 The spectrum of the Active-NPC inverter output current for f_s=5000 Hz, L=8mH, M=0.8, PF=1.

Figs. 4-43 to 4-45 present the power loss distribution for f_s=8000 Hz, M=0.8 and PF=1, the Active-NPC inverter current injected to the electric grid, the PWM output voltage and the spectrum of the Active-NPC inverter output current.

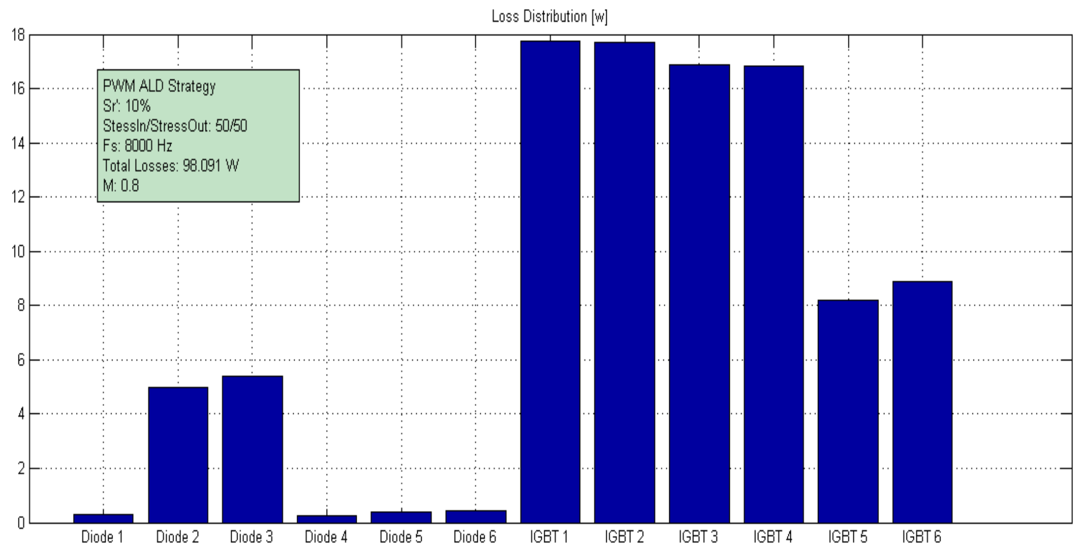

Figure 4-43 Power loss distribution for f_s=8000 Hz, L=8mH, M=0.8, PF=1.

(a)

(b)

(c)

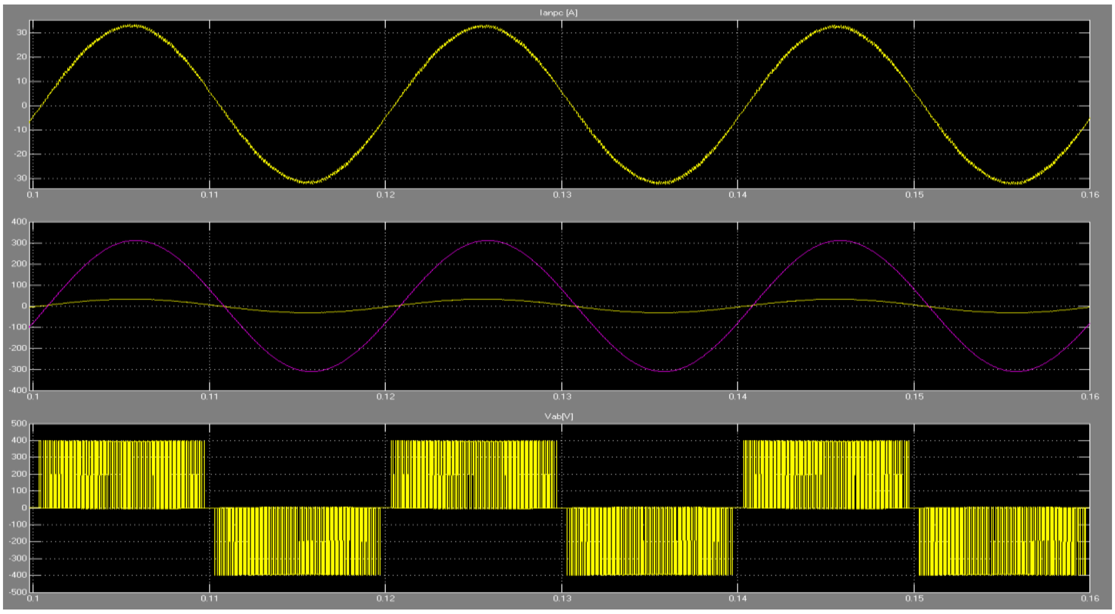

Figure 4-44(a) Inverter current injected into the electric grid (A), (b) Active-NPC inverter output current and grid voltage,(c) Active-NPC inverter PWM output voltage (V).

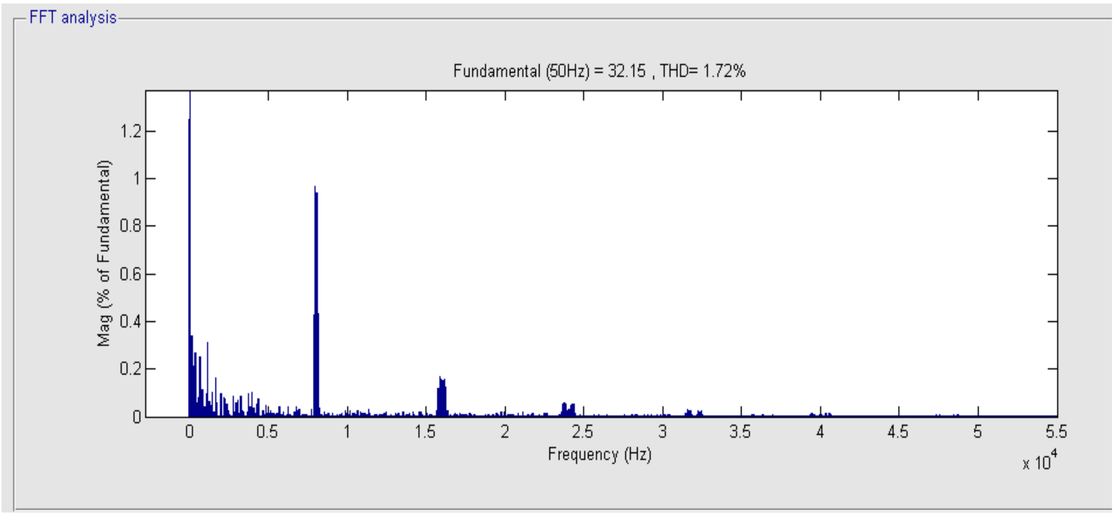

Figure 4-45 The spectrum of the Active-NPC inverter output current f_s=8000 Hz, L=8mH, M=0.8, PF=1.

Figs. 4-46 to 4-48 present the power loss distribution for f_s=10000 Hz, M=0.8 and PF=1, the Active-NPC inverter current injected to the electric grid, the PWM output voltage and the spectrum of the Active-NPC inverter output current.

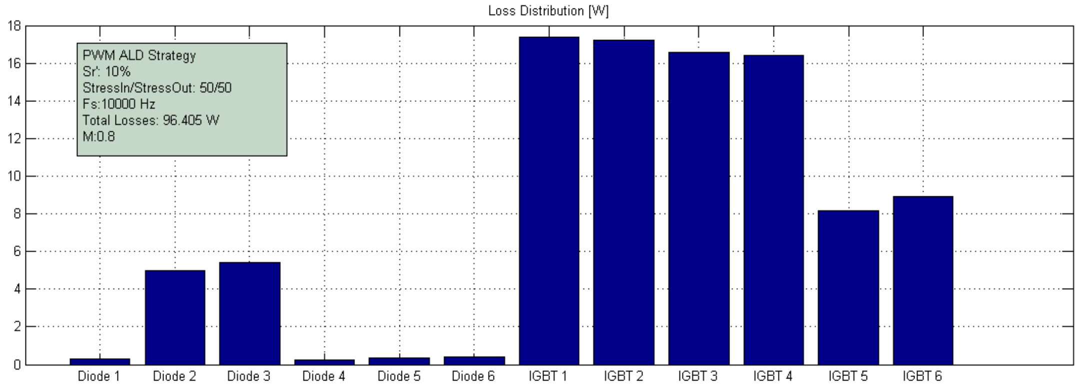

Figure 4-46 Power loss distribution for f_s=10000 Hz, L=8mH, M=0.8, PF=1.

(a)

(b)

(c)

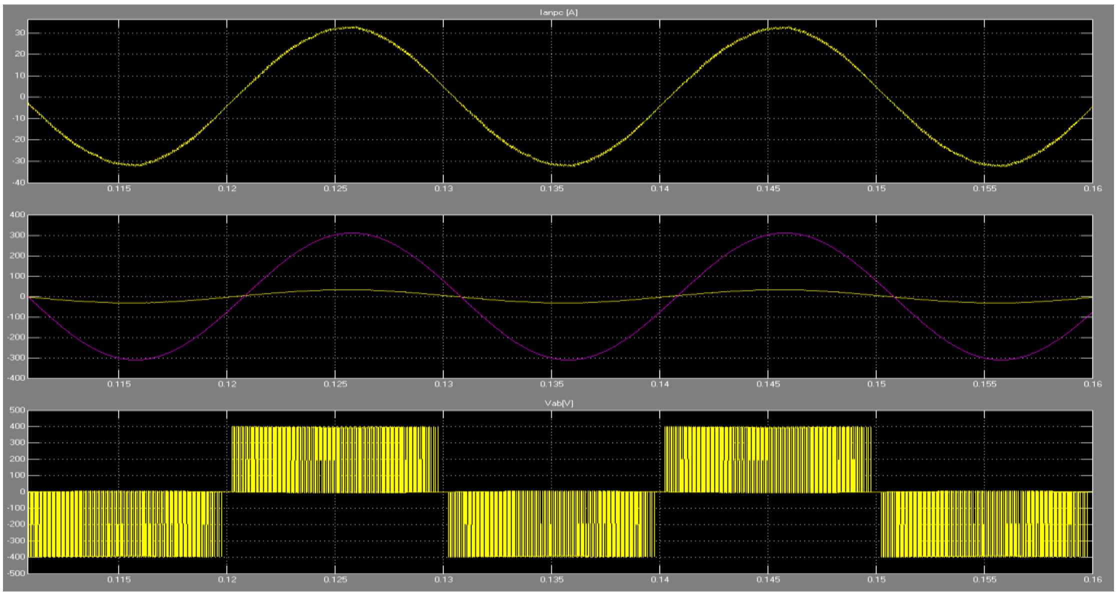

Figure 4-47(a) Inverter current injected into the electric grid (A), (b) Active-NPC inverter output current and grid voltage,(c) Active-NPC inverter PWM output voltage (V).

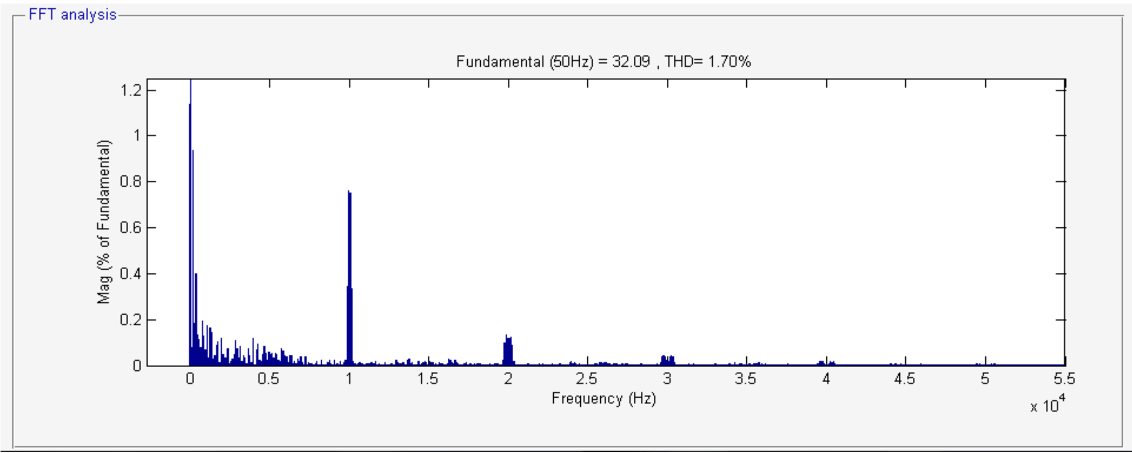

Figure 4-48 The spectrum of the Active-NPC inverter output current for f_s=10000 Hz, L=8mH, M=0.8, PF=1.

4.1.5 PWM-4 Strategy (Adjustable Losses Distribution Active-NPC) 40-60 Stress In-Stress Out

Figs. 4-49 to 4-51 present the power loss distribution for f_s=3000 Hz, M=0.8 and PF=1, the Active-NPC inverter current injected to the electric grid, the PWM output voltage and the spectrum of the Active-NPC inverter output current.

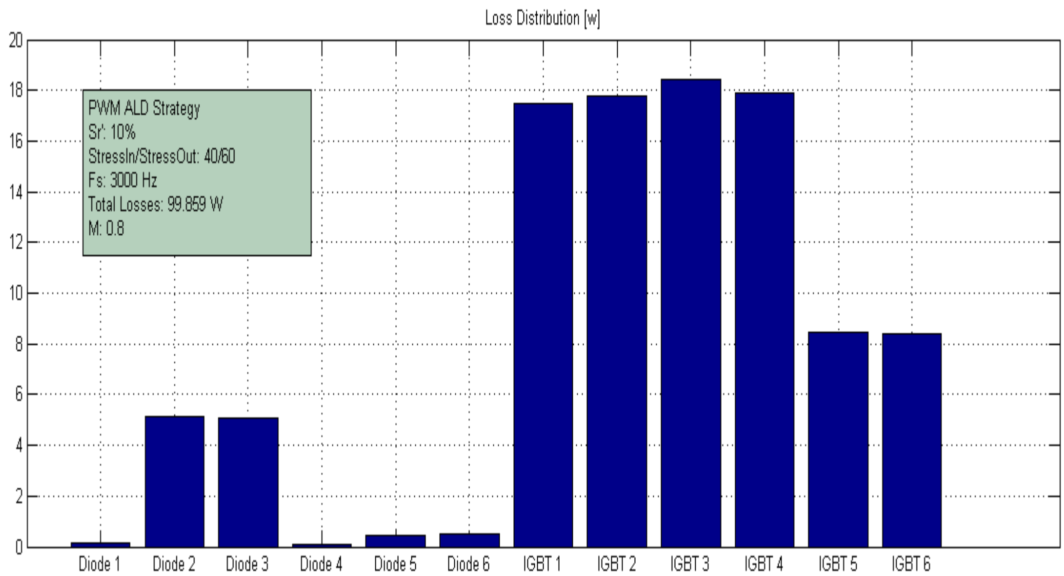

Figure 4-49 Power loss distribution for f_s=3000 Hz, L=8mH, M=0.8, PF=1.

(a)

(b)

(c)

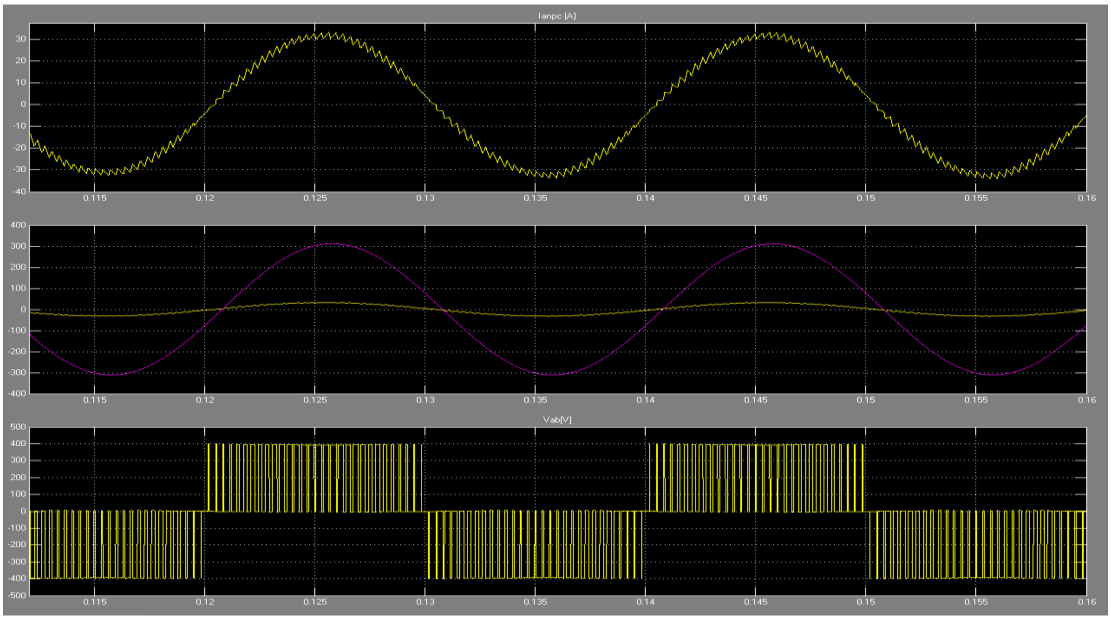

Figure 4-50(a) Inverter current injected into the electric grid (A), (b) Active-NPC inverter output current and grid voltage,(c) Active-NPC inverter PWM output voltage (V).

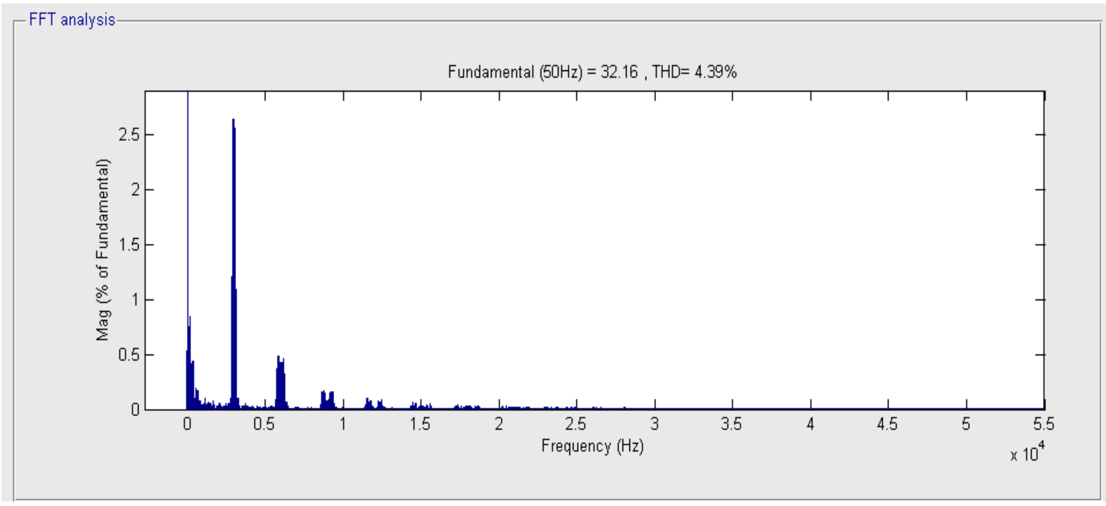

Figure 4-51 The spectrum of the Active-NPC inverter output current for f_s=3000 Hz, L=8mH, M=0.8, PF=1.

Figs. 4-52 to 4-54 present the power loss distribution for f_s=5000 Hz, M=0.8 and PF=1, the Active-NPC inverter current injected to the electric grid, the PWM output voltage and the spectrum of the Active-NPC inverter output current.

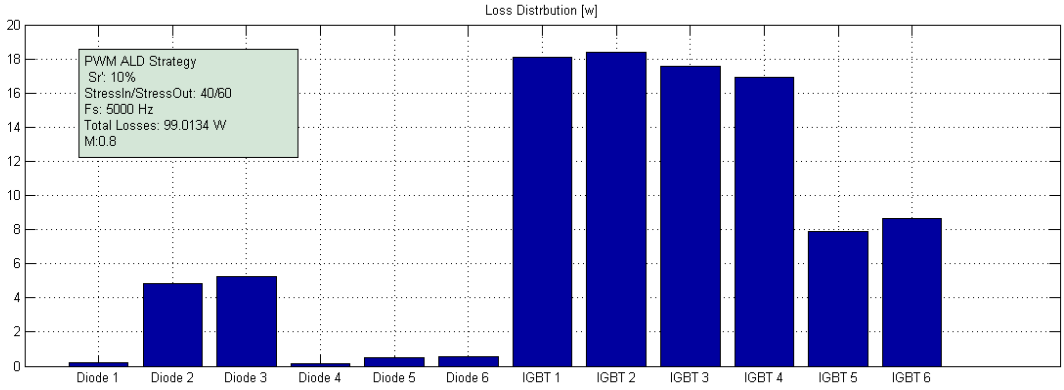

Figure 4-52 Power loss distribution for f_s=5000 Hz, L=8mH, M=0.8, PF=1.

(a)

(b)

(c)

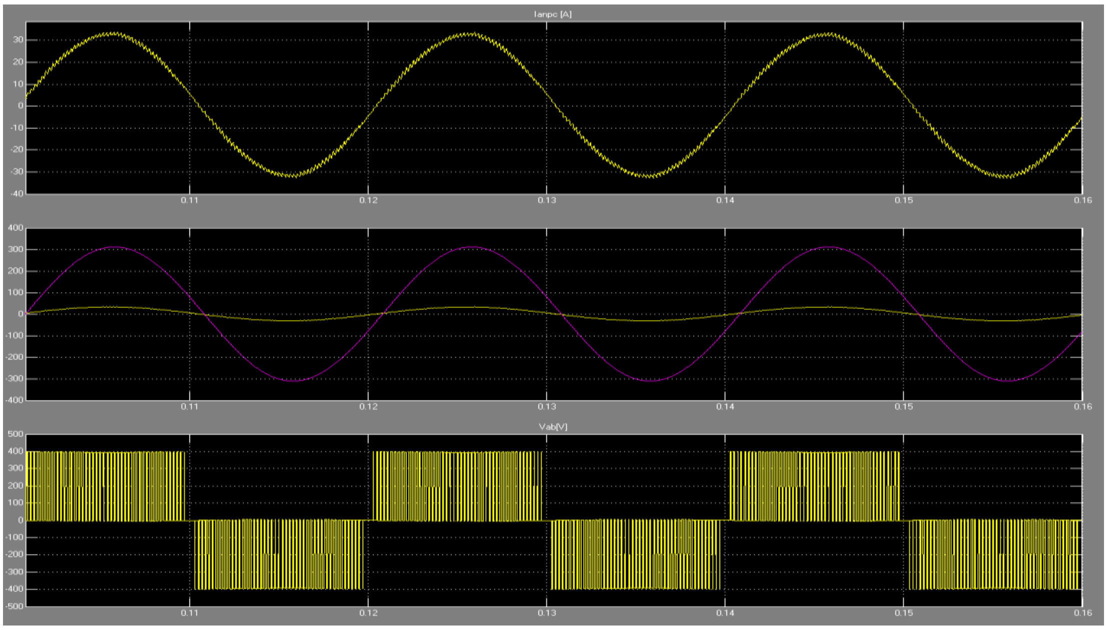

Figure 4-53(a) Inverter current injected into the electric grid (A), (b) Active-NPC inverter output current and grid voltage,(c) Active-NPC inverter PWM output voltage (V).

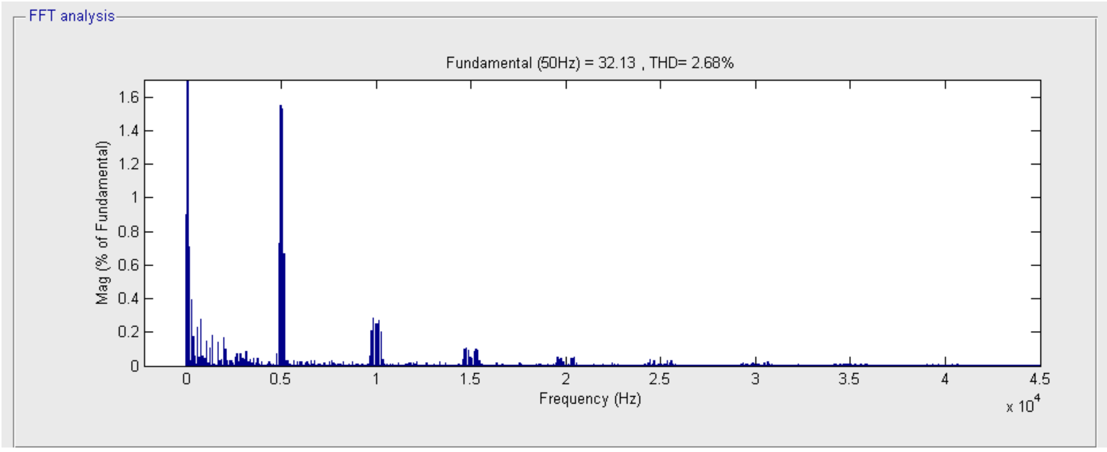

Figure 4-54 The spectrum of the Active-NPC inverter output current for f_s=5000 Hz, L=8mH, M=0.8, PF=1.

Figs. 4-55 to 4-57 present the power loss distribution for f_s=8000 Hz, M=0.8 and PF=1, the Active-NPC inverter current injected to the electric grid, the PWM output voltage and the spectrum of the Active-NPC inverter output current.

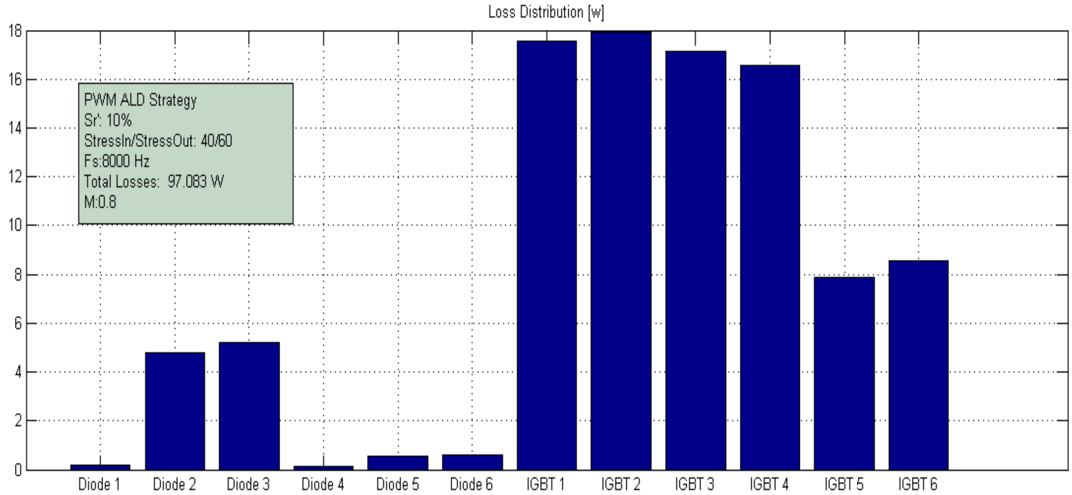

Figure 4-55 Power loss distribution for f_s=8000 Hz, L=8mH, M=0.8, PF=1.

(a)

(b)

(c)

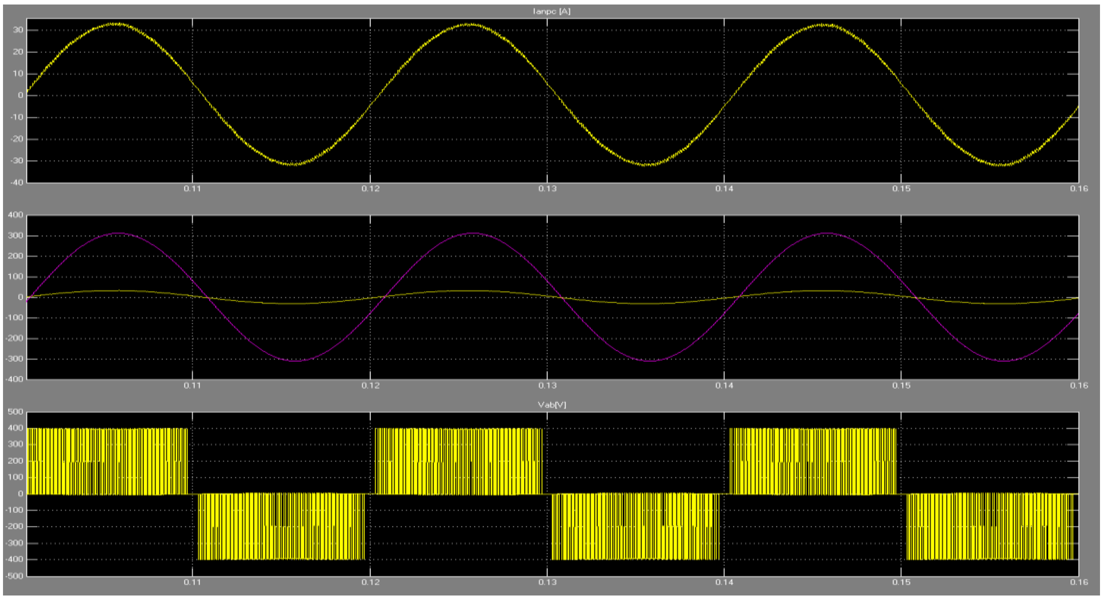

Figure 4-56(a) Inverter current injected into the electric grid (A), (b) Active-NPC inverter output current and grid voltage,(c) Active-NPC inverter PWM output voltage (V).

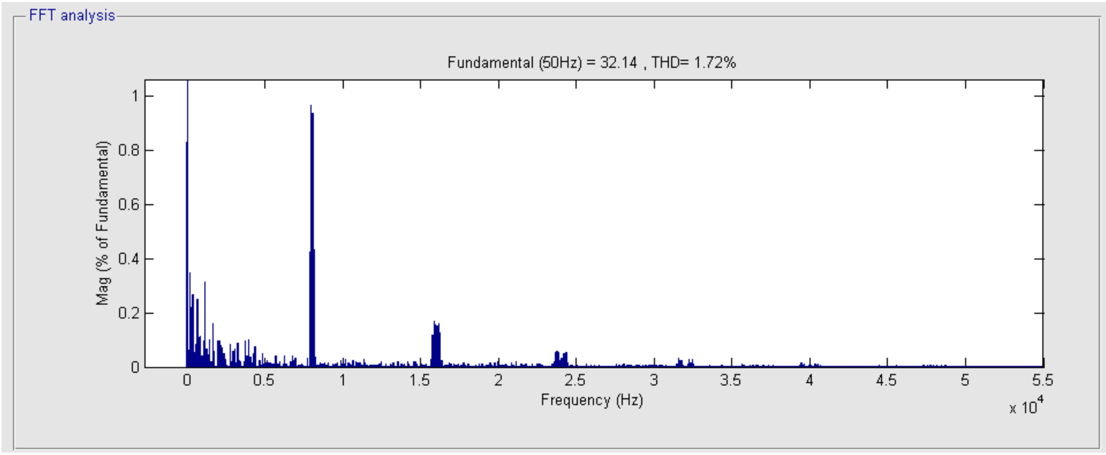

Figure 4-57 The spectrum of the Active-NPC inverter output current for f_s=8000 Hz, L=8mH, M=0.8, PF=1.

Figs. 4-58 to 4-60 present the power loss distribution for f_s=10000 Hz, M=0.8 and PF=1, the Active-NPC inverter current injected to the electric grid, the PWM output voltage and the spectrum of the Active-NPC inverter output current.

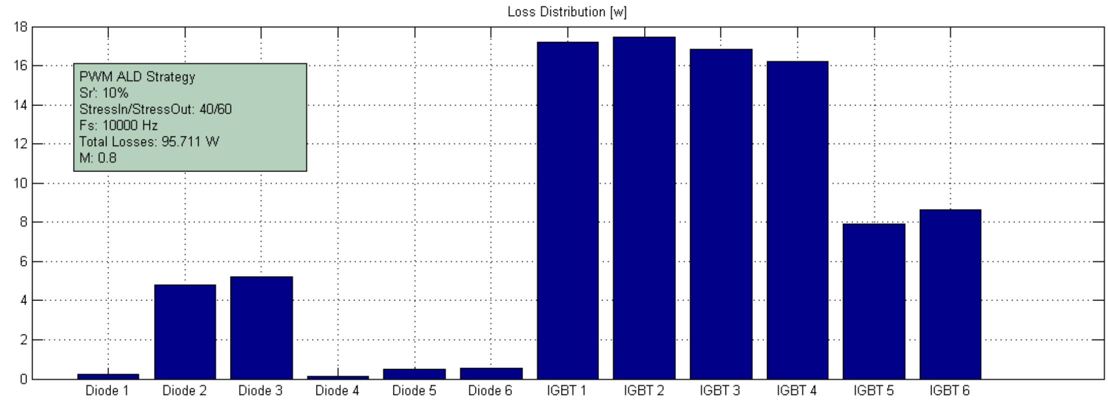

Figure 4-58 Power loss distribution for f_s=10000 Hz, L=8mH, M=0.8, PF=1.

(a)

(b)

(c)

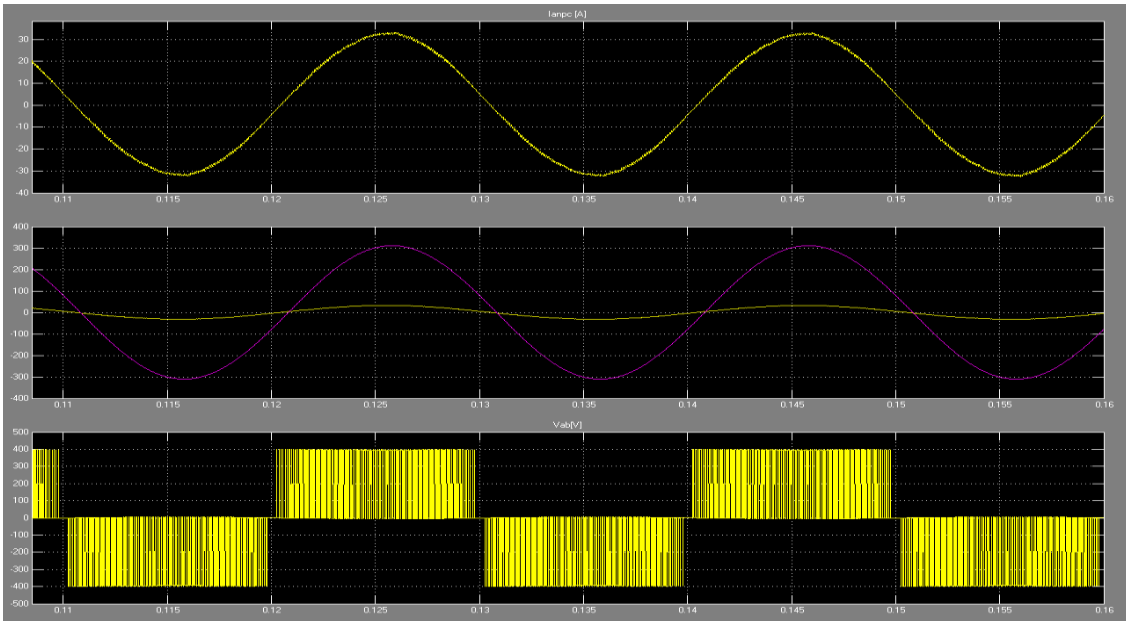

Figure 4-59(a) Inverter current injected into the electric grid (A), (b) Active-NPC inverter output current and grid voltage,(c) Active-NPC inverter PWM output voltage (V).

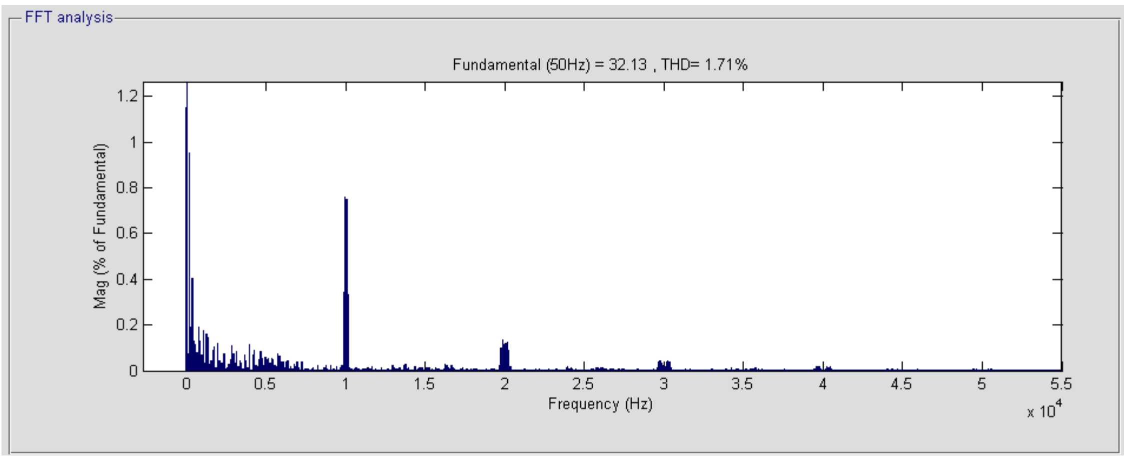

Figure 4-60 The spectrum of the Active-NPC inverter output current for f_s=10000 Hz, L=8mH, M=0.8, PF=1.

4.2 Optimization Results

In the following graphs and tables, the optimization results are presented for different switching frequencies for an Active-NPC inverter with V_{DC}=400 V and P_o=5 kW.

4.2.1 Objective function: Minimum Sum of Total Losses of the Power Semiconductors

Firstly, Table 4-1 is a summary table containing all the results of the past-proposed strategies and the results of the optimization model with genetic algorithms.

Table 4-1. Total power losses (W) of the past-proposed PWM strategies and proposed optimization model for L=8mH, M=0.8, PF≈1

f_s (Hz)	**Strategy**					
	PWM1	**PWM2**	**PWM3**	**ALD(50/50)**	**ALD(40/60)**	**Opt. Model (GA)**
3000	110.49	110.7437	100.45	100.649	99.859	94.9409
5000	110.036	110.0373	98.48	99.94	99.0134	91.6981
8000	109.159	109.4123	96.924	98.091	97.2914	91.3407
10000	108.48	108.7453	96.0751	96.405	95.717	90.233

Additionally, in order to present the percentage deviation between the results of the proposed optimization model and the past-proposed PWM strategies, Table 4-2 is also provided:

Table 4-2. Reduction of total power losses % (PWMs-Opt. Model/ Opt. Model) for L=8mH, M=0.8, PF≈1

f_s (Hz)	Strategy				
	PWM1	**PWM2**	**PWM3**	**ALD(50/50)**	**ALD(40/60)**
3000	16.37%	16.64%	5.8%	6.01%	5.18%
5000	19.99%	19.99%	7.39%	8.98%	7.97%
8000	19.5%	19.78%	6.11%	7.39%	6.51%
10000	20.22%	20.51%	6.48%	6.84%	6.07%

Observing the above matrices it is concluded that, the genetic algorithm reduced the power losses of the Active-NPC inverter from 5.18% (ALD (40/60)) up to 20.51% (PWM2), compared with the optimization model. In general, PWM1 and PWM2 strategies, consume about 16.5-20% more power, while PWM3 (Double Frequency) and ALD strategies consume about 5-9% more power, compared with the proposed optimization model. Despite being mentioned in previous publications that the power losses remain at the same levels independently of the Optimal strategy calculated, the above results show that with the best choice of the firing angles and the suitable strategy, there can be up to 20.51% less power losses.

Analytically, the following figures present the proposed optimization model results and the optimal strategies that have been derived, with an inductance L=8 mH as output filter.

Figs. 4-61 to 4-63 present the power loss distribution for f_s=3000 Hz, M=0.8 and PF=1, the Active-NPC inverter current injected to the electric grid, the PWM output voltage and the spectrum of the Active-NPC inverter output current.

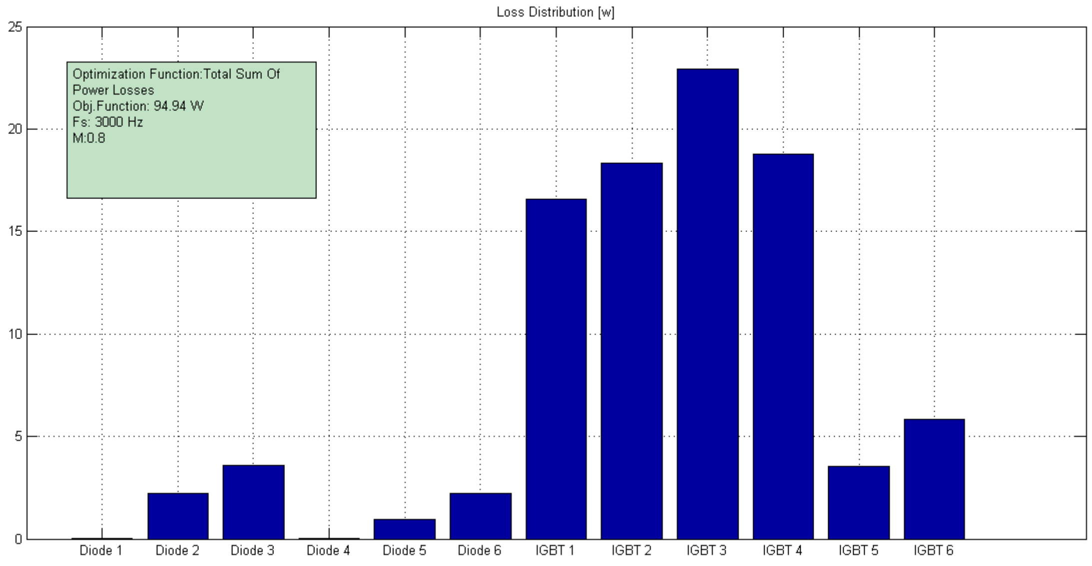

Figure 4-61 Power loss distribution for fs=3000 Hz, L=8mH, M=0.8, PF=1.

(a)

(b)

(c)

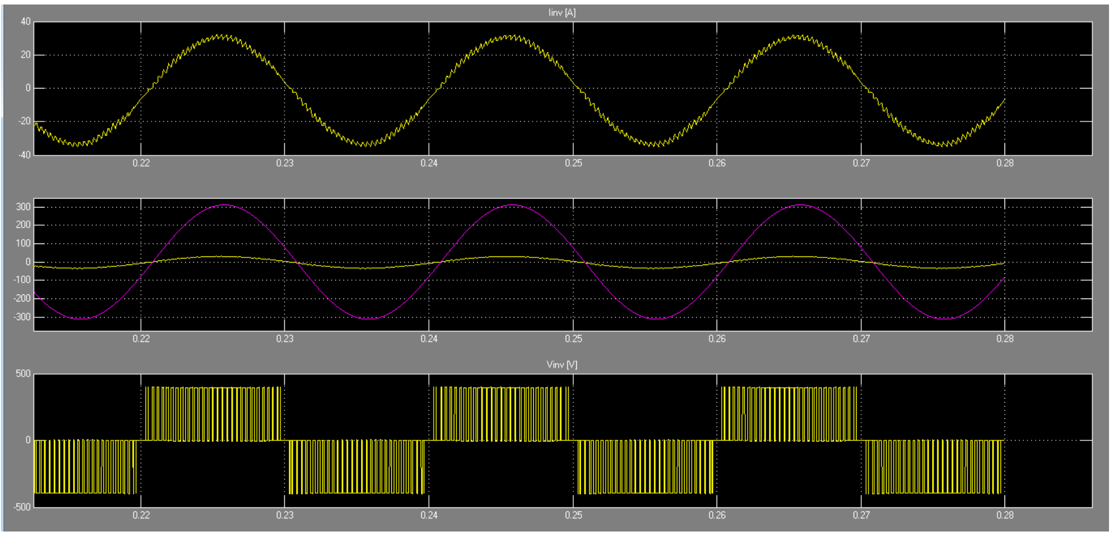

Figure 4-62 (a) Inverter current injected into the electric grid (A), (b) Active-NPC inverter output current and grid voltage,(c) Active-NPC inverter PWM output voltage (V).

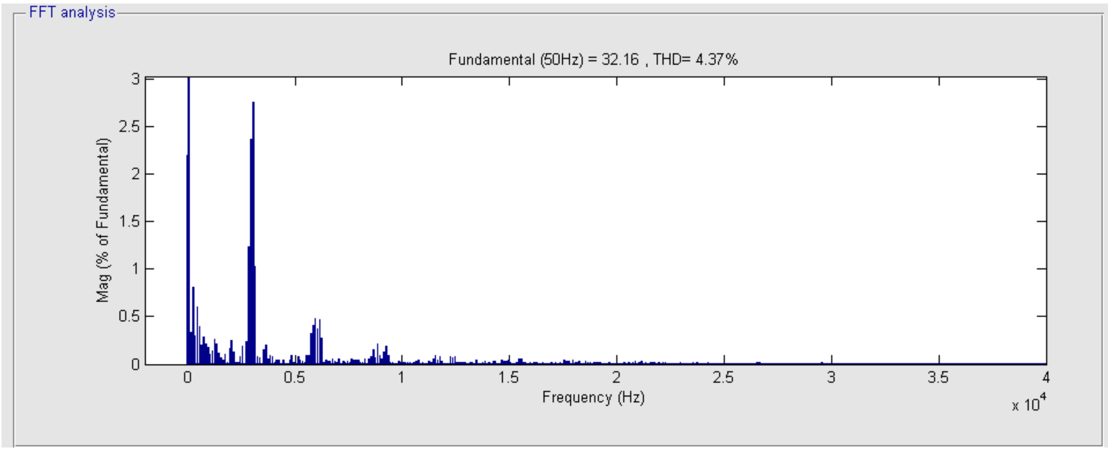

Figure 4-63 The spectrum of the Active-NPC inverter output current for f_s=3000 Hz, L=8mH, M=0.8, PF=1.

Optimal strategy calculated: $\mathbf{0_{out}^-}$**,** $\mathbf{P_2}$**,** $\mathbf{0^-/\,0_1^-/0^+}$**,** $\mathbf{0_{out}^+}$**,** $\mathbf{N_2}$**,** $\mathbf{0_{out}^-}$ (Table 3-2)

The strategy calculated as optimal contains P_2 as positive state, N_2 as negative and three different zero paths. In more details in positive side the algorithm selected a strategy with two-way zero paths $\mathbf{0^-/\ 0_1^-/0^+}$, $\mathbf{0_{out}^+}$ and during the negative side only one $\mathbf{0_{out}^-}$. Fig.4-64 presents the optimal firing angles of the Active-NPC inverter for f_s= 3000 Hz, L=8mH, M=0.8 and PF=1.

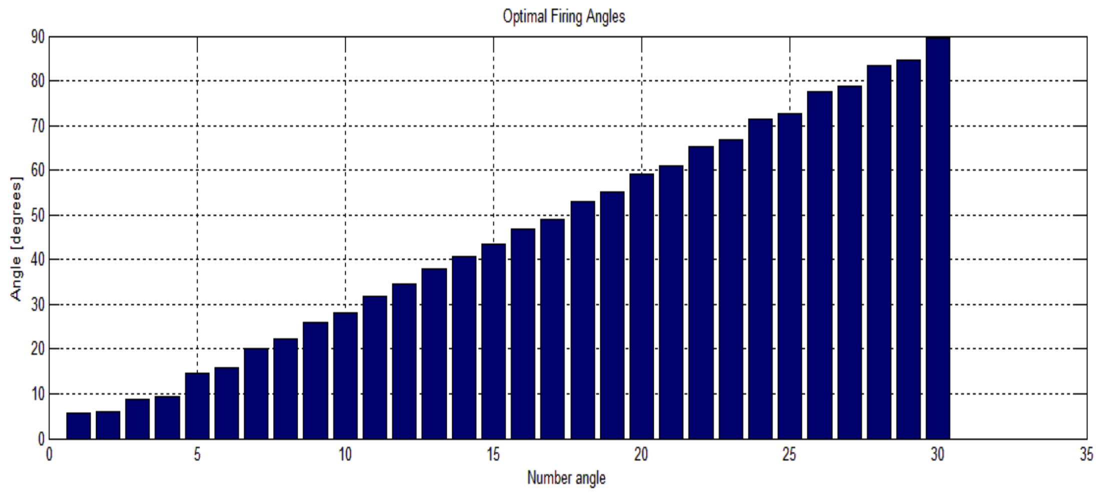

Figure 4-64 Optimal firing angles of Active-NPC inverter for f_s=3000Hz L=8mH, M=0.8 and PF=1.

Figs. 4-65 to 4-67 present the power loss distribution for f_s=5000 Hz, M=0.8 and PF=0.99, the Active-NPC inverter current injected to the electric grid, the PWM output voltage and the spectrum of the Active-NPC inverter output current.

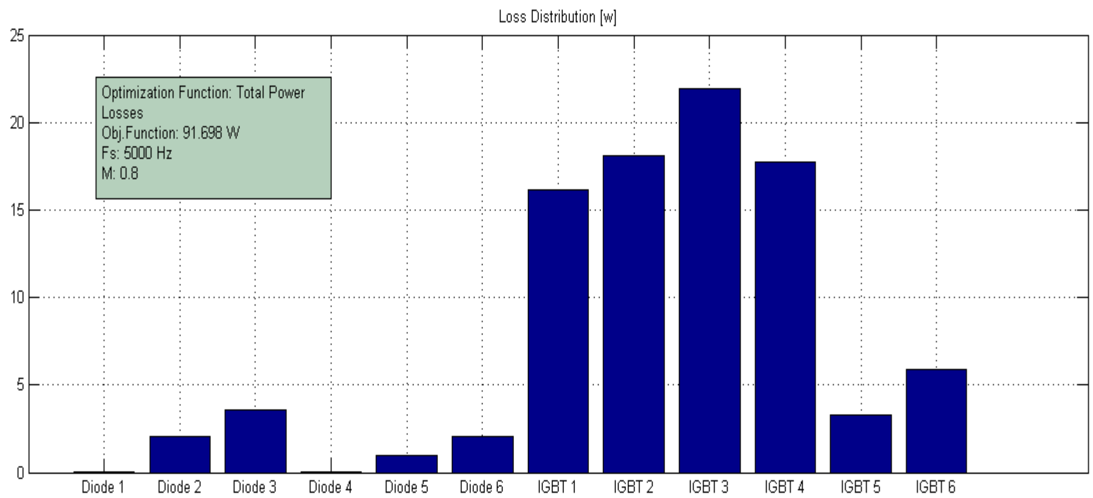

Figure 4-65 Power Loss distribution for f_s=5000 Hz, L=8mH, M=0.8, PF=0.99.

(a)

(b)

(c)

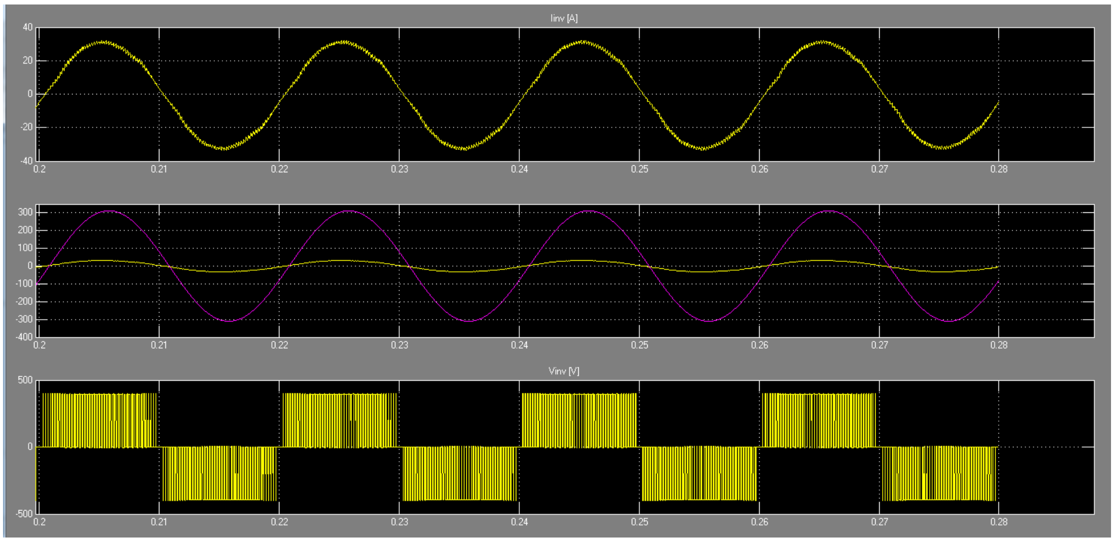

Figure 4-66(a) Inverter current injected into the electric grid (A), (b) Active-NPC inverter output current and grid voltage,(c) Active-NPC inverter PWM output voltage (V).

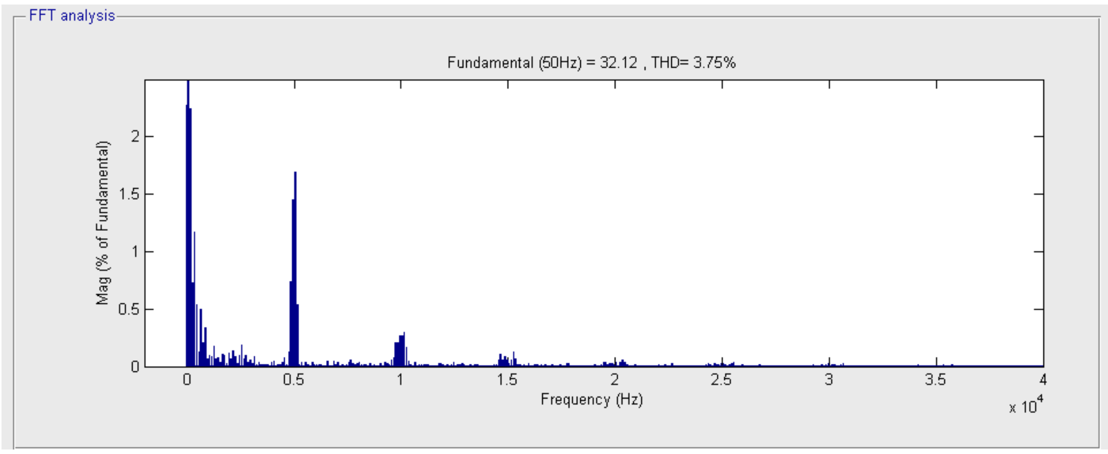

Figure 4-67 The spectrum of the Active-NPC inverter output current for f_s=5000 Hz, L=8mH, M=0.8, PF=0.99.

Optimal strategy calculated: $\mathbf{0_{out}^{-}}$**, P**$_2$**,** $\mathbf{0^{-}/\ 0_1^{-}/0^{+}}$**,** $\mathbf{0_{out}^{+}}$**, N**$_2$**,** $\mathbf{0_{out}^{-}}$ (Table 3-2)

Genetic Algorithm derived as optimal a strategy containing P_2 as positive state, N_2 as negative and three different zero paths. In positive side, the algorithm selected a strategy with two-way zero paths $\mathbf{0^{-}/\ 0_1^{-}/0^{+}}$, $\mathbf{0_{out}^{+}}$ and during the negative side only one $\mathbf{0_{out}^{-}}$. It is observed that the same strategy has been derived as in the case of f_s= 3000 Hz. Fig.4-68 presents the optimal firing angles of the Active-NPC inverter for f_s= 5000 Hz, L=8mH, M=0.8 and PF=1.

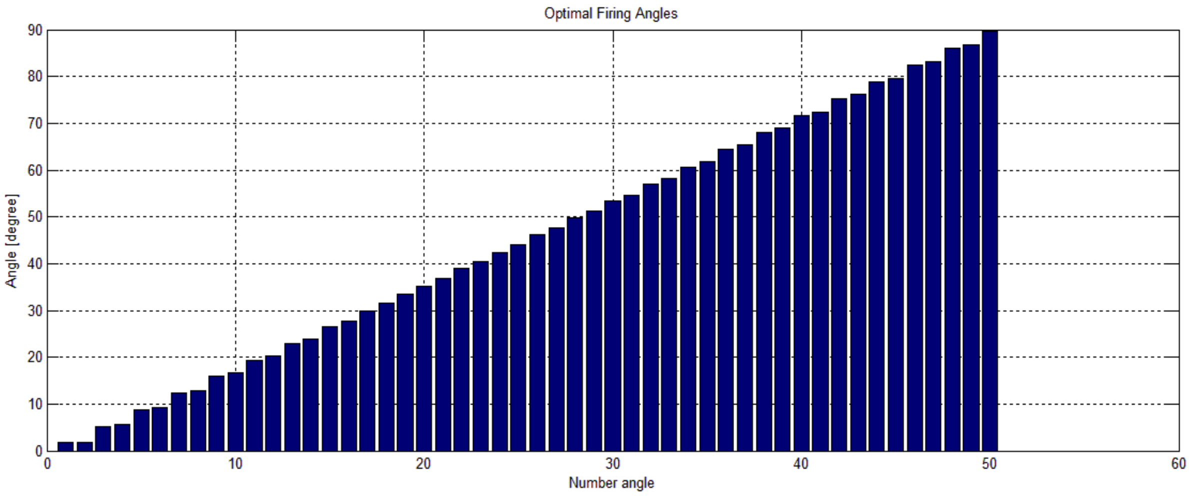

Figure 4-68 Optimal firing angles of Active-NPC inverter for fs=5000 Hz L=8mH, M=0.8 and PF=1

Figs. 4-69 to 4-71 present the power loss distribution for f_s=8000 Hz, M=0.8 and PF≈1, the Active-NPC inverter current injected to the electric grid, the PWM output voltage and the spectrum of the Active-NPC inverter output current.

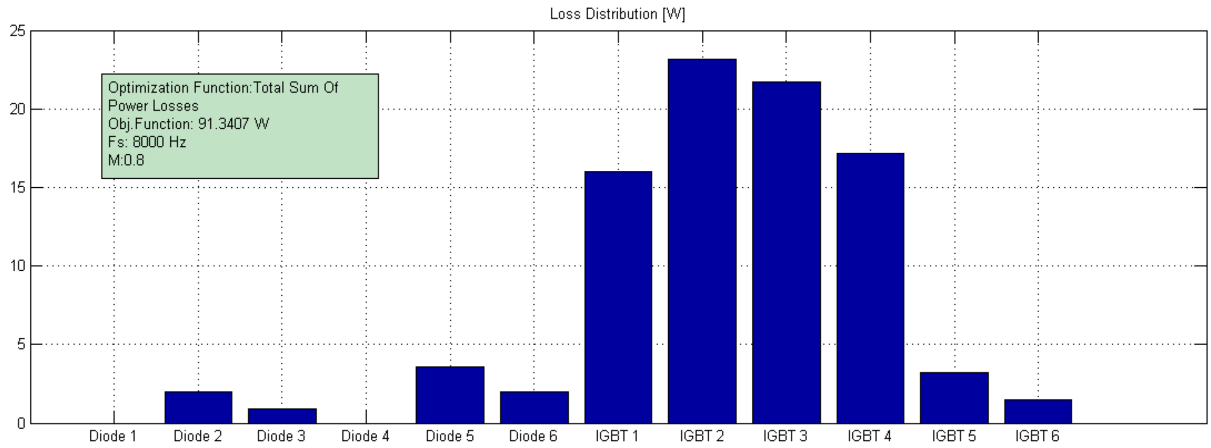

Figure 4-69 Power loss distribution for f_s=8000 Hz, L=8mH, M=0.8, PF≈1.

(a)

(b)

(c)

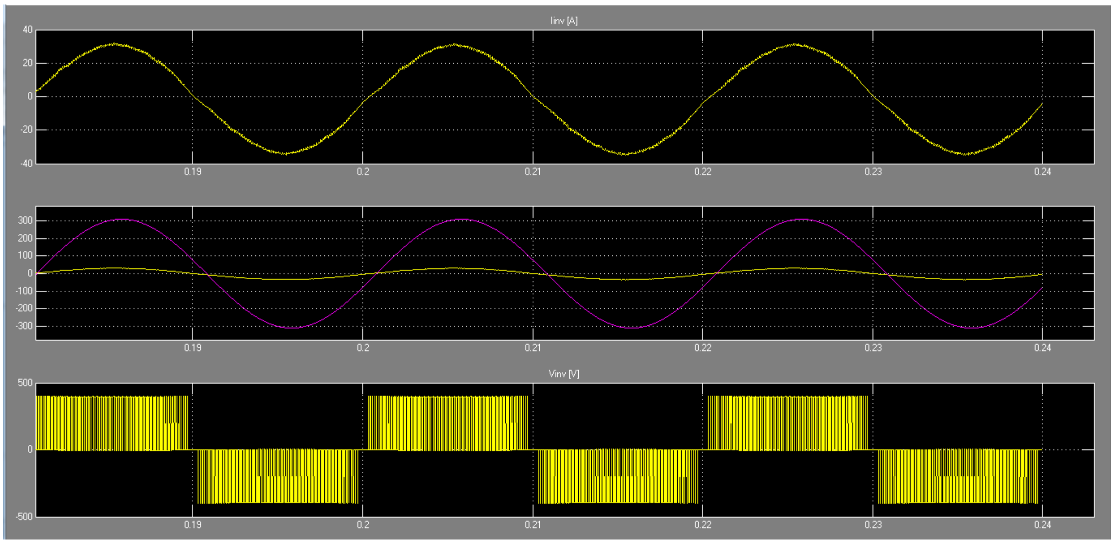

Figure 4-70 (a) Inverter current injected into the electric grid (A), (b) Active-NPC inverter output current and grid voltage,(c) Active-NPC inverter PWM output voltage (V).

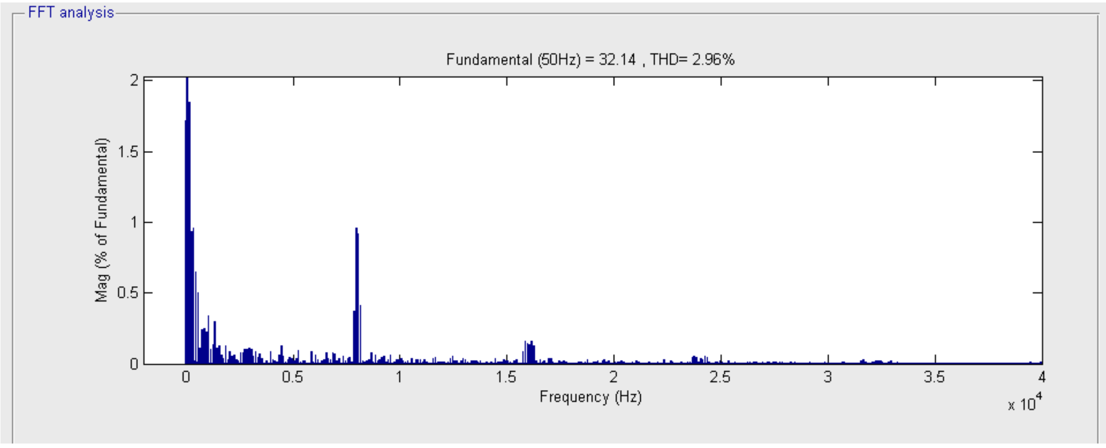

Figure 4-71 The spectrum of the Active-NPC inverter output current for f_s=8000 Hz, L=8mH, M=0.8, PF≈1.

Optimal strategy calculated: 0_{out}^-, P_2, 0_{out}^-, 0_{out}^+, 0_{out}^-, N_2, 0_{out}^- (Table 3-2)

The Genetic Algorithm calculated as optimal a strategy containing P_2 as positive state, N_2 as negative and two different zero paths. In positive side, the algorithm selected a strategy with two-way zero paths **0_{out}^-, 0_{out}^+** and during the negative side only one **0_{out}^-**. Fig.4-72 presents the optimal firing angles of the Active-NPC inverter for f_s= 8000 Hz, L=8mH, M=0.8 and PF≈1.

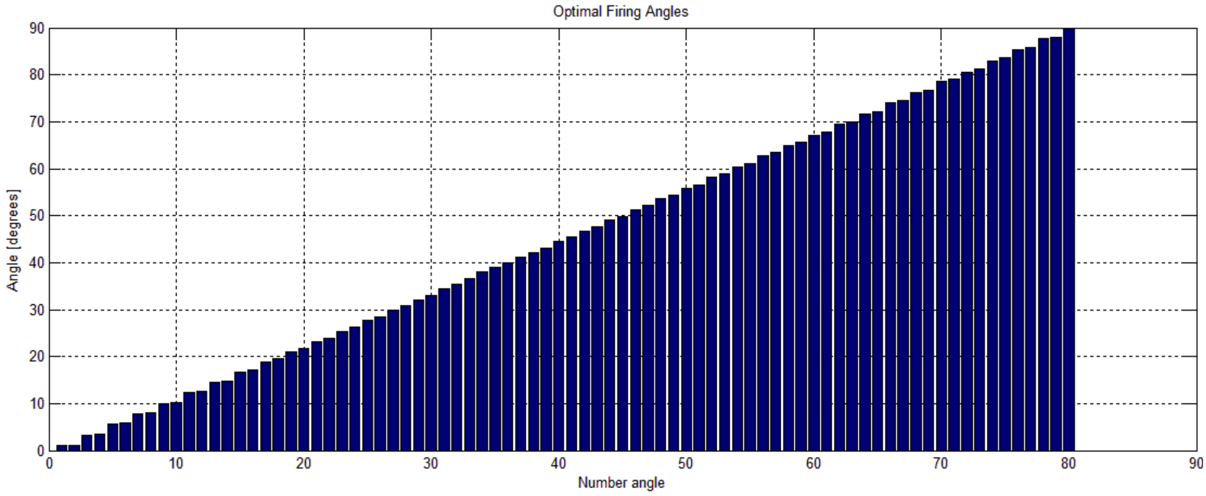

Figure 4-72 Optimal firing angles of Active-NPC inverter for fs= 8000Hz L=8mH, M=0.8 and PF≈1.

Figs. 4-73 to 4-75 present the power loss distribution for f_s=10000 Hz, M=0.8 and PF=0.98, the Active-NPC inverter current injected to the electric grid, the PWM output voltage and the spectrum of the Active-NPC inverter output current.

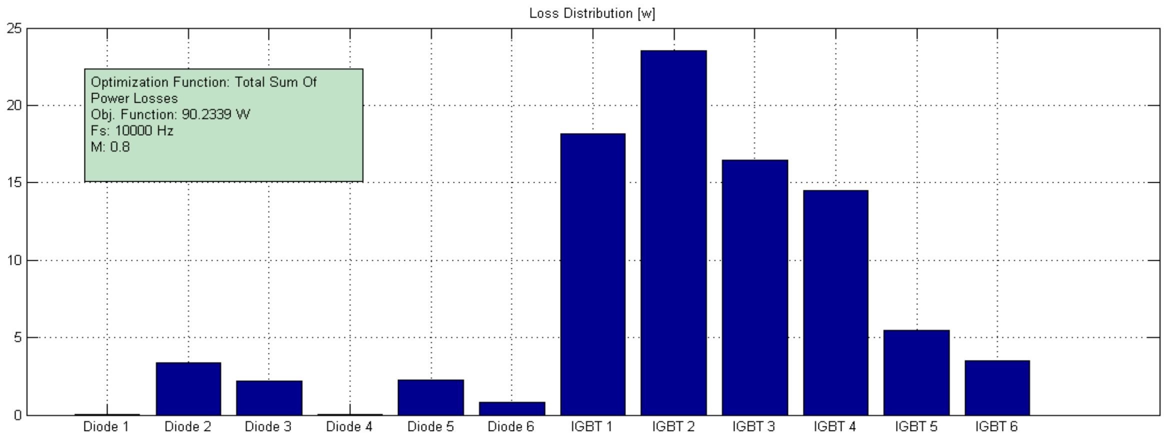

Figure 4-73 Power loss distribution for f_s=10000 Hz, L=8mH, M=0.8, PF=0.98.

(a)

(b)

(c)

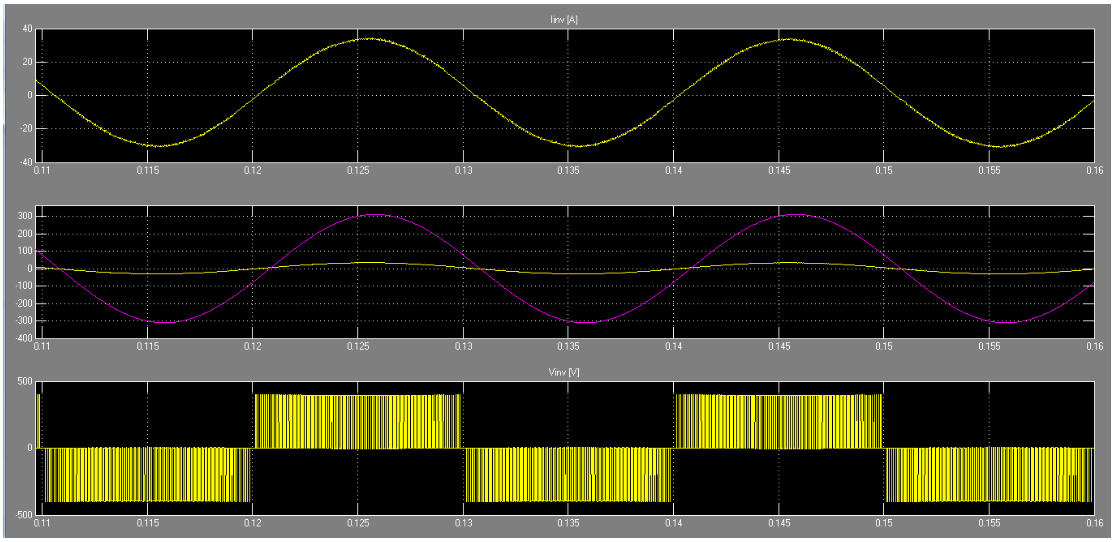

Figure 4-74 (a) Inverter current injected into the electric grid (A), (b) Active-NPC inverter output current and grid voltage,(c) Active-NPC inverter PWM output voltage (V).

.

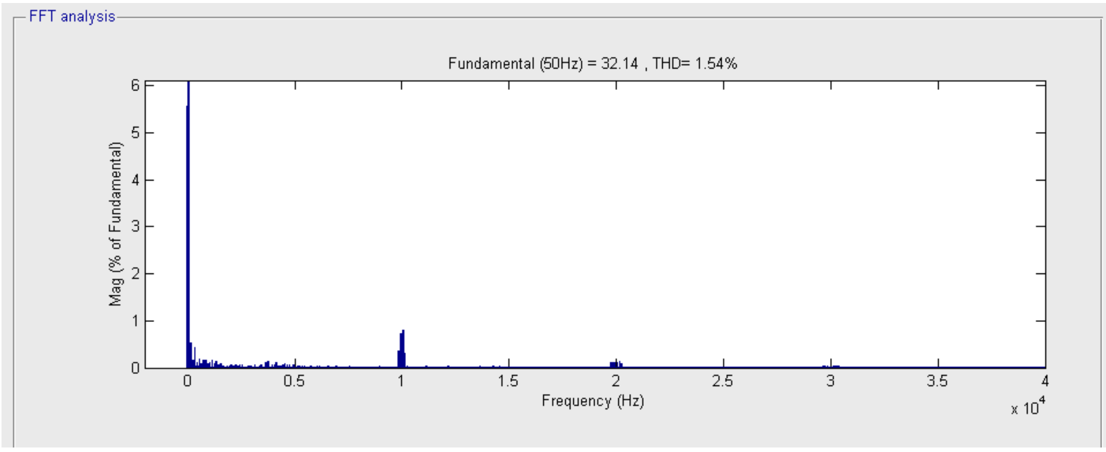

Figure 4-75 The spectrum of the Active-NPC inverter output current for f_s=10000 Hz, L=8mH, M=0.8, PF=0.98.

Optimal strategy calculated: $0_1^+/0^-$, P_2, 0_{out}^+, N_2, 0_{out}^-, $0_1^+/0^-$ (Table 3-2)

The optimal strategy calculated contains P_2 as positive state, N_2 as negative and three different zero paths. In positive side, the algorithm selected a strategy with only one zero path $\mathbf{0_{out}^+}$ and during the negative side a two way-zero path $\mathbf{0_{out}^-}$, $\mathbf{0_1^+/0^-}$. Fig.4-76 presents the optimal firing angles of the Active-NPC inverter for f_s= 8000 Hz, L=8mH, M=0.8 and PF=0.98.

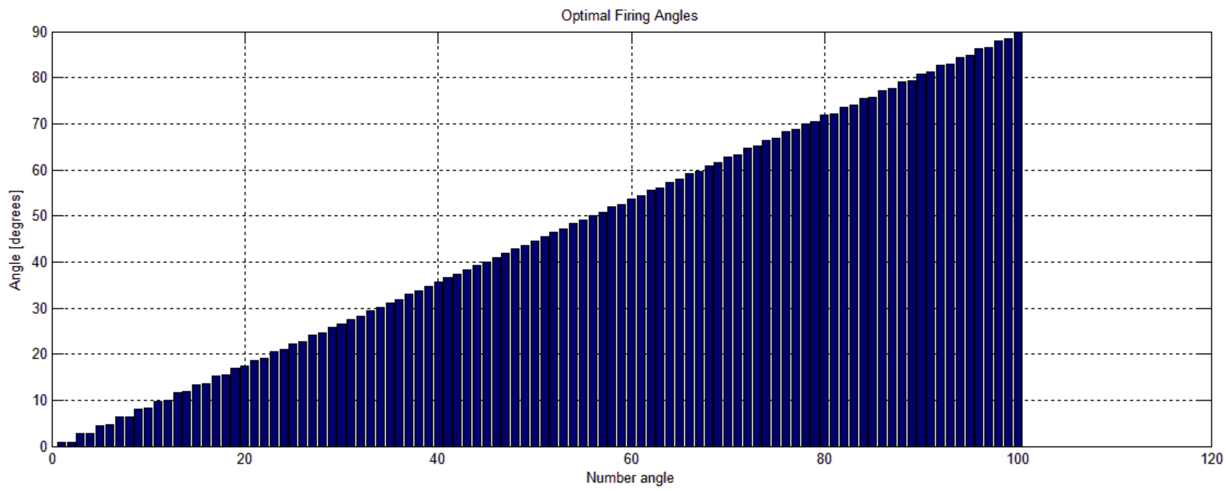

Figure 4-76 Optimal firing angles of Active-NPC inverter for fs=10000 Hz L=8mH, M=0.8 and PF=0.98.

Table 4-3 shows the summary of the above optimization results for the "total power losses" objective function, referring to the optimal zero switching states, calculated at the proposed optimization method.

Table 4-3. Summary table of optimization results for the "total power losses" objective function		
Strategy	**Switching State**	**Times Selected**
PWM2	0^-	0
PWM2/DF/ALD	$0^+/0_2^+/0_{IN}^+$	0
DF/ALD	$0_1^+/0^-$	1
PWM1/DF/ALD	$0^-/\ 0_1^-/0^+$	2
ALD	0_{out}^+	4
ALD	0_{out}^-	4

From the above matrix and results it is concluded that in most cases genetic algorithm selected up to three different zero ways. Moreover, the zero paths 0_{out}^+ and 0_{out}^- used in every case for zero-state commutations and it can be observed that, usually, in positive states two zero paths where chosen, while in negative paths only one.

4.2.2 Objective Function: Optimal Distribution of Power Losses among the Power Semiconductors

Table 4-4 includes the results of the past-proposed PWM strategies and the results of the proposed optimization method using genetic algorithms. The objective function in this case is the “sum of squared differences” of the power losses of the IGBTs and diodes.

Table 4-4. Sum of squared differences results in past-proposed PWM strategies and the proposed optimization method for L=8mH, PF≈1.

f_s (Hz)	Strategy					
	PWM1	PWM2	PWM3	ALD (50/50)	ALD (40/60)	Opt. Model
3000	1.8673e+04	9.172e+03	1.011e+04	7.710e+03	7.732e+03	7.5352e+03
5000	1.8574e+04	9.049e+03	9.759e+03	7.564e+03	7.573e+03	7.2610e+03
8000	1.8372e+04	8.897e+03	9.210e+03	7.160e+03	7.168e+03	7.1502e+03
10000	1.825e+04	8.742e+03	9.0379e+03	6.870e+03	6.874e+03	6.6192e+03

The percentage reduction of the objective function achieved by the proposed optimization method compared to the past-proposed PWM strategies is presented is in Table 4-5.

Table 4-5. The percentage reduction of the objective function value achieved by the proposed optimization method % (PWMs-Opt. Model/ Opt. Model)

f_s (Hz)	Strategy				
	PWM1	PWM2	PWM3	ALD(50/50)	ALD(40/60)
3000	148%	21.7%	34.2%	2.33%	2.62%
5000	156%	24.6%	34.4%	4.18%	4.30%
8000	157%	24.4%	28.8%	1.43%	2.59%
10000	176%	32.5%	36.5%	3.79%	3.85%

The Genetic Algorithm based approach reduced the "sum of squared differences" of power losses through the Active-NPC semiconductors from 176% up to 1.43% in relation to the past-proposed PWM methods. From Table 4-5, we can see that power losses are a lot more balanced (up to 176%) comparing with PWM1 strategy, while the others strategies, with more zero paths, reach up to 1.43% (ALD 50-50) genetic algorithm results.

Analytically, the following figures present the optimization results of the proposed method, the resulting waveforms and the strategies that have been derived, with an inductance L=8 mH as output filter.

Figs. 4-77 to 4-79 show the power loss distribution for f_s=3000 Hz, M=0.8 and PF=1, the Active-NPC inverter current injected to the electric grid, the PWM output voltage and the spectrum of the Active-NPC inverter output current.

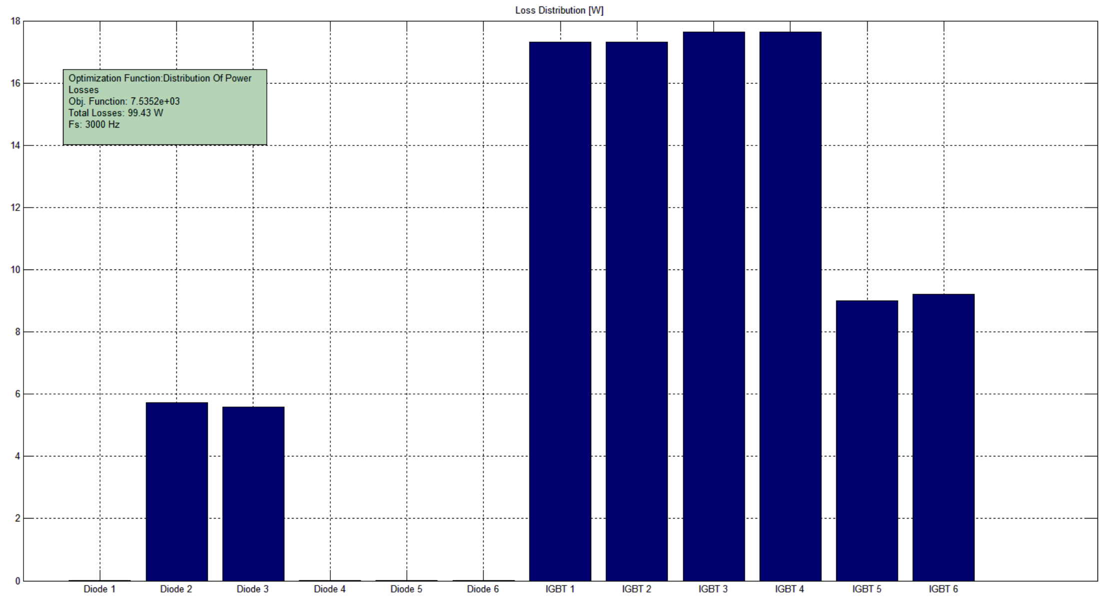

Figure 4-77 Power loss distribution for f_s=3000 Hz, L=8mH, M=0.8, PF=1.

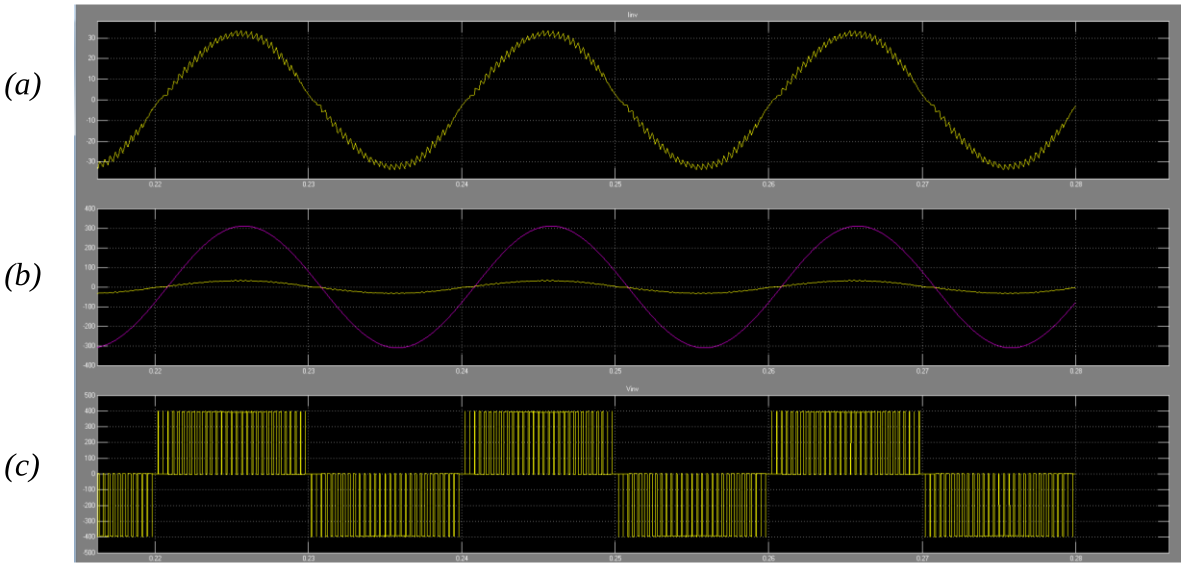

Figure 4-78(a) Inverter current injected into the electric grid (A), (b) Active-NPC inverter output current and grid voltage,(c) Active-NPC inverter PWM output voltage (V)

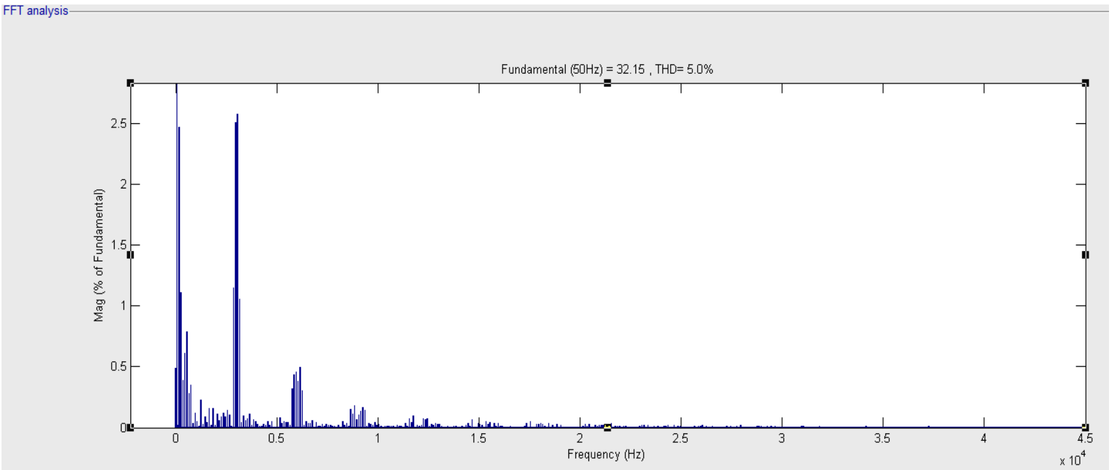

Figure 4-79 The spectrum of the Active-NPC inverter output current for f_s=3000 Hz, L=8mH, M=0.8, PF=1.

Optimal strategy calculated: $\mathbf{0^-}$, $\mathbf{P_1}$, $\mathbf{0^-/\,0_1^-/0^+}$, $\mathbf{N_2}$, $\mathbf{0^-}$ (Table 3-2).

The strategy calculated as optimal contains $\mathbf{P_1}$ as positive state, $\mathbf{N_2}$ as negative and two different zero paths. In the positive side, the algorithm selected a strategy with only one zero path $\mathbf{0^-/\,0_1^-/0^+}$ and during the negative side again one zero way path $\mathbf{0^-}$. Fig.4-80 presents the optimal firing angles of the Active-NPC inverter for f_s= 3000 Hz, L=8mH, M=0.8 and PF=1.

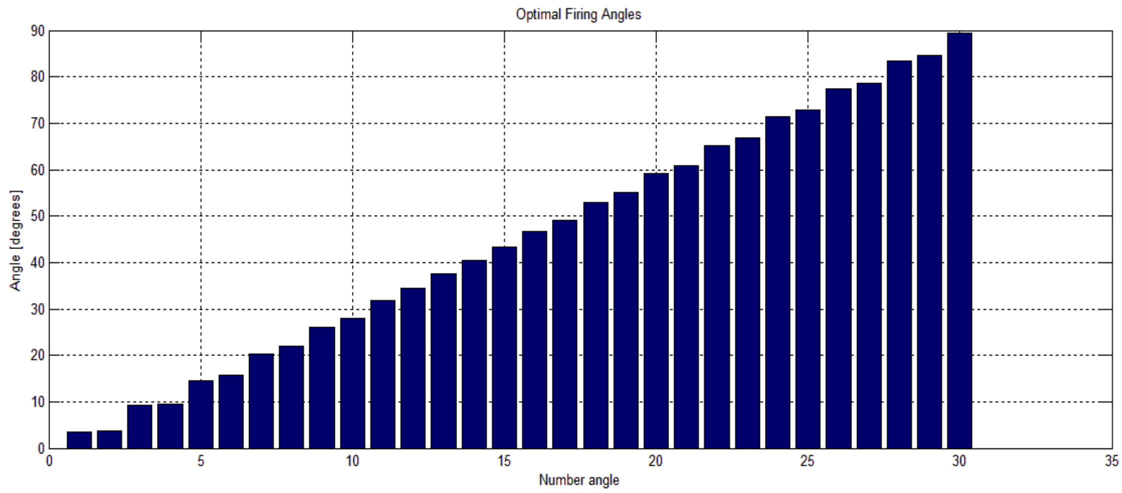

Figure 4-80 Optimal firing angles of Active-NPC inverter for fs= 3000Hz, L=8mH, M=0.8 and PF=1.

Figs. 4-81 to 4-83 present the power loss distribution for f_s=10000 Hz, M=0.8 and PF=1, the Active-NPC inverter current injected to the electric grid, the PWM output voltage and the spectrum of the Active-NPC inverter output current.

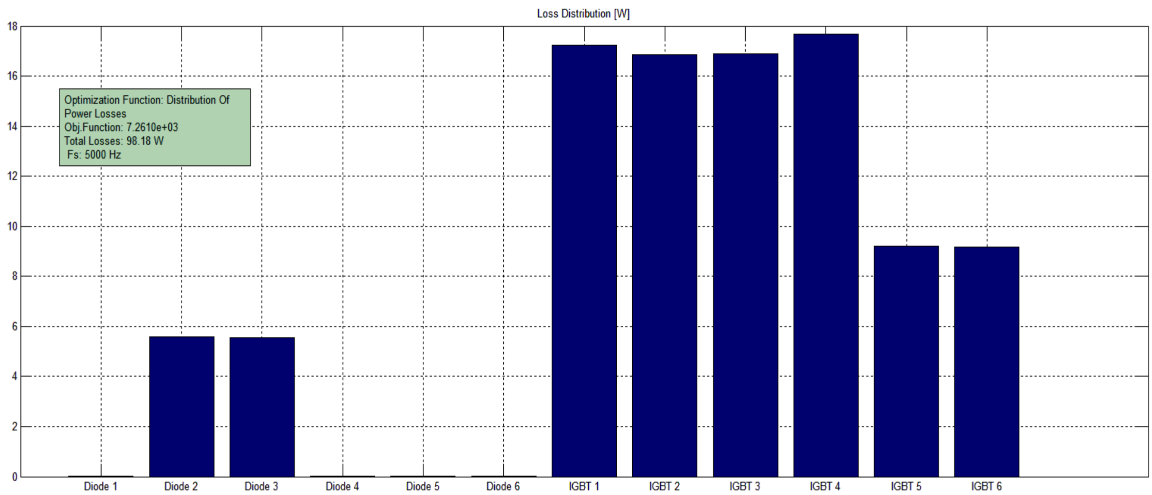

Figure 4-81 Power loss distribution for f_s=5000 Hz, L=8mH, M=0.8, PF=1.

(a)
(b)
(c)

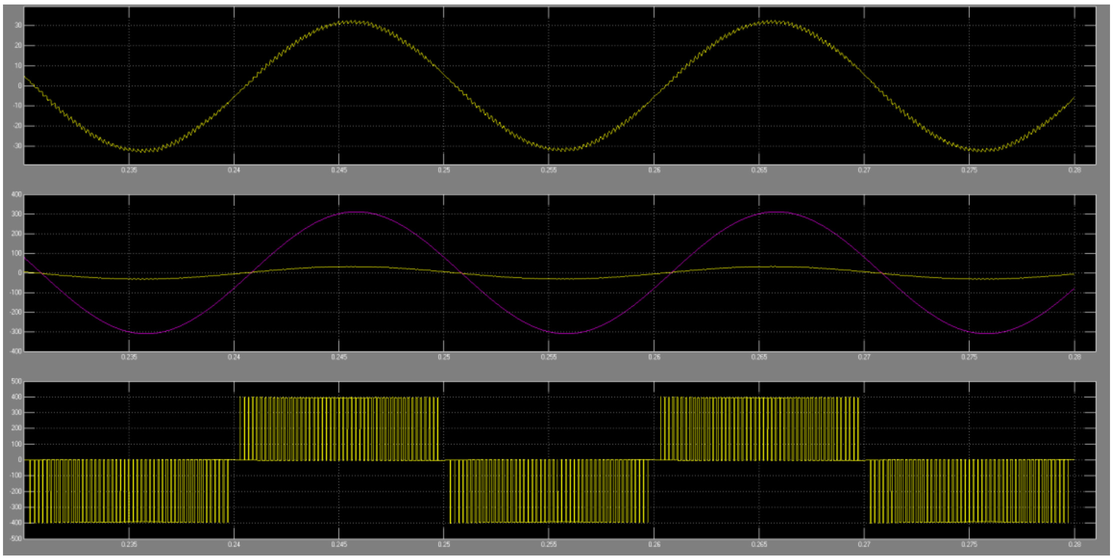

Figure 4-82(a) Inverter current injected into the electric grid (A), (b) Active-NPC inverter output current and grid voltage,(c) Active-NPC inverter PWM output voltage (V)

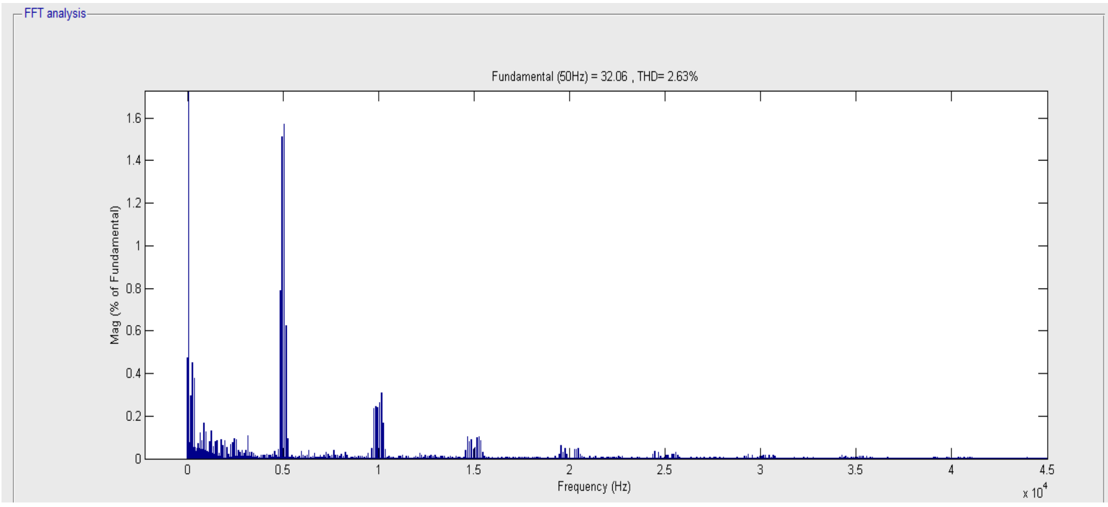

Figure 4-83 The spectrum of the Active-NPC inverter output current f_s=5000 Hz, L=8mH, M=0.8, PF=1.

Optimal strategy calculated: 0^-, P_2, $0^+/0_2^+/0_{IN}^+$, $0^-/\ 0_1^-/0^+$, N_2, 0^- (Table 3-2)

The strategy calculated as optimal contains P_2 as positive state, N_2 as negative and three different zero paths. In positive side, the algorithm selected a strategy with two way zero paths **$0^+/0_2^+/0_{IN}^+$, $0^-/\ 0_1^-/0^+$** and during the negative side one zero way path **0^-**. Fig.4-84 presents the optimal firing angles of the Active-NPC inverter for f_s= 5000 Hz, L=8mH, M=0.8 and PF=1.

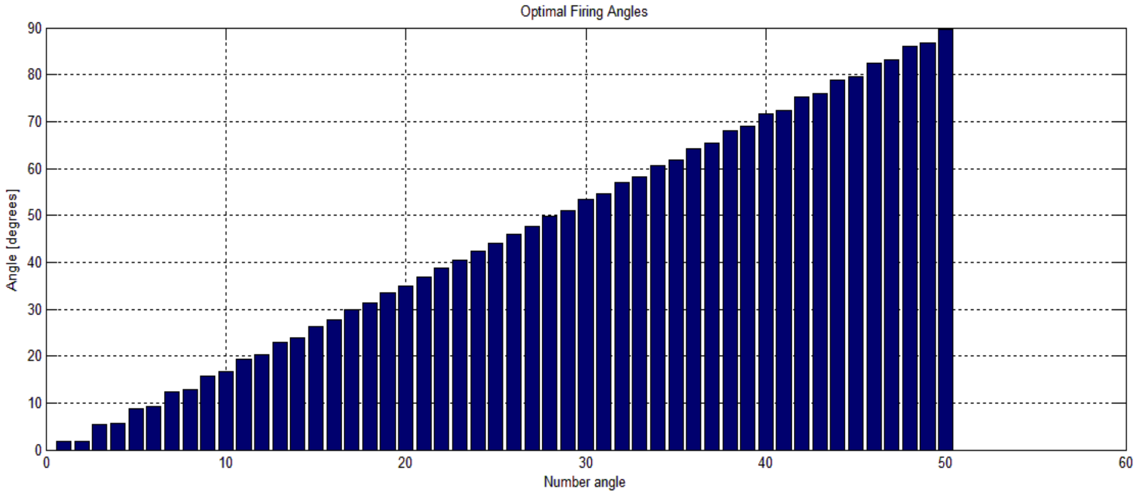

Figure 4-84 Optimal firing angles of Active-NPC inverter for fs= 5000Hz, L=8mH, M=0.8 and PF=1.

Figs. 4-85 to 4-87 present the power loss distribution for f_s=8000 Hz, M=0.8 and PF=1, the Active-NPC inverter current injected to the electric grid, the PWM output voltage and the spectrum of the Active-NPC inverter output current.

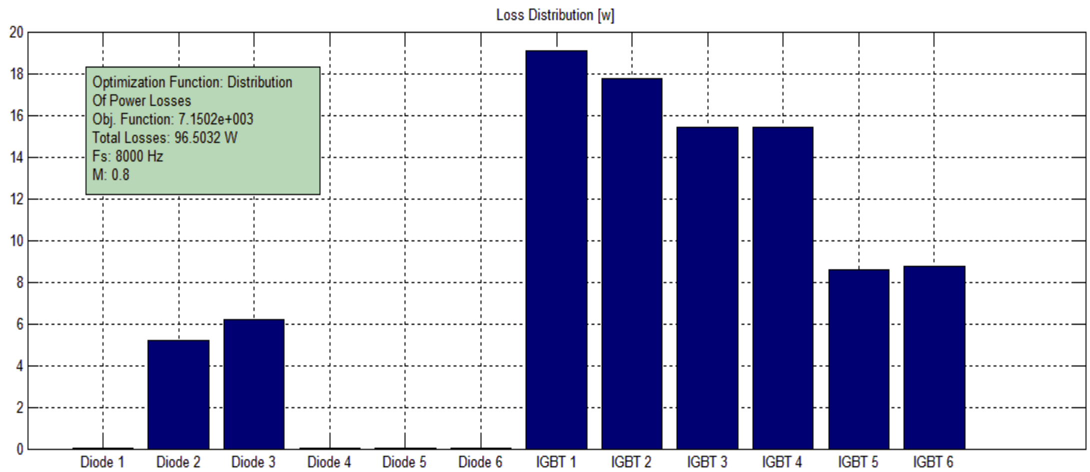

Figure 4-85 Power loss distribution for f_s=8000 Hz, L=8mH, M=0.8 PF=1.

(a)

(b)

(c)

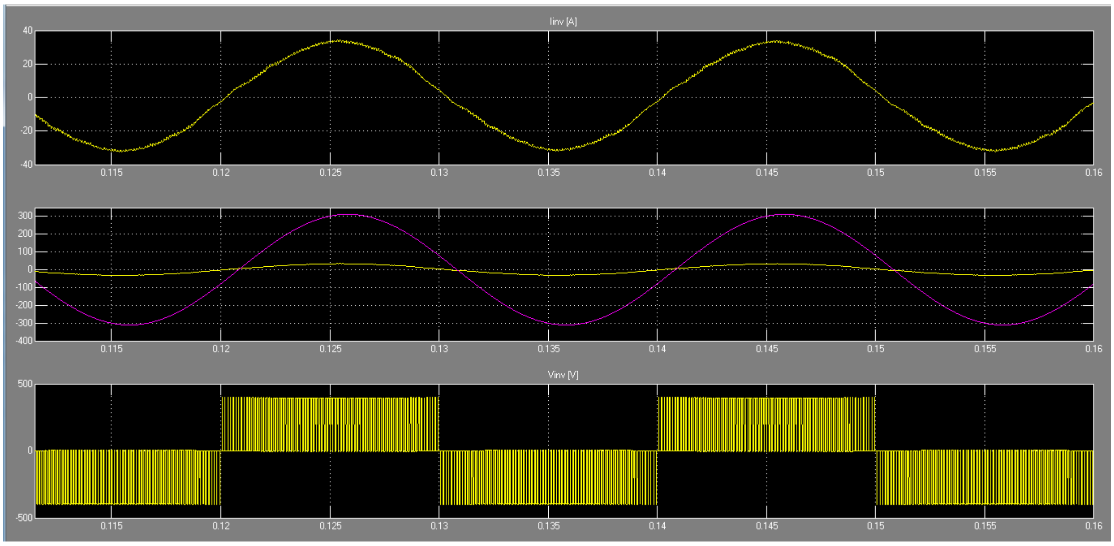

Figure 4-86 (a) Inverter current injected into the electric grid (A), (b) Active-NPC inverter output current and grid voltage,(c) Active-NPC inverter PWM output voltage (V).

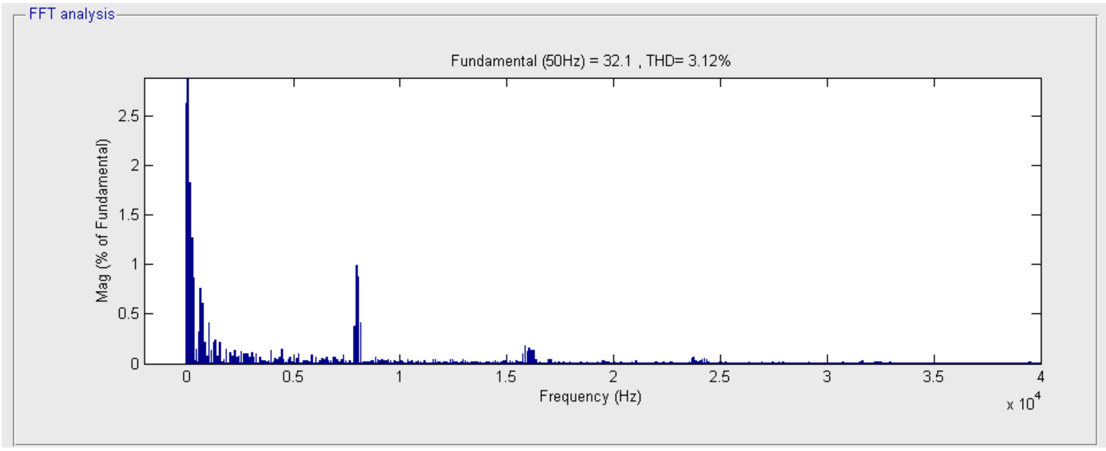

Figure 4-87 The spectrum of the Active-NPC inverter output current for f_s=8000 Hz, L=8mH, M=0.8 PF=1.

Optimal strategy calculated: $0_1^+/0^-$, P_1, $0^+/0_2^+/0_{IN}^+$, N_2, $0_1^+/0^-$ Table (3-2)

The strategy calculated as optimal contains **P_1** as positive state, **N_2** as negative and two different zero paths. In positive side, the algorithm selected a strategy with one way zero path **$0^+/0_2^+/0_{IN}^+$** and during the negative side again only one zero way path **$0_1^+/0^-$**. Fig.4-88 presents the optimal firing angles of the Active-NPC inverter for f_s= 8000 Hz, L=8mH, M=0.8 and PF=1.

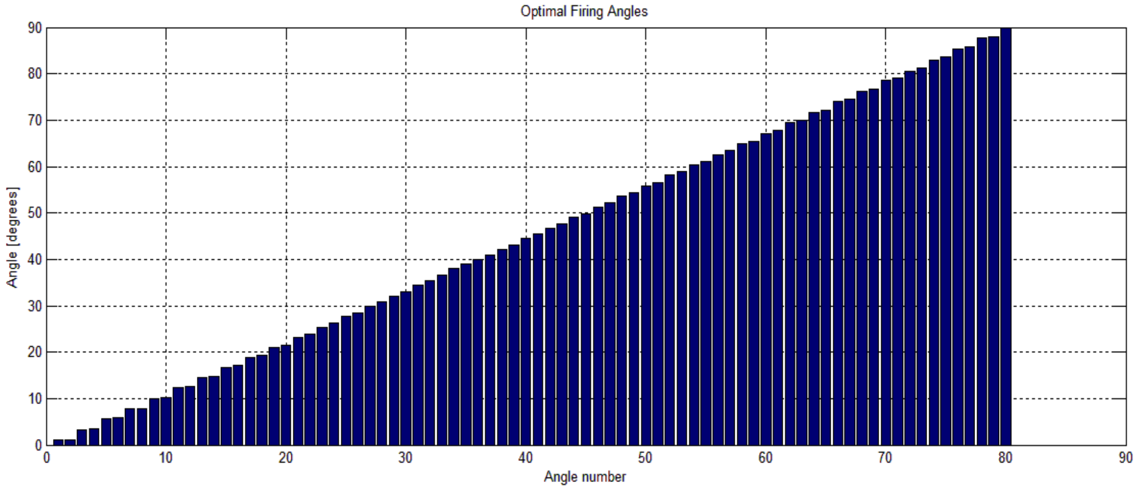

Figure 4-88 Optimal firing angles of Active-NPC inverter for fs= 8000Hz, L=8mH, M=0.8 and PF=1.

Figs. 4-89 to 4-91 present the power loss distribution for f_s=10000 Hz, M=0.8 and PF≈1, the Active-NPC inverter current injected to the electric grid, the PWM output voltage and the spectrum of the Active-NPC inverter output current.

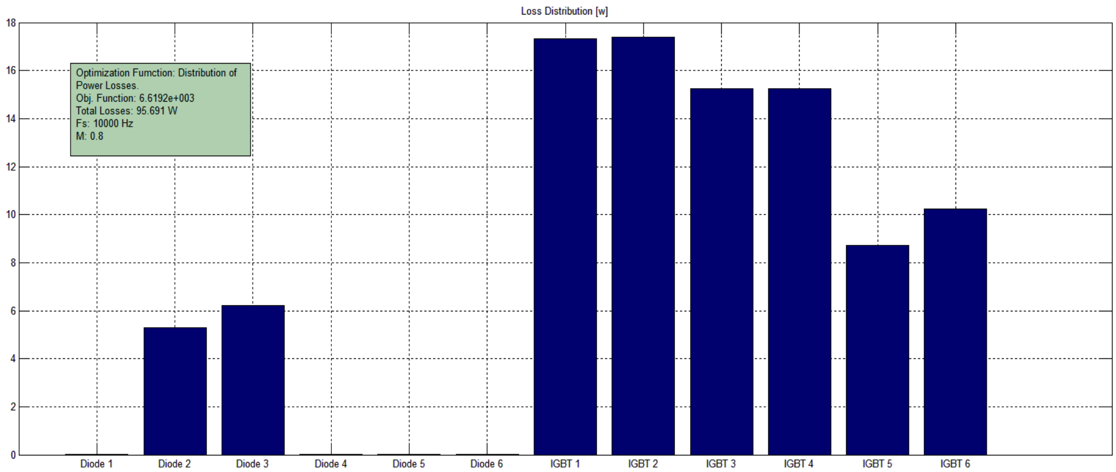

Figure 4-89 Power loss distribution for f_s=10000 Hz, L=8mH, M=0.8, PF≈1.

(a)

(b)

(c)

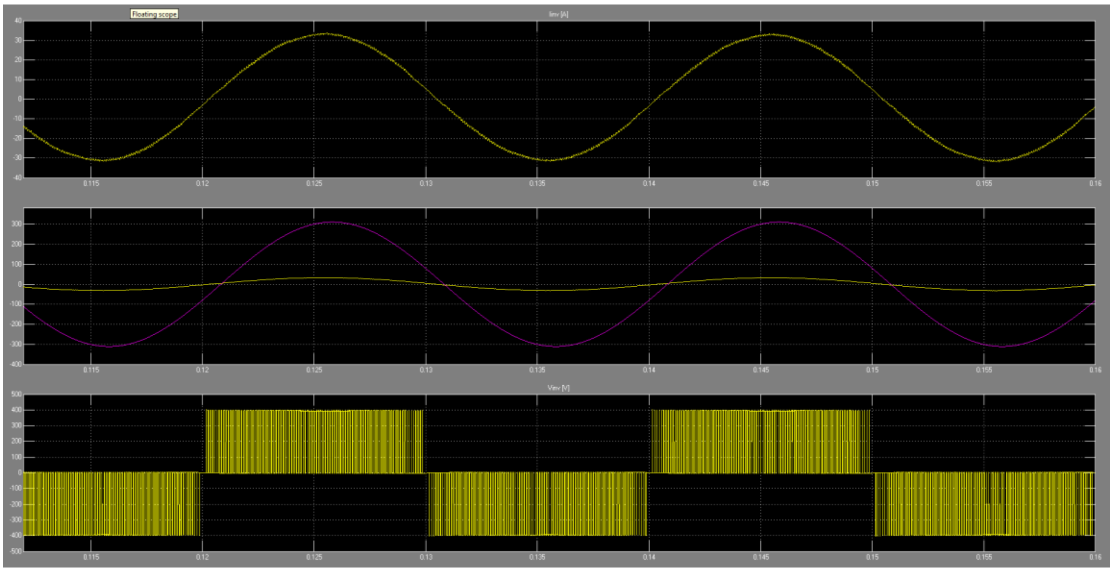

Figure 4-90(a) Inverter current injected into the electric grid (A), (b) Active-NPC inverter output current and grid voltage,(c) Active-NPC inverter PWM output voltage (V).

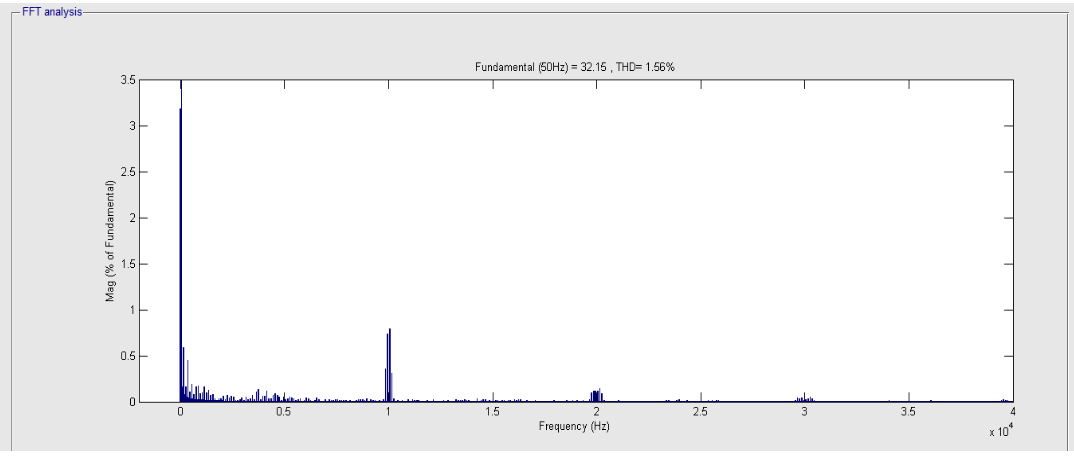

Figure 4-91 The spectrum of the Active-NPC inverter output current for f_s=10000 Hz, L=8mH, M=0.8, PF≈1.

Optimal strategy calculated: $0_1^+/0^-$, P_2, $0^-/ 0_1^-/0^+$, N_2, $0_1^+/0^-$ (Table 3-2)

The strategy calculated as optimal contains $\mathbf{P_2}$ as positive state, $\mathbf{N_2}$ as negative and two different zero paths. In positive side, the algorithm selected a strategy with one way zero path **$0^-/ 0_1^-/0^+$** and during the negative side again only one zero way path **$0_1^+/0^-$**. Fig.4-92 presents the optimal firing angles of the Active-NPC inverter for f_s= 10000 Hz, L=8mH, M=0.8 and PF≈1.

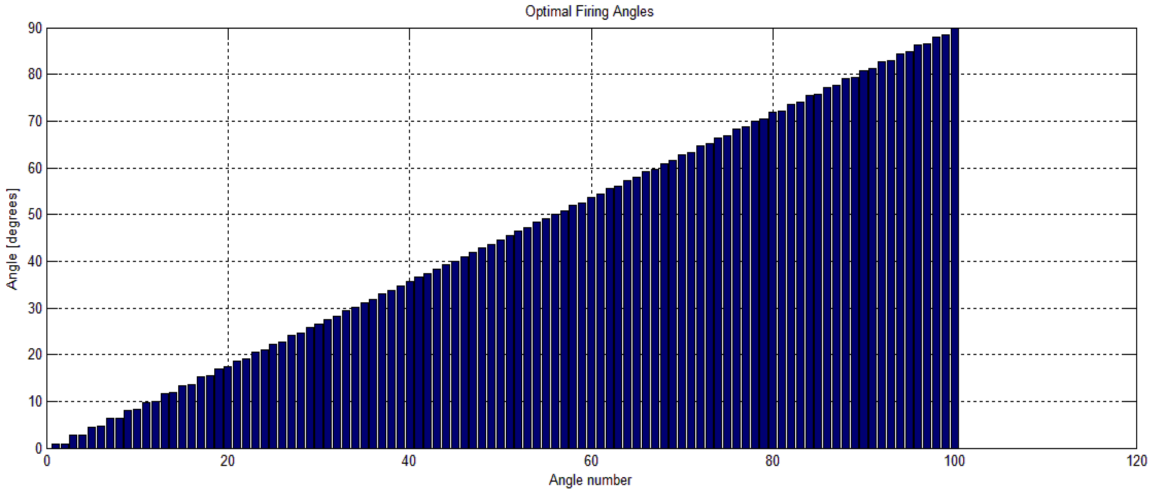

Figure 4-92 Optimal firing angles of Active-NPC inverter for fs= 10000 Hz, L=8mH, M=0.8 and PF≈1.

Table 4-6 shows a summary of the above optimization results for the “sum of squared differences” objective function, referring to the optimal zero switching states, calculated at the proposed optimization method.

Table 4-6. Summary table of optimization results for the “sum of squared differences” of power losses objective function.

Strategy	Switching State	Times Selected
PWM2	0^-	2
PWM2/DF/ALD	$0^+/0_2^+/0_{IN}^+$	2
DF/ALD	$0_1^+/0^-$	2
PWM1/DF/ALD	$0^-/ 0_1^-/0^+$	3
ALD	0_{out}^+	0
ALD	0_{out}^-	0

From the above matrix and results it is concluded that in most cases genetic algorithm selected two or three different zero-ways. Moreover, the zero paths 0^- , $0^+/0_2^+/0_{IN}^+$, $0_1^+/0^-$ and $0^-/ 0_1^-/0^+$ were selected and it can be observed that despite the main concept of the past-proposed PWM methods for balancing the power losses is the selection of more zero paths, the proposed optimization method used only up to three. It should be noted that despite the less zero paths, the proposed optimization method also optimizes the firing angles.

Table 4-7. TDD results in past-proposed PWM strategies and the proposed optimization method for L=8mH, PF≈1

f_s (Hz)	Strategy					
	PWM1	PWM2	PWM3	ALD (50/50)	ALD (40/60)	Opt. Model (Sum/Distribution)
3000	4.22%	4.22%	2.31%	4.39%	4.39%	4.37% / 5%
5000	2.69%	2.70%	1.70%	2.68%	2.68%	3.75% / 2.63%
8000	1.73%	1,74%	1.16%	1.72%	1.72%	2.96% / 3.12%
10000	1.74%	1.74%	1.06%	1.7%	1.71%	1.54% / 1.56%

Concerning the total harmonic distortion results, which are presented in Table 4-7, it is observed that the proposed optimization method, except of the case with f_s = 10 kHz, has worse performance than the other PWM methods. However, the resulting THD satisfies the constraints of the IEEE standard.

Fig. 4-93 presents the efficiency of the Active-NPC inverter of the past-proposed PWM and the proposed optimization method in which the objective function is the total sum of power losses among power semiconductors.

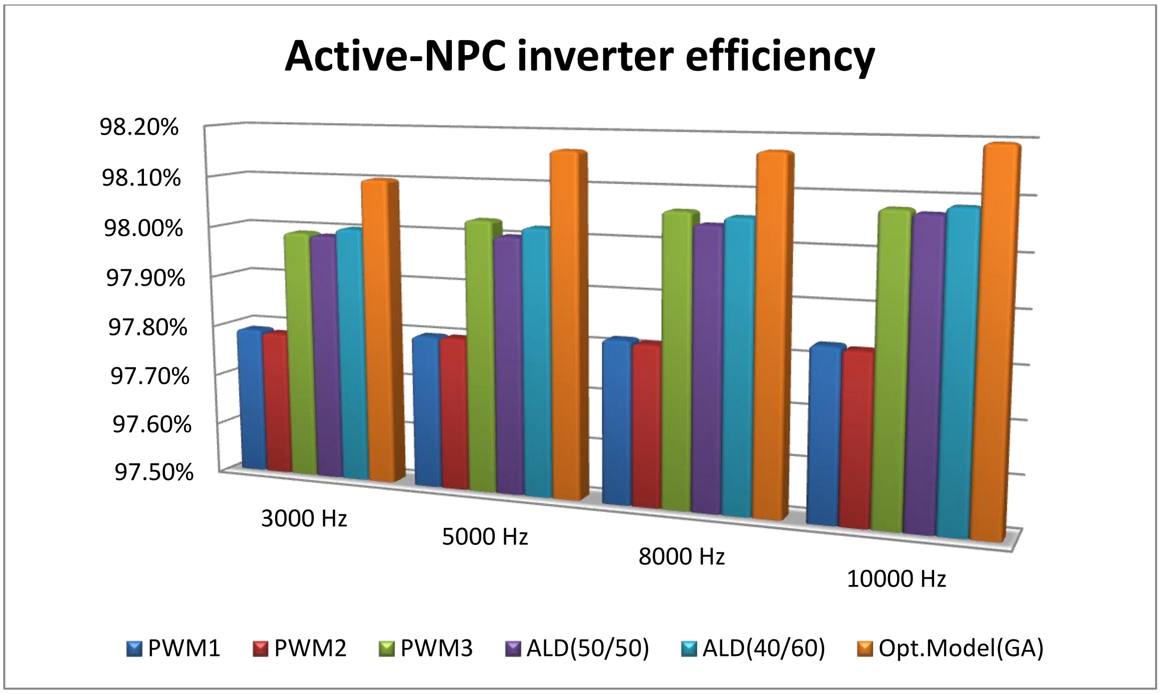

Figure 4-93 The Active-NPC inverter efficiency of the past-proposed PWM strategies and the proposed optimization method.

Finally, Fig. 4-94 presents the efficiency of the Active-NPC inverter of the past-proposed PWM and the proposed optimization method in which the objective function is the sum of squared differences of power losses among power semiconductors.

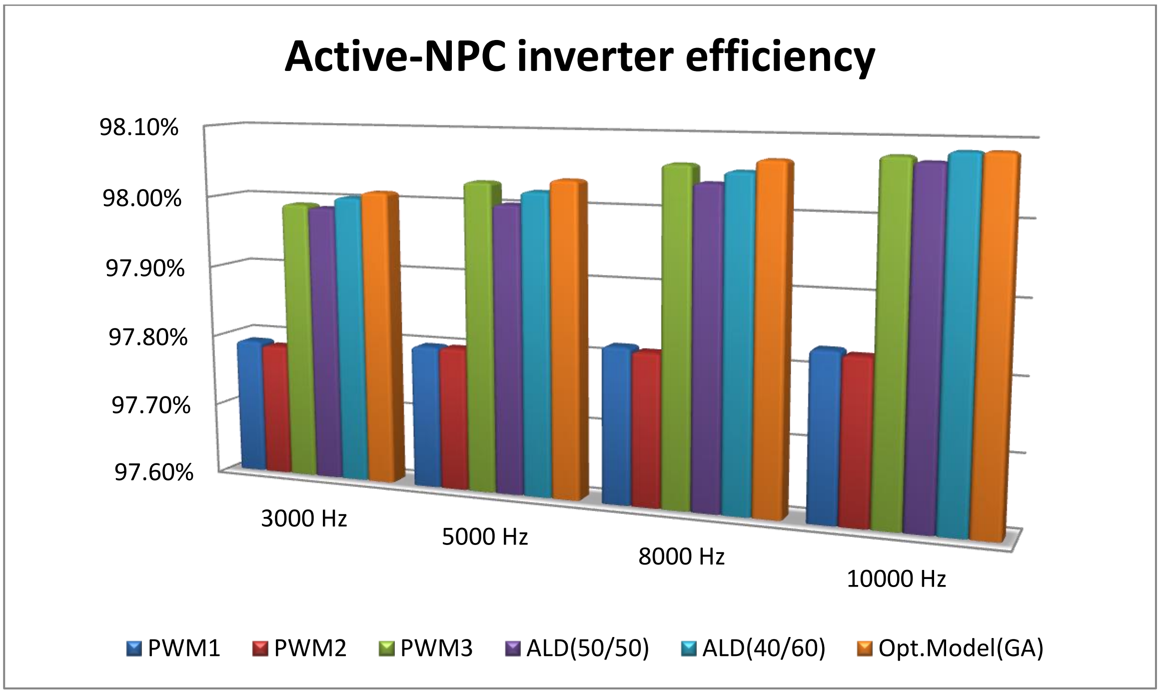

Figure 4-94 The Active-NPC inverter efficiency of the past-proposed PWM strategies and the proposed optimization method.

To sum up, there is not a specific strategy that gives the best result either for the total losses, either for the best distribution of power losses. It can be mentioned that some combinations of commutations are often selected by the algorithm and every strategy has one positive and one negative selection for different input parameters. As it can be observed, the proposed algorithm did not choose more than three different zero paths, in difference with the past-proposed strategies where the more paths are used, the better results they had.

5. Conclusions

5. Conclusions

In this thesis, genetic algorithms have been used to optimize the power losses distribution and the total losses of the Active-NPC inverter topology. In particular, genetic algorithm gives a set of angles of the output voltage waveform and a strategy. Simulink simulates the circuit, exports the power losses of every semiconductor and Matlab computes the minimum sum of the squared differences of power losses between all devices and the total sum of power losses, which are the objective functions of the algorithm. Through this iterative model, genetic algorithm decides which set of angles and strategy should be extracted, in order to have more balanced and less power losses, respectively through the Active-NPC inverter semiconductors. It has to be said that all possible switches transitions have taken into consideration, in order to create all possible strategies, simulate them and decide which strategy of the optimized set of angles gives the best result. This set of angles, except from the output voltage waveform symmetry constraints, also obeys IEEE standards for interconnecting distributed power sources with Electric Power Systems, by examining the total demand distortion (TDD). Simulations using Simulink have been performed for evaluating the performance of different Active-NPC inverter control strategies and comparing the past-proposed strategies with the method developed in this thesis. The genetic algorithm parameters have been derived from optimization experiments through Matlab.

The combination of angles detection and strategy selection produces less and/or more balanced power losses. Having as objective function the total power losses, the proposed method picked the strategy and found the appropriate angles that resulted from 5.18% (ALD (40/60)) up to 20.51% (PWM2) less power losses of the Active-NPC inverter semiconductors. With regard to power losses distribution, genetic algorithm results reduced the corresponding objective function value from 1.43% up to 176% compared to the past-proposed PWM techniques. Finally, it is noticed that the genetic algorithm optimization process chose only up to three different zero paths, in contrast with the pas-proposed PWM strategies, where the more zero paths used, the better results they had.

An improvement and extension could be the utilization of C language for deriving results faster and a construction of a graphic user interface (GUI), in order to be more convenient to the user.

6. Bibliography

[1] Lin Ma, Tamas Kerekes, Remus Teodorescu, Xinmin Jin, Marco Liserre and Pedro Rodriguez, "The PWM Strategies of Grid-connected Distributed Generation Active-NPC Inverters", IEEE Energy Conversion Congress and Exposition, pp. 920 – 927, 20-24 Sept. 2009.

[2] Muhammad H. Rashid "Power Electronics Handbook", Academic Press 2001.

[3] Gonzalez, R. Lopez, J. Sanchis, P. Marroyo, L, 'Transformer-less Inverter for Single-Phase Photovoltaic Systems', Power Electronics, IEEE Transactions on Vol. 22, Issue 2, , pp. 693 – 697, March 2007.

[4] T. Bróckner, S. Bernet, H. Góldner, "*The Active-NPC Converter and Its Loss-Balancing Control*", IEEE Transactions on Industrial Electronics, Vol.52, pp.855-868, 2005.

[5] A. Nabae, I. Takahashi, and H. Akagi, "A new neutral-point-clamped PWM inverter," IEEE Transactions on Industrial Applications., Vol. 17, pp. 518–523, Sep. / Oct. 1981.

[6] D. Floricau, E. Floricau and M. Dumitrescu, "Natural Doubling of the Apparent Switching Frequency using Three-Level ANPC Converter", International School on Nonsinusoidal Currents and Compensation, pp.1 – 6, 10-13 June 2008.

[7] C. Attaianese, M. Di Monaco, and G. Tomasso. "Three-Phase Three-Level Active-NPC Converters for High Power Systems", International Symposium on Power Electronics, Electrical Drives, Automation and Motion, 2010.

[8] N. Mohan, T.Underland, W.Robbins "Ηλεκτρονικά Ισχύος", β' έκδοση, εκδόσεις Α.Τζιόλα 1996.

[9] Tsitsopoulos Nikolaos, "Optimization control of DC/AC inverters using genetic Algorithms", Technical University of Crete, 2006.

[10] IEEE std-1547 "Standard for Interconnecting Distributed Resources with Electric Power Systems", July 2003

[11] www.mathworks.com, Matlab and Simulink Product Family.

[12] www.mathworks.com/help/toolbox/gads/gaoptimset.html

[13] D.Floricau, G.Gateau, A Leredde, R. Teodorescu “The Efficiency of Three-Level Active-NPC Converter for Different PWM Strategies”, 13th European Conference on Power Electronics and Applications, pp.1-9, 8-10 Sept 2009.

[14] Lin Ma, Tamas Kerekes, Remus Teodorescu, Xinmin Jin, Dan Floricau, Marco Liserre “The High Efficiency Transformer-less PV Inverter Topologies Derived From NPC Topology”, 13th European Conference on Power Electronics and Applications, pp.1-10, 8-10 Sept. 2009.